Progress in Energy and Combustion Science 45 (2014) 1–53

Contents lists available at ScienceDirect

Progress in Energy and Combustion Science

journal homepage: www.elsevier.com/locate/pecs

Review

Progress in particle resuspension from rough surfaces by turbulent flows

Christophe Henry [a, *], Jean-Pierre Minier [b]

[a] Institute of Fluid-Flow Machinery, Polish Academy of Science, Fiszera 14 st., Gdańsk 80-231, Poland
[b] EDF R&D, Fluid Dynamics, Power Generation and Environment, 6 quai Watier, Chatou 78400, France

ARTICLE INFO

Article history:
Received 11 February 2014
Accepted 2 June 2014
Available online

Keywords:
Colloid
Particle
Resuspension
Detachment
Reentrainment

ABSTRACT

This article deals with the resuspension phenomenon whereby particles adhering on a wall surface can be re-entrained by a flowing fluid. This is an area where significant progress has been achieved over the last years from an experimental, theoretical and numerical point of view. A first purpose of the present work is to report on the advances that have clarified our understanding of the physics of particle resuspension. It will be seen that new pictures have emerged about the physical processes involved in particle resuspension and, correspondingly, that new models have been proposed. A second purpose of the review is to put forward a general framework that allows both experimental analysis and new modelling ideas to be developed in terms of the fundamental interactions at play. These interactions are made up by the particle–fluid, particle–surface and particle–particle forces which are, in turn, related to the three specific fields of fluid dynamics, interface chemistry and surface roughness. Such a separation is helpful to highlight the actual physical processes while emphasising their relative importance in different situations and to provide useful guidelines for the necessary modelling efforts. In particular, it is stressed that new models which capture particle motion along a wall and simulate the complete particle dynamics represent an improvement over more classical static approaches. It is proposed that these new approaches be pursued and brought to higher levels of maturity.

In this paper, attention is first focussed on the case where only a single layer of particles is sticking on the surface and, thus, can be re-entrained. A detailed review of the experimental works brings out the essential mechanisms and particle resuspension is shown to result from a balance between particle–fluid interactions and particle–surface interactions influenced by surface heterogeneities (roughness). The numerical models which have been proposed are then thoroughly discussed with respect to a new hierarchy of modelling approaches which is introduced. The present paper also outlines the mechanisms of multilayer particle resuspension which is still an open subject and where our present understanding remains preliminary. In this situation, resuspension is shown to be also governed by particle–fluid and particle–surface interactions but with the addition of particle–particle interactions (through cohesion forces or impaction). Finally, suggestions about the areas that still need to be addressed as well as about the issues that remain to be improved are addressed.

Contents

* Corresponding author.
E-mail addresses: christophe.henry@mines-paris.org (C. Henry), jean-pierre.minier@edf.fr (J.-P. Minier).

http://dx.doi.org/10.1016/j.pecs.2014.06.001
0360-1285/

1. Introduction

The present review deals with the issue of particle resuspension, a field where much progress has been made experimentally, theoretically and numerically since the detailed review of Ziskind [1].

1.1. The resuspension phenomenon

Resuspension (also referred to as re-entrainment, removal or detachment) corresponds to the process where particles sticking on a surface are reentrained away from the surface. Depending on the field, resuspension can either be required so as to limit surface fouling (for instance dust accumulation on solar cells [2]) or has to be avoided when deposited particles are hazardous materials (such as radioactive particles in nuclear power plants [3] or contaminant particles in hospitals). The resuspension phenomenon has thus been extensively studied in a wide range of fields which are illustrated by the following examples.

- Re-entrainment of sediments (particles with sizes ranging from a few tens of micrometres to a few millimetres) is a key issue in sediment dynamics [4] and also in soil resuspension [5].
- Dust resuspension is a matter of concern for the environment since a release of road dust (particulate matter with diameters smaller than 10 μm) greatly impacts pollution levels [6] and, also, since resuspended dust can be carried by winds [7] (sometimes leading to the formation of sand dunes in desert).
- Resuspension of airborne particles is investigated both for indoor environment [8] (including ventilation systems [9,10] or walking-induced resuspension [11]) and for outdoor environment (e.g. industrial pills and pesticide applications [9]) due to their potential threat on human health.

- Similarly, re-entrainment of aerosolised drug particles used in dry powder inhalers (DPI) [12] or in spray drying systems [13] has been studied.
- Resuspension also affects the food industry (e.g. re-entrainment of spores from bacillus species [14], or spray systems used in the production of milk powders [15]).
- The energy industry is also concerned by the issue of particle removal (for instance by the release of radioactive products in nuclear reactors or heat exchangers [16]) and by the release of potentially harmful particles in case of fire [17].
- Resuspension is a significant issue in filtration systems [18] and membrane fouling [19] with applications in pharmaceutical, food, wastewater and desalination industries. More specifically, in membranes, the formation of a filter cake can improve the collection efficiency but induces a significant increase of the pressure drop leading to higher energy consumptions. Thus, particle removal is commonly used in membranes to ensure optimal filtration.
- In biology, removal of bioparticles is widely studied, for instance in the field of biocolloid contamination and retention in porous media (e.g. viruses, bacteria and protozoa) [20,21] or in biofilm formation [22].
- Studies have also investigated removal of explosive particles and TNT-polymer composite particles from fingerprints [23] and clothes [24] or surfaces [25].

From this quick overview, it is seen that resuspension can take place in numerous environments and, also, that it can involve particles with different properties (size, nature, etc.) as well as a wide range of scales. Furthermore, an additional challenge comes from the multidisciplinary aspect of the overall phenomenon: indeed, resuspension contains issues related to fields as different as fluid dynamics (particle–fluid interactions), interface chemistry (particle–surface or particle–particle interactions), material physics (surface roughness and other heterogeneities), solid mechanics (surface deformation), physics of granular matter (morphology of resuspended materials, forces and energy propagation within these materials) and biology (in the case of bioparticles). This multidisciplinary nature as well as the various industrial/environmental applications gives a clue as to why resuspension still remains the object of ongoing investigations.

Clearly, the general question of resuspension is extremely diverse and classifications are needed. To start with, a distinction between three categories of materials can be proposed [26,27]: particulate (by solid particles), organic (by organic species), biological (accumulation of biological organisms) materials. In the present paper, we have chosen to focus our attention on the resuspension phenomenon for solid particles. Yet, when relevant, we will still refer to some existing works on the resuspension of biological or organic materials in order to underline similarities in the mechanisms/physics at play in resuspension (here in the more general sense).

1.2. Guidelines for particle resuspension

In the studies devoted to particle resuspension, the terminology varies often, depending on the point of view chosen in each article, and this can be a source of unnecessary confusion. Therefore, at this stage, it is worth giving the definitions of the important notions related to resuspension that will be used in the present article.

(def-1) Particle resuspension (or re-entrainment) refers to the removal of particles from surfaces after the break-up of the particle–surface contact/bond. Reentrained particles are thus suspended particles that are transported by the fluid (eventually in the vicinity of the surface).
(def-2) Particle detachment refers to the break-up of the particle–surface contact and can thus be only one part of the whole resuspension mechanism (for instance if particles move on the surface before being detached).
(def-3) Sticking (or deposited or adhering) particles correspond to particles that are in contact with the surface and that can be resuspended.
(def-4) Retention should not be mistaken with adhesion since it refers to matter being trapped in a media (without necessarily having adhesion to the media). Retention is often encountered in porous media [28].
(def-5) An aggregate is a group of particles in suspension forming a larger structure whereas a cluster is a group of particles deposited on a surface and forming a larger structure.
(def-6) Fragmentation, or de-agglomeration, corresponds to the separation of a large structure (for instance an agglomerate or a cluster) into several smaller ones.
(def-7) Particle bouncing on surfaces can occur when incoming particles have enough energy to bounce back into the flow [29]. In that sense, bouncing particles could be regarded as resuspended since the surface–particle contact has been disrupted. In the present study, we consider that particle bouncing does not correspond to particle resuspension since particles did not adhere first to the surface (but adhesion forces are still present and lead to a dissipation of the particle kinetic energy). Thus, we only consider resuspension as the removal of particles already sticking on a surface.
(def-8) Saltation occurs when large inertial particles (e.g. sand) are re-entrained from a surface but are too large to remain in suspension and thus hit again the surface later on [7]. Upon impacting the surface once again, these particles can lead to the resuspension of other materials present on the surface.
(def-9) Abrasion refers to the erosion of a surface by exposure to scraping or other mechanical constraints on the surface (e.g. by ice in clouds [30], bombardment of saltated particles [7,31]).

With respect to these definitions, the present paper is mainly concerned with the resuspension of particles from surfaces exposed to a (laminar or turbulent) flow. However, even within these limits, reviewing resuspension is not a straightforward task as a variety of different standpoints can be chosen. For example, some reviews have been recently released but in which resuspension was only discussed for specific cases, such as indoor resuspension [32]. In the present work, a more general point of view is retained: the mechanisms and physics of particle resuspension are analysed regardless of any specific application and the attempt made here is to underline their universal character.

1.3. Aim of the present review

The present review is focussed on putting forward recent advances on particle resuspension for both large inertial particles (such as sediments) and small colloidal particles (particles with a size ranging from a few nanometres up to a few micrometres, for which Brownian motion plays a predominant role). These advances gather new insights into the physical mechanism at play as well as new developments in modelling approaches. More specifically, the main objectives are.

(i) To emphasise the fact that particle resuspension depends on a coupling between three major physical interactions: particle–fluid, particle–surface and particle–particle

interactions (the latter one being mainly significant for multilayer resuspension).
(ii) To highlight the dependence of particle resuspension on geometrical factors such as the presence of surface heterogeneities or deposit morphologies.
(iii) To analyse the relative importance/role of these physical interactions and geometrical factors in particle resuspension.
(iii) To provide an in-depth discussion of the various modelling approaches proposed in the literature for monolayer particle resuspension and to propose a unified modelling framework to address that situation.
(iv) To underline the open issues related to multilayer resuspension and the intricate coupling between particle deposition and resuspension.

In many practical situations, particle resuspension is closely related to particle deposition as the net flux of deposited particles on a surface results from the difference between the flux of particles being carried to the surface (deposition) and the flux of particles being carried away from the surface (resuspension). A recent comprehensive review on particle deposition has been proposed where the analysis in terms of the three major physical interactions mentioned in the point (i) above has been shown to be helpful to bring a much-clearer description of the processes involved [33]. The present review is a continuation of this first work and, with this companion paper [33], represents an effort to provide a complete picture of the general issue of particle interactions with walls (which involves, in particular, deposition and resuspension as key mechanisms).

1.4. Organisation of the present review

Within this scope, the paper is organised as follows. An overview of the key elements of the fundamental interactions is made in Section 2. A detailed review of the experimental works brings out the essential mechanisms at play for monolayer deposits in Section 3, with an emphasis on the new pictures that have emerged recently. Then, fundamental aspects of particle motion along walls and of the detailed steps involved in the mechanisms of particle resuspension are described in Section 4. The various modelling approaches that have been proposed to simulate particle resuspension from monolayers are addressed in Section 5, where a new classification and a discussion on the importance of a unified modelling framework are developed. Finally, the present paper proposes in Section 6 a discussion on the open issues of multilayer resuspension. In Section 7, the conclusion sums up the key elements of particle resuspension that have been brought forth and the open issues that remain to be tackled are discussed.

2. Overview of the fundamental interactions

The aim of this section is to provide an introduction to the main aspects of the fundamental interactions (particle–fluid, particle–surface and particle–particle) which constitute one of the guidelines of the present review. As each of these aspects would require a monograph should comprehensive descriptions be expected, we limit ourselves to presenting the central points of the theoretical formulations underlying these interactions. A first account of surface heterogeneities, which bring important modifications for particle–surface and particle–particle interactions and have a key role in resuspension, is also presented. In that respect, the important notions, such as the particle relaxation timescale, the characteristic features of turbulent boundary layers and the DLVO theory, are introduced here as they are helpful to discuss experimental data in Section 3. The specific aspects related to the expressions of the forces and moments exerted on deposited particles and to surface roughness effects are developed in more details later on in Section 4.

Layout of this section. The salient points of particle transport are outlined in Section 2.1.1 which introduces the central notion of the particle relaxation timescale before a presentation of turbulent boundary layers and near-wall units in Section 2.1.2 and an introduction to the idea of coherent structures in Section 2.1.3. Particle–surface interactions are discussed in the frame of the DLVO theory in Section 2.2 while particle–particle interactions are addressed in Section 2.3. Finally, surface heterogeneities, especially surface roughness, are introduced in Section 2.4.

2.1. Particle–fluid interactions

2.1.1. Particle transport and the particle relaxation time scale

For particle-laden flows, particle transport is best presented by adopting a Lagrangian point of view. Then, particle transport results naturally from the action of the forces acting on each particle and which enter the particle momentum equation as

$$\frac{\mathrm{d}\mathbf{x}_\mathrm{p}}{\mathrm{d}t} = \mathbf{U}_\mathrm{p}, \tag{1a}$$

$$m_\mathrm{p}\frac{\mathrm{d}\mathbf{U}_\mathrm{p}}{\mathrm{d}t} = \mathbf{F}_{\mathrm{f}\to\mathrm{p}} + \mathbf{F}_\mathrm{ext} \tag{1b}$$

where $\mathbf{x}_\mathrm{p}$ is the location of the particle centre of mass, $\mathbf{U}_\mathrm{p}$ its velocity and m_p the mass of the particle. In the momentum equation Eq. (1b), $\mathbf{F}_{\mathrm{f}\to\mathrm{p}}$ represents the forces of the fluid on the particle while $\mathbf{F}_\mathrm{ext}$ stands for the action of external fields such as gravity. In the description of the particle dynamics, the first equation, Eq. (1a), is not to be overlooked as it indicates that particle transport (which is treated without approximation by Lagrangian approaches [34,35] is indeed directly related to the effects of the forces exerted on the particle. Thus, this question amounts to the formulation of the forces exerted on a particle in a surrounding fluid flow (the situation of a particle located at the wall and only partially surrounded by the fluid flow is a limit case and is specifically addressed in Section 4.1.1). Though apparently simple and considered as soon as the mid-19th century, the issue of the precise derivation of the various forces exerted on a particle due to a fluid flow has proved extremely difficult. Present formulations retain the so-called drag, lift, added-mass and Basset forces [36,37] which are added to gravity forces, though the expression of these forces can vary according to different authors. In this section, we leave out the lift force which is discussed in Section 4.1.1 for deposited particles and we neglect the Basset (or historical) force. Then, the present consensus about the forces acting on a particle in a fluid flow means that the particle momentum equation can be written as

$$m_\mathrm{p}\frac{\mathrm{d}\mathbf{U}_\mathrm{p}}{\mathrm{d}t} = \frac{\pi d_\mathrm{p}^3}{6}\rho_\mathrm{f}\frac{\mathrm{D}\mathbf{U}_\mathrm{s}}{\mathrm{D}t} + \frac{\pi d_\mathrm{p}^3}{6}\left(\rho_\mathrm{p}-\rho_\mathrm{f}\right)\mathbf{g} + \frac{1}{2}\frac{\pi d_\mathrm{p}^2}{4}\rho_\mathrm{f}C_\mathrm{D}|\mathbf{U}_\mathrm{s}-\mathbf{U}_\mathrm{p}| \times (\mathbf{U}_\mathrm{s}-\mathbf{U}_\mathrm{p}) + \frac{\pi d_\mathrm{p}^3}{6}C_\mathrm{A}\rho_\mathrm{f}\left(\frac{\mathrm{D}\mathbf{U}_\mathrm{s}}{\mathrm{D}t}-\frac{\mathrm{d}\mathbf{U}_\mathrm{p}}{\mathrm{d}t}\right) \tag{2}$$

where ρ_f is the fluid density, ρ_p the particle density, d_p its diameter and $\mathbf{U}_\mathrm{s}$ the velocity of the fluid seen by particles as they move across the fluid flow. Relying on a point-approximation for particles, this velocity of the fluid seen is expressed as the local instantaneous value of the fluid velocity at the same time and at the particle position, which means that we have $\mathbf{U}_\mathrm{s}(t) = \mathbf{U}_\mathrm{f}(t,\mathbf{x}_\mathrm{p}(t))$ where $\mathbf{U}_\mathrm{f}(t,\mathbf{x})$ represents the fluid velocity field. In Eq. (2), the first two terms on the rhs (right-hand side) correspond to the fluid acceleration and to the buoyancy term while the third term is the general form for the

drag force, involving the drag coefficient C_D, and the fourth term is the added-mass force. The added-mass force is expressed with an added-mass coefficient C_A (usually taken simply as $C_A = 1/2$) and is a function of the difference between the acceleration of the fluid seen (along its own trajectory) and the particle acceleration. Note that the drag force is expressed in terms of the velocity slip $\mathbf{U}_r = \mathbf{U}_s - \mathbf{U}_p$ while the added-mass force is written as a function of the acceleration slip.

The added-mass force can be of importance for example for small sediments in a liquid medium when $\rho_p \sim \rho_f$. However, for particles heavier than the fluid $\rho_p \gg \rho_f$, it can be shown that the drag force is the dominant force [35–37] and the particle momentum equation is then reduced to

$$\frac{d\mathbf{U}_p}{dt} = \frac{\mathbf{U}_s - \mathbf{U}_p}{\tau_p} + \mathbf{g}. \tag{3}$$

where the drag force has been written so as to bring out the particle relaxation timescale τ_p which is given by

$$\tau_p = \frac{\rho_p}{\rho_f} \frac{4d_p}{3C_D|\mathbf{U}_r|}. \tag{4}$$

This timescale is the key notion for particle transport and accounts for the particle inertia. More precisely, τ_p stands for the timescale over which particle velocities adjust to the local fluid velocity seen. Precise expressions for the drag coefficient are discussed later on in Section 4.1.1. As an illustration of existing drag force expressions, it is sufficient here to introduce the drag force in the Stokes regime, where $C_D = 24/\mathrm{Re}_p$ (with $Re_p = |\mathbf{U}_r| d_p/\nu_f$ the particle Reynolds number and ν_f the fluid kinematic viscosity). The Stokes regime is valid when $\mathrm{Re}_p \leq 1$ and is often a good approximation for small particles. In that case, the drag force retrieves the classical form where $\mathbf{F}^{\mathrm{Drag}}_{f\to p} = 3\pi\rho_f\nu_f d_p \mathbf{U}_r$ and the particle relaxation timescale is then given by the well-known expression

$$\tau_p = \frac{\rho_p}{\rho_f} \frac{d_p^2}{18\nu_f}. \tag{5}$$

It can be noted that, if the added-mass force is deemed important, the notion of the particle relaxation timescale still holds and simple manipulations of Eq. (2) show that the expression of τ_p is slightly modified to give (still in the Stokes regime)

$$\tau_p = \left(\frac{\rho_p + 1/2\rho_f}{\rho_f}\right) \frac{d_p^2}{18\nu_f}. \tag{6}$$

The above considerations have been developed for hydrodynamical effects, assuming that particles are not sensitive to Brownian motion. Yet, for colloidal particles, this is not the case anymore and it is important to account for Brownian effects in the particle dynamics. This is simply done by adding a white-noise term to the particle momentum equation, which becomes a generalisation of the historical Langevin equation, and the system of equations (retaining only the drag force, for the sake of simplicity) has the following form

$$d\mathbf{x}_p(t) = \mathbf{U}_p(t)\, dt \tag{7a}$$

$$d\mathbf{U}_p(t) = \frac{\mathbf{U}_s(t) - \mathbf{U}_p(t)}{\tau_p} dt + \mathbf{g}\, dt + K_{Br}\, d\mathbf{W}(t) \tag{7b}$$

In the particle momentum equation, which is now a stochastic differential equation, the diffusion coefficient K_{Br} is given by $K_{Br} = \sqrt{(2k_B T_f)/(m_p \tau_p)}$ where k_B is the Boltzmann constant and T_f the fluid temperature. This form of the particle momentum equation is the most general expression and is valid for both inertial particles (for which K_{Br} becomes negligible) and colloidal particles (for which gravity becomes negligible). More details can be found in [33]. In the context of particle deposition and resuspension, we are basically interested in particle motion in the near-wall region which corresponds to a specific region referred to as the (possibly turbulent) boundary layer whose properties need to be given.

2.1.2. Turbulent boundary layers and near-wall units

In the following, we consider the basic situation of a channel flow with an axis representation sketched in Fig. 1(a). Classical analysis of a fluid flow in the fully developed region (where velocity statistics no longer change with x) indicates that the balance of mean forces in the wall-normal direction is characterised by the wall shear stress τ_w (see a detailed presentation in the reference textbook on turbulent flows [38]. The wall shear stress can be expressed by $\tau_w = \rho_f \nu_f (d\langle U_f\rangle/dy)_{y=0}$ where $\langle U_f\rangle$ is the mean fluid longitudinal velocity.

To characterise the near-wall region, it is relevant to introduce the so-called wall units, which are derived from the wall shear stress τ_w and the kinematic viscosity ν_f. First of all, a friction velocity u_τ is defined from the wall shear stress and the fluid density as $u_\tau = \sqrt{\tau_w/\rho_f}$. Based on this friction velocity u_τ (in ms^{-1}) and on the fluid viscosity ν_f (in $\mathrm{m}^2\,\mathrm{s}^{-1}$), a length scale δ_ν and a time scale τ_ν can be defined as:

$$\delta_\nu = \frac{\nu_f}{u_\tau}, \quad \tau_\nu = \frac{\nu_f}{u_\tau^2} \tag{8}$$

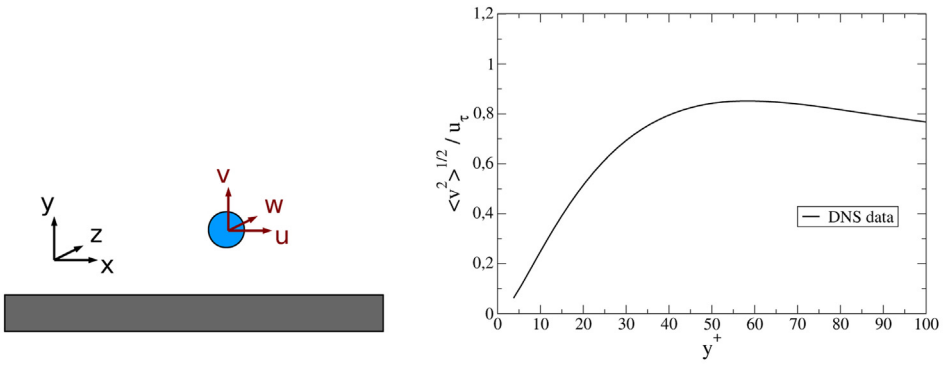

(a) Sketch of the axes used in the near-wall regions

(b) DNS results for the wall-normal fluid kinetic energy $< v^2 >$ in the near-wall region

Fig. 1. Quantities in the near-wall region. Reprinted from [33]. Copyright 2012 with permission from Elsevier.

Then, dimensionless quantities are introduced, such as the dimensionless distance from the wall $y^+ = y/\delta_\nu$ or the dimensionless near-wall velocity $\mathbf{U}_f^+ = \mathbf{U}_f/u_\tau$. For particle transport, this means also that we can define the non-dimensional particle relaxation timescale as $\tau_p^+ = \tau_p u_\tau^2/\nu_f$. Obviously, the viscosity ν_f is fluid-dependent while the friction velocity u_τ is flow-dependent and the behaviour of fluid velocity statistics are thus fluid and flow dependent. However, the key result is that, once properly made non-dimensional, all quantities follow universal laws (referred to as the "law of the wall") in the near-wall region for arbitrary large Reynolds numbers [38].

In particular, this allows to define the viscous sublayer where viscous effects are dominant: this zone is usually taken as the sublayer starting at the wall with a thickness of about $\delta_{VS}^+ \sim 5$ (or, somewhat more loosely, as $\delta_{VS}^+ \sim 5-10$ when no buffer layer is considered between the viscous and logarithmic layers) and where the mean longitudinal velocity scales as $\langle U_f^+ \rangle \simeq y^+$. In the same way, the well-know logarithmic region (or log law region) can be isolated as the part of the inner layer where viscosity does not play a role and where the mean longitudinal velocity scales as $\langle U_f^+ \rangle \simeq 1/\kappa \ln[y^+] + B$ where B is a constant and κ the von Karman constant. The thickness of the boundary layer is defined as the distance to the wall where the wall unit scaling overlap with the outer layer scaling (the bulk of the flow). The precise evaluation of this distance remains somewhat arbitrary (or dependent on the Reynolds number [38]). Yet, in practise, the thickness of the turbulent boundary layer in the near-wall region can be estimated as being of the order of $l_{BL} \approx 100-200\delta_\nu$.

These variations of the fluid mean longitudinal velocity are important in the context of particle resuspension as they are typically used in the expression of the drag force as well as in the moment of the hydrodynamical forces exerted on a deposited particle (these issues are addressed in Section 4.1.1). Another characteristic and noteworthy feature concerns the second-order moments of the fluid velocity ($\langle \mathbf{u}^2 \rangle$) which exhibit strong variations through the boundary layer and a marked anisotropy [38,39]. This is true in particular for the wall-normal fluid kinetic energy $\langle v^2 \rangle$ (see Fig. 1(b)) which is the particle driving force that induces the particle flux towards the wall (since there is no transport due to the mean wall-normal fluid velocity given that $\langle V \rangle = 0$ [38]). On the other hand, in the immediate vicinity of the wall (thus, in the viscous sublayer), velocity fluctuations remain small but with a stronger increase of the longitudinal fluctuating energy $\langle u^2 \rangle$ (which scales as y^2) compared to the wall-normal one (which scales as y^4). The damped fluctuations in the wall-normal direction mean that direct lift-off forces will be reduced (apart from intense but rare 'events') and the importance of the longitudinal fluctuations over the fluctuations in the normal direction suggests also that particle motion along the wall surface will be triggered with more likelihood than a direct pull-off. These questions are at the core of the resuspension mechanisms and will be developed in the next sections, particularly in Section 4 and in Section 5.

2.1.3. Near-wall coherent structures

With the introduction of the near-wall units, turbulent boundary layers are usually characterised by bringing out the profiles of velocity statistics in terms of the normalised wall-normal distance y^+. In addition to this statistical assessment of near-wall fluid motions, new information has been provided by fine experimental observations [40,41] as well as by results from Direct Numerical Simulations (DNS) [42,43]. Both have paved the way for a new vision of turbulent boundary layers.

Indeed, the classical statistical approach provides information typically on the first (one-point) velocity moments and, less often, on two-point velocity correlations (through measurements). Though correct, these statistical assessments do not reveal the instantaneous realisations, or 'pictures', of the velocity field in the near-wall region. In that sense, it would be misleading to imagine the reality of the velocity field as, for example, a Gaussian noise around the mean velocity profiles. Indeed, direct experimental visualisations have revealed that boundary layers are made up by the random succession of fluid 'coherent structures', which can be loosely defined as regions of the fluid exhibiting a certain order in space and time (see the illustration in Fig. 2). In that respect, DNS has proved itself to be a valuable approach as turbulent boundary layers are very thin layers where experimental measurements are therefore difficult to carry out precisely. If we regard a DNS as a 'numerical experiment' that complements experimental measurements (and give access to variables difficult to measure such as the turbulent kinetic energy dissipation rate), more precise descriptions of coherent structures in turbulent boundary layers have emerged.

In practise, a quantitative and universal definition of these coherent structures has proved difficult [38]. Nevertheless, the concept introduces new interesting aspects and has allowed, in particular, new insights into the physics of particle transport in near-wall regions. Indeed, recent analyses carried out using particle tracking in DNS [44–46] have highlighted the key role played by fluid structures for particle transport. As displayed in Fig. 2, these studies have revealed that particles moving towards the wall tend

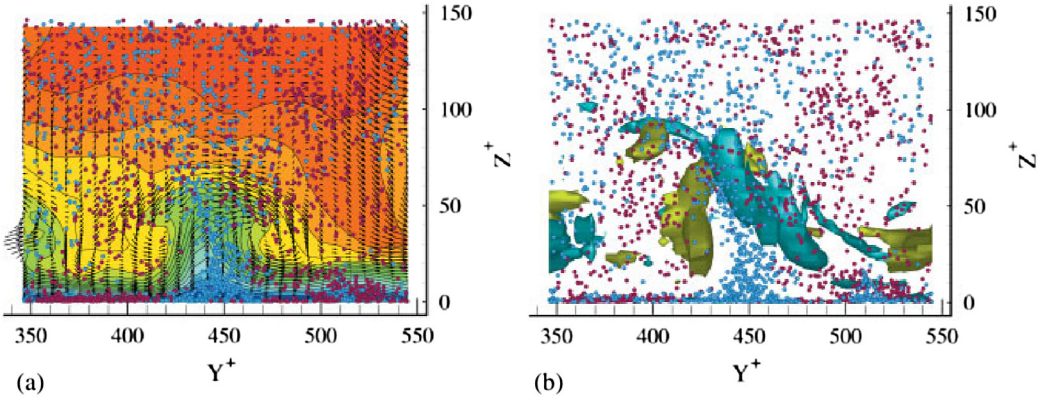

Fig. 2. Cross-section of the flow field and front view of particles in the near-wall region (a) and front view of particles and structures in the near-wall region (b) [46]. Vectors represent the fluid velocity, and colour isocontours map the values of the streamwise velocity component (left figure). Green isosurface identify counter-clockwise rotating vortices while pale blue isosurfaces identify clockwise rotating vortices (right figure). Purple particles have a wall-normal velocity oriented towards the wall while blue particles have a wall-normal velocity oriented away from the wall. Reprinted from [46]. Copyright 2009 with permission from Elsevier.

to be correlated with a fluid coherent structure called 'sweep' (spatially-coherent fluid motion with a velocity directed towards the wall) while particles moving away from the wall tend to be correlated with a fluid structure called 'ejection' (spatially-coherent fluid motion with velocity directed towards the bulk of the flow). Furthermore, local particle concentrations, referred to as the preferential concentration effect, have been linked with the existence of low-speed streaks where particles tend to be trapped [42,46,47]. Clearly, these DNS simulations have demonstrated that analyses based on near-wall fluid coherent structures are relevant, especially to understand fine details of particle dynamics in turbulent boundary layers. Recently, models for particle deposition have started to follow that path by developing stochastic descriptions where particles are transported as the result of their interactions with a random succession of modelled coherent structures [48] (details and illustrations of such modelling approaches can be found in Ref. [33]).

In the following, we will simply refer to fluid coherent structures as a spatially-coherent motion which exist for some time: these structures are thus first defined by some typical features (for instance, for sweeps and ejections by their velocity sign with respect to the wall-normal direction or by a quadrant analysis) and are characterised by a timescale (which measures their lifetime), a length scale and, more importantly, a velocity scale (which defines their intensity). More elaborate definitions can be found in the specialised literature which has developed for near-wall coherent structures (see Refs. [38,39,44,46,49–51]). It will be seen in Section 3, and especially in Section 3.1, that these notions are important to distinguish between the various mechanisms involved in particle resuspension.

2.2. Particle–surface interactions

When particles are in the immediate vicinity of a wall surface (i.e. for separation distances lower than a few tens of nanometres), the magnitude of particle–surface interactions is comparable to, or even greater than, particle–fluid interactions. These particle–surface interactions are traditionally described using the DLVO theory - named after the works of Derjaguin–Landau [52] and Verwey–Overbeek [53] – which considers that interbody interactions are the sum of the van der Waals (VDW) interaction and of the Electrostatic Double-Layer (EDL) interaction [54–56]:

- VDW forces are volume forces arising from dipole-dipole interactions (more details can be found in [33,54,55,57,58]). Apart from some exceptional situations, it is important to note that VDW forces are attractive forces.
- EDL forces occur between two charged bodies immersed in a liquid [56]. In that case, a double-layer is spontaneously formed around each body due to the electrostatic affinity of ions (the concentration of counterions close to the surface is higher). The overlap of two double-layers upon particle–surface encounter leads either to attractive EDL forces for oppositely charged surfaces or repulsive EDL forces for similarly charged surfaces (more details in [33,54,55,57,59,60]).

There is an ample literature devoted to particle–surface interactions, especially for colloids for which these forces are indeed important, with references textbooks [54,56] and recent reviews [33,55]. In the context of this chapter, it is sufficient to bring out the key aspects which are relevant for the later discussions on the resuspension mechanisms. This can be best done by considering a simple formulation for the DLVO force between a perfectly spherical particle and a perfectly smooth plane which is given by

$$F_{\mathrm{DLVO}} = -\frac{A_{\mathrm{H}} R_{\mathrm{part}}}{6h^2} + 4\pi\varepsilon_0\varepsilon_{\mathrm{r}}\phi_{\mathrm{p}}\phi_{\mathrm{w}}R_{\mathrm{part}}\kappa\,\exp(-h\kappa) \tag{9}$$

where h represents the distance between the two surfaces (in terms of the distance of the centre of the particle to the wall surface d, we have $h = d - R_{\mathrm{part}}$ with R_{part} the particle radius). The first term on the rhs of Eq. (9) is the VDW force and is expressed with the so-called Hamaker constant A_{H} (in J). The second term on the rhs corresponds to the EDL contributions (note that both forces, VDW and EDL, derive from a potential) and is expressed as an exponentially decaying function of the distance to the surface h divided by the Debye length κ^{-1}. This Debye length is defined by

$$\kappa^{-1} = \sqrt{\frac{\varepsilon_0\varepsilon_r k_{\mathrm{B}} T_{\mathrm{f}}}{2e^2\, I}} \tag{10}$$

where ε_0 is the dielectric permittivity of vacuum (in $\mathrm{F.m^{-1}}$), ε_{r} the dielectric constant of the liquid medium, k_{B} the Boltzmann constant (in $\mathrm{J.K^{-1}}$), T_{f} the fluid temperature (in K), e the electron charge (in C) and I_{IS} the solution ionic strength (which is a measure of the ion concentration in the solution). The EDL force involves also the particle potentials ϕ_{p} and of the surface potential ϕ_{w} (often taken as the zeta potentials, in V).

More elaborated formulas of the DLVO force than the one retained in Eq. (9) are available in the references mentioned above but the interest of this expression is to reveal the most important features. It is seen that the form of the EDL contribution explains that the Debye length is usually referred to as the 'screening length' since it is the length scale above which the electrostatic double-layer interactions are screened and become negligible. An interesting point is that the VDW does not depend on the liquid pH and is the only contribution for particles in a gas flow. On the other hand, the expression of the EDL force shows that there are separate contributions from typically the zeta potentials, the ionic strength and the Debye length which are all functions of the pH of the liquid. This explains that the influence of particle–surface interactions is discussed with reference to the DLVO theory and, in particular, by considering the specific influences of these quantities (zeta potential, ionic strength, etc.) as will be done in Section 3.2.

Further understanding is brought by considering a typical evolution of the DLVO potential energy with the separation distance between a 1 μm particle and a plate in repulsive electrostatic conditions, as displayed in Fig. 3. It can be seen that the VDW attraction is predominant at small separation distances and large separation distances, while the EDL repulsion dominates the interaction energy at intermediate separations. The peak in the DLVO curve corresponds to the so-called *energy barrier* E_{barr}, which can prevent incoming particles from reaching the surface.

In the context of particle deposition, this energy barrier appears as a useful notion to predict whether incoming particles (due to hydrodynamical particle transport in the near-wall region) can actually deposit (when their kinetic energy is high enough to overcome the energy barrier) or will bounce back from the wall surface. In terms of the hydrodynamical near-wall units introduced in Section 2.1.2, the location of the energy barrier y^+_{EB} is typically of the order of $y^+_{\mathrm{EB}} \sim 10^{-2} - 10^{-3}$ which means that the particle–surface interactions, though essential, take place in a nearly-vanishing region (with respect to the hydrodynamical length scale in the boundary layer) and is best treated as a boundary condition. Yet, taking into account the central notion of the energy barrier allows to build a formulation where particle transport and particle–surface interactions are intimately coupled so as to obtain a complete and consistent description of particle deposition (see a detailed presentation of this approach in [33]).

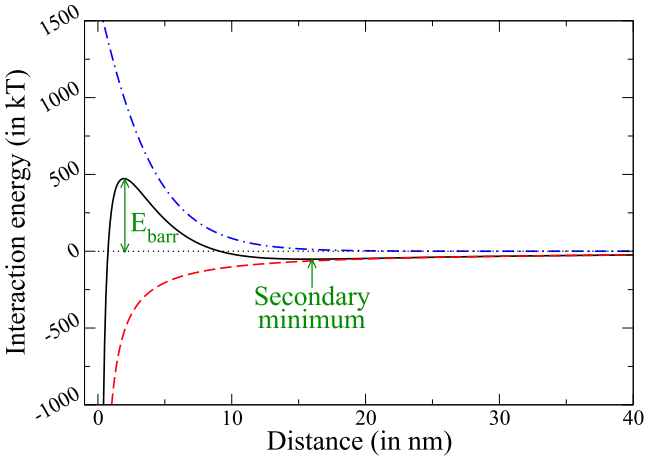

Fig. 3. DLVO interaction energy between a sphere and a plate: – – VDW interaction energy, · – EDL interaction energy, — DLVO interaction energy. Reprinted from [33]. Copyright 2012 with permission from Elsevier.

So far, the DLVO force has been presented typically for a particle close to a wall surface but still within the fluid (so that $h > 0$). From the example considered in Fig. 3, it is also seen that particles which overcome the energy barrier fall in the potential well of the VDW contribution and that the resulting attractive force appears to become infinite at the particle–surface contact. As such, DLVO forces can seem inappropriate to predict adhesion forces. Yet, by introducing a contact distance (related to the Bohr repulsion), it will be seen that DLVO can still be applied for adhesion forces, which represents a strong advantage as the same expression can then be used both for particles approaching the wall and for particles in contact with this wall surface. This point is taken up and addressed in detail in the discussion of contact theories developed in Section 4.1.2.

As reviewed recently by Liang et al. [55], the DLVO theory can sometimes fail to predict the interaction energy at nanoscale separation distances. Therefore, in some specific situations, extended-DLVO theories have been proposed to account for additional forces (such as solvation forces, acid-base interactions, steric or capillary forces [33,55,56]). However, it should be borne in mind that such extended-DLVO theories depend highly on the situations considered (for example, capillary forces occur only when particles deposit in humid environments). These extensions are also considered at the end of Section 4.1.2.

To sum up, the DLVO theory remains a reference for particle–surface forces and, apart from particular situations that need to be addressed specifically and on a case-to-case basis, it can be considered that the DLVO theory provides a satisfactory framework for particle–surface interactions.

2.3. Particle–particle interactions

The occurrence of particle–particle interactions in a particle-laden flow is closely related to particle concentration. Indeed, when the particle concentration is low (which means that we are considering a dilute flow regime), particle–particle interactions are rare events which do not play a significant role in the overall picture of the particle fundamental interactions. However, when the particle concentration increases, particle–particle interactions happen more often and start to have an impact. For instance, in concentrated particle suspensions, it is common to observe particle agglomeration, i.e. the formation of an aggregate due to the collision of pair of particles that can stick together and form a larger 'particle' whose inertia and, consequently, dynamics are modified. Similarly, particle–particle interactions are predominant when surfaces are covered by particles: in that case, multilayers of particles are formed on the surface. In the analysis of the formation of multilayer deposits, it has been shown recently that these particle–particle interactions play a central role and that, by properly accounting for them, the various structures of multilayer deposits that have been observed can be correctly predicted [33].

Although it is important to introduce particle–particle interactions separately from particle–surface ones, the expression of these forces is often done through the same DLVO theory, typically by substituting a sphere-sphere geometry to the sphere-plate one considered in Section 2.2. This is also helpful to reveal that particle–particle interactions have a similar double nature as particle–surface ones. Indeed, particle–surface interactions involve first an hydrodynamical step (called the 'transport step' [33]) and an interface chemistry step (called the 'adhesion step' [33]). In the same manner, particle–particle interactions involve also a similar hydrodynamical step where particles are brought together by the underlying action of a turbulent fluid (this is the 'collision step') and another interface chemistry step (which can be called the 'agglomeration step'). This decomposition is the basis of recent fine-grained modelling approaches of agglomeration [61–63] and of more classical and more macroscopic population-balance approaches [54,56,64,65]. In the context of the present section which is an introduction to the main notions of the fundamental interactions, this means that the characteristics features of DLVO forces, as discussed in the Section 2.2, remain valid. In particular, since particles are usually charged accordingly (unless separately-charged particles are introduced in a solution), the particle–particle EDL contribution to the DLVO forces leads typically to a repulsive term. Thus, the notion of an energy barrier is particularly relevant for particle–particle interactions.

2.4. The role of surface heterogeneities

Particle–particle as well as particle–surface interactions have been shown to depend also on local heterogeneities on the surface, such as surface roughness or surface charge heterogeneities [57]. Consequently, numerous approaches have been proposed to account either for surface roughness [66–72] or surface charge heterogeneities [73–78] (or even both). Given the central role played by surface roughness in the resuspension mechanism, it is worth introducing the characteristics of surface heterogeneities by considering how they are accounted for in some modelling approaches.

2.4.1. Surface roughness

As far as modelling of surface roughness is concerned, a distinction between two different approaches for surface roughness can be made:

(a) Modified Derjaguin approaches [66] propose a simple model in which surface roughness is described as a collection of hemispherical asperities on a smooth surface. Thus, surface roughness is represented by at least two parameters: the asperity height (or radius) and the number of asperities per unit area (or the surface coverage fraction S_{cov}). The overall interaction energy between a rough plate and a sphere U_{SR} is obtained by assuming that the interaction energies are additive and is thus given by the weighted sum of the sphere–plate interaction U_{SP} and of all sphere-asperity interactions U_{SA}:

$$U_{SR} = (1 - S_{cov})U_{SP} + \sum_{\text{asperities}} U_{SA} \quad (11)$$

The various models available in the literature differ from each other in the description of surface roughness (including or not polydispersion, with a single asperity or multiple asperities, etc.) and in the formulas retained for the calculation of VDW and EDL interactions [66,69,70,79]. For instance, a recent stochastic model based on this approach describes rough surfaces by a collection of hemispherical asperities placed randomly on the surface (more precisely within the region where particle-asperity are significant) respecting the distribution in asperity size and the surface coverage (see Fig. 4).

Statistical information on the effect of surface roughness on the energy barrier is then obtained by performing Monte Carlo simulations [79].

(b) Surface Element Integration (SEI) methods have been developed recently by Bhattacharjee et al. [68,80,81]. This method consists of calculating the energy barrier by integrating the interaction energy per unit area between two infinite half-space over the exact surface topography (that is obtained by experimental measurements), as depicted in Fig. 5. SEI methods are thus similar to the Derjaguin integration method, except that no assumption is made on the curvature radius of the bodies (that have to be much larger than the separation distance in the Derjaguin integration method).
The main advantage of the SEI method is that it can be applied accurately to any geometry. For instance, the SEI method has been shown to provide accurate predictions between a spheroidal particle and a flat plate [82] or for spherical particles in cylindrical pores [83].

This representation of surface roughness has been addressed here mostly in the context of particle deposition that is for particles approaching a wall (see Fig. 4) since surface roughness modifies the energy barrier and the resulting deposition rate [33]. Yet, most of the characteristics presented above remain important, if not central, for the resuspension phenomenon. Their effects are already present in experimental studies (see Section 3) and complementary accounts of surface roughness will be detailed in Section 4.1.2 in the context of adhesion forces (which can be slightly more complicated due to the possible inclusion of surface deformation). It will then be seen that the role of surface roughness is at the core of the discussions, developed in Section 5, about the existing modelling approaches.

2.4.2. *Surface charge heterogeneities*

Similarly to surface roughness, two modelling approaches have been proposed in the literature to include surface charge heterogeneities in the DLVO interaction. A simplified model (which is accurate, provided that the potential patches are much larger than the particle size) describes the interaction between heterogeneously charged surfaces as the interaction energy between surfaces having a constant charge/potential whose value is given by the potential of the surfaces facing each others [73,76,84,85]. Another refined approach (similar to the SEI approach) proposes to evaluate the interaction energy by integrating numerically the interaction energy per unit area between two-infinite flat plates over the exact surface topography and with the corresponding local surface potential [75,77,78,86,87]. The issue of surface charge heterogeneities is taken up again, with more details, in Section 4.1.2.

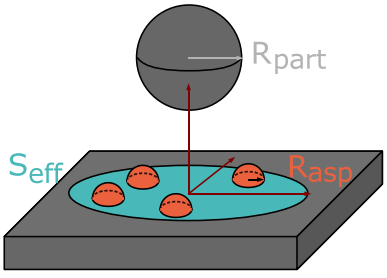

Fig. 4. Description of surface roughness using hemispherical asperities placed randomly underneath each incoming particle. Reprinted from [79]. Copyright 2011 with permission from American Chemical Society.

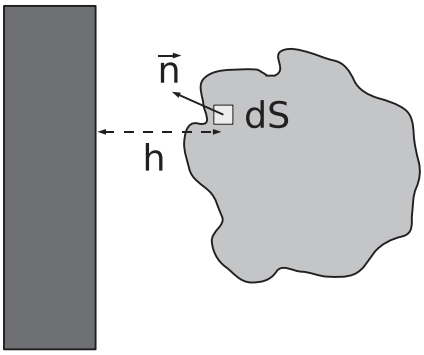

Fig. 5. Schematic representation of the SEI method applied to a sphere–plate interaction: the interaction energy (over each surface element dS) is integrated numerically over the exact surface topography.

3. Experimental studies of resuspension from monolayer deposits

This section is devoted to the description and analysis of experimental studies of particle resuspension from monolayer deposits while the case of resuspension from multilayer deposits will be treated later in Section 6. Monolayer resuspension has been extensively studied in the literature (see for instance previous reviews on the topic [1,32,88,89]) since it represents the first step towards an understanding of the whole resuspension phenomenon (both monolayer and multilayer). Yet, to provide a self-contained description, we have chosen to recall some existing experimental works on monolayer resuspension while emphasising how more recent works have extended our current understanding of this phenomenon. In particular, the various interactions at play in monolayer resuspension as well as their relative impact on particle reentrainment are underlined. Indeed, several experimental data have shown that particle–fluid interactions, particle–surface interactions as well as substrate heterogeneities have a significant impact on particle reentrainment [90–98]. However, the pictures emerging from these experimental data are not always clear, for example with respect to the role of sliding/rolling motion or burst-type ejections. In that sense, this section will not only report on recent experimental progress but will also put forward a new analysis which will be shown to be helpful to clarify the occurrence and importance of these mechanisms.

Layout of this section: This section is organised with respect to the various interactions at play in resuspension: the effect of particle–fluid interactions on resuspension is presented in Section 3.1, the role of particle–surface interactions is described in Section 3.2 while the impact of surface heterogeneities on resuspension is discussed in Section 3.3.

3.1. The role of particle–fluid interactions in resuspension

3.1.1. Particle–fluid interactions

The role of a fluid flow on particle resuspension has been studied experimentally for years. For instance, Hubbe in 1985 [90] measured the reentrainment of titanium dioxide colloids (with a size ranging from 144 nm up to 700 nm) immersed in a liquid solution from cellulose and glass substrates exposed for 60 s to a shear stress in coaxial cylinders. Particles adhering to an element of the surface were recorded using light scattering methods at various times corresponding to higher shear stresses τ_f. Typical images are displayed in Fig. 6 which shows that the number of particles adhering to a glass surface decreases when the shear stress is increasing. As displayed in Fig. 7, further analysis and a compilation of these images provided graphs for the evolution of the resuspension rate (or the fraction of particles remaining on the surface) with the flow conditions: it can be seen that the number of resuspended particles increases when the flow velocity is higher.

A large number of studies have used similar techniques to measure the amount of particles remaining on surfaces after exposure to a flow (see also previous reviews [1,88,89]). In this paper, we have chosen to make a distinction between experiments performed in rectangular channels (such as wind tunnels) where the flow is relatively simple and those performed in more complex flows (such as porous media or impinging jets). On the first hand, many experiments have focussed on particle resuspension in simple shear flows (see Table 1 for a list of such experiments in chronological order) since it is a relevant case in atmospheric resuspension (sand, sediments, dusts) and for resuspension in ventilation ducts. On the second hand, other experiments have investigated resuspension in more complex flows (see Table 2 for a list of such experiments in chronological order) in the context of resuspension from filtration systems (porous media) and walking-induced resuspension (with complex flow patterns close to the surface). It is worth noting that similar observations have been made regardless of the flow conditions. This was not a foregone conclusion especially in the case of porous media where complex flow and deposit structures can arise due to the intricate flow geometry.

From all these observations of particle resuspension in various flow conditions (see also previous reviews [1,88,89]), it appears clearly that the amount of resuspended particles increases with increasing fluid velocity (or shear stress) regardless of the flow conditions (either a flow over a smooth surface [112] or in porous media [108] or even an impinging jet on a surface [106]). As a result, a threshold velocity (or shear stress) for particle resuspension has often been defined as the velocity required to remove half of the particles initially deposited on the surface [102]. For example, Niño et al. [98] measured the resuspension of 704 nm TiO_2 particles from glass substrates exposed to a liquid flow in a rectangular channel. As displayed in Fig. 8, the threshold shear stress (here expressed as a dimensionless quantity $\tau^+ = u_\tau^2 \rho_f / (g d_p (\rho_p - \rho_f))$) has been characterised as a function of the particle Reynolds number $Re_p = u_\tau d_p / \nu_f$ (where u_τ is the friction velocity introduced in Section 2.1.2): it can be seen that resuspension increases when the particle size increases ($Re_p \nearrow$, $\tau_f^+ = \text{cte}$) and when the fluid velocity is higher ($Re_p \nearrow$, $\tau_f^+ \nearrow$). It can also be seen that recent experiments have confirmed the trends underlined in previous reviews while exploring in more details the effect of turbulence on particle resuspension.

3.1.2. Resuspension mechanisms

Yet, even though these experimental findings highlight the effect of particle–fluid interactions on the resuspension phenomenon, they fail to capture the detailed mechanisms that lead to particle resuspension. Therefore, similar measurement techniques have been developed to investigate the dynamics of particle resuspension, i.e. the evolution in time of reentrained particles [102]. For that purpose, high-speed video (or fast-image) recordings are often used to keep track of particle motion close to the surface in a rectangular channel or in centrifuge experiments (the mechanisms of resuspension have seldom been studied in porous media since direct observations of particle positions are intricate and require transparent media). However, the main difficulty that arises in analysing and summarising the mechanisms of particle resuspension is that experiments have been performed in various conditions and, in particular, the size of particles ranges from colloids up to millimetre sand particles.

Therefore, in the present review, we have chosen to analyse the mechanisms of particle resuspension in terms of the size of the particles involved. Broadly speaking, to characterise particles in boundary layers, two dimensionless parameters with respect to wall units can be obtained: the first one is the dimensionless particle relaxation time $\tau_p^+ = (d_p^2 u_\tau^2 / 18 \nu_f^2)(\rho_p / \rho_f)$ while the second one is the dimensionless particle size $d_p^+ = d_p u_\tau / \nu_f$. Since particle deposition is mainly governed by particle transport [33], deposition is generally studied using the particle relaxation time τ_p^+ as the main parameter. Yet, in the case of resuspension, hydrodynamic interactions acting on deposits depend on their size and d_p^+ can play a significant role. Thus, in the following, the dynamics and mechanisms of the resuspension phenomenon are analysed using the dimensionless particle size d_p^+ and comparing it to the extent of the viscous sublayer δ_{VS} (generally estimated as $\delta_{VS}^+ \sim 5 - 10$, as indicated in Section 2.1.2). This new analysis allows to clarify experimental evidence by dividing particles between 'small particles' (meaning that $d_p^+ \lesssim \delta_{VS}^+$) and 'large particles' (meaning that $d_p^+ \gtrsim \delta_{VS}^+$):

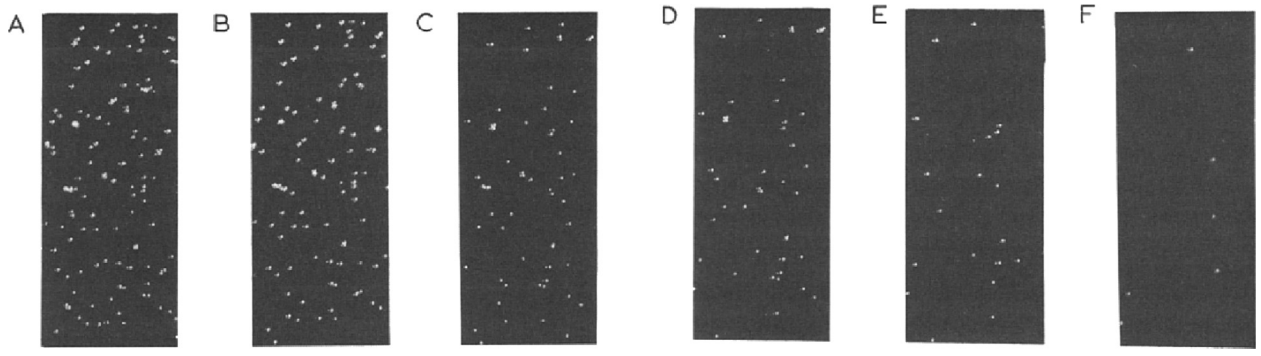

Fig. 6. Light scattering images of TiO_2 particles on glass substrates at pH 3 after 60 s exposure to a constant shear stress τ_f (with increasing increments): (A) initial population, (B) $\tau_f = 14.3$ Pa , (C) $\tau_f = 26.9$ Pa, (D) $\tau_f = 31.9$ Pa, (E) $\tau_f = 42.9$ Pa, (F) $\tau_f = 55.4$ Pa. Reprinted from [90]. Copyright 1985 with permission from Elsevier.

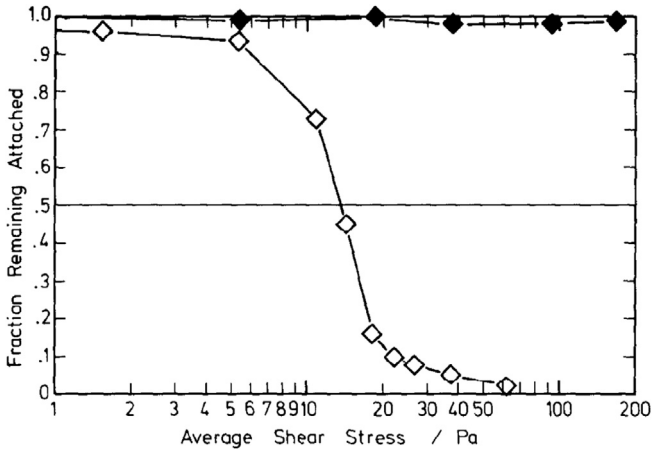

Fig. 7. Evolution of the fraction of TiO_2 particles remaining on the surface: ⋄ particles exposed to increasing shear stress and ◆ particles in absence of flow. Reprinted from [90]. Copyright 1985 with permission from Elsevier.

- For small particles (see also Table 3 for a list of experiments underlining the resuspension mechanism for small particles), particle motion is characterised by rolling or sliding motions on the surface. The first insights into the mechanism of particle resuspension have been obtained with experimental data measuring particle resuspension both in a channel flow and in centrifuge experiments [91,101,113,114]. In centrifuge experiments, particle removal in the wall-normal direction was found to be smaller than removal in the tangential direction. Moreover, no correlations between wall-normal centrifuge experiments and removal in fluid flow have been found. These observations have favoured the vision of a resuspension mechanism due to tangential forces that trigger resuspension at smaller velocities rather than by normal pull-off forces [101,113]. More recently, experimental data using video analysis have provided images of rolling particles and thus further confirmed previous experimental data with precise optical observations. For instance, Jiang et al. [115] measured the resuspension of 30 μm glass particles from stainless steel surfaces exposed to a turbulent airflow (70 ms^{-1}) in a rectangular channel using video techniques (this corresponds to a dimensionless diameter $d_p^+ \simeq 7$). Even for these particles whose diameters are at the high-limit of the present class of small particles, the snapshots of an entrained particle show that such particles are first rolling (or sliding) on the surface before being separated from the surface and reentrained in the fluid (see Fig. 9). This rolling/sliding motion has been further confirmed by other experiments in various hydrodynamic conditions (for example, in porous media [108], in wind tunnels [94,96]).
- Large particles (see also Table 4 for a list of experiments underlining the resuspension mechanism for large particles): the motion of particles whose size is large compared to wall units ($d_p^+ \gtrsim \delta_{VS}^+$) is characterised by 'burst-type' resuspension with a specific role played by coherent structures. The role of coherent structures in particle resuspension is thus due to the overlap of particles with the logarithmic sublayer (where such

Table 1
List of experiments that have studied the effect of particle–fluid interactions on monolayer resuspension in rectangular flows.

Experiment	Particles	Surface	Flow	Measurement technique	Main observations
Hubbe, 1985 [90]	TiO_2 colloids (144–700 nm)	Cellulose and glass	Turbulent fluid flow ($0.6 < \tau_f < 312$ Pa) in coaxial cylinders	Light scattering images	Increasing reentrainment with increasing shear stress
Hubbe, 1985 [91]	TiO_2 colloids (144–700 nm)	Glass	Shear flow (coaxial cylinder) and centrifuge (normal and transversal)	Light scattering images	Detachment governed by transversal forces, increasing detachment with increasing particle size and shear
Wu et al., 1992 [99]	Uranine, pollen, polymer, lycopodium (5 μm up to 42 μm)	Glass, plexiglass, leaves	Airflow in wind tunnel	Video analysis	Dependence of resuspension on particle size and air velocity
Meinders and Busscher, 1993 [100]	Polystyrene (736 μm)	Glass	Parallel-plate liquid flow chamber	Image analysis	Influence of shear rate on resuspension
Braaten, 1994 [101]	Lycopodium, glass, nickel, pollen (18–34 μm)	Glass	Centrifuge and airflow in wind tunnel	Microscope particle counting	Threshold velocity is inversely dependent to the particle diameter
Phares et al., 2000 [102]	Ammonium fluorescein (8.4–15.7 μm) and polystyrene (6.6–13.6 μm)	Glass	Laminar channel flow and impinging gas jet	Image analysis	Measurement of threshold shear stress for various sizes and velocities
Nino et al., 2003 [98]	Glass (38–94 μm) and silica sand (112–530 μm)	Glass	Liquid flow in a rectangular channel	High-speed video	Dependence of threshold velocity on the particle Reynolds number (increasing resuspension for larger particles or higher fluid velocities)
Ibrahim et al., 2003 [94]	Stainless steel, glass and lycopodium (25–77 μm) $d_p^+ \leq 4$	Glass	Turbulent airflow (0–23 m/s) in wind tunnel	Microvideo recording	Increasing resuspension with higher flow velocity
Ibrahim et al., 2004 [95]	Stainless steel (70 nm)	Glass	Turbulent airflow in wind tunnel	Microvideo recording	No effect of acceleration, higher threshold velocity for laminar than for turbulent flows
Mukai et al., 2009 [103]	Salt (1–20 μm)	Sheet metal, linoleum, carpet	Airflow in wind tunnel	Change in particle concentration	Higher removal for larger flow rate, higher turbulence intensity and larger particles
Wang et al., 2012 [104]	Calcium salt (0.4–10 μm)	Stainless steel	Airflow in ventilation duct	Changes in particle concentration	Higher release rate for high velocities and large particles

Table 2
List of experiments that have studied the effect of particle–fluid interactions on monolayer resuspension in more complex flows.

Experiment	Particles	Surface	Flow	Measurement technique	Main observations
Ryan and Gschwend, 1994 [105]	Hematite (150 nm)	Quartz grains	Liquid flow in packed bed column	Particle concentration derived from turbidity	Higher resuspension rate for increasing fluid velocity
Smedley et al., 1999 [106]	Polystyrene (8.3 μm)	Glass	Impinging gas jet (normal incidence)	Image analysis	Increase of resuspension with higher pressure
Smedley et al., 2001 [107]	Polystyrene (12 μm)	Glass	Impinging gas jet (oblique incidence)	Image analysis	Highest removal obtained for oblique incidence
Bergendahl and Grasso, 2000 [108]	Polystyrene latex (1.0 μm)	Glass bead	Liquid flow in porous media	Light scattering	Higher resuspension with increasing flow rate
Zhang et al., 2002 [109]	Glass (40–50 μm)	Steel	Impinging air jet (various incident angle)	Image processing	Dependence on air pressure and incident angle on resuspension
Fletcher et al. [24]	Monodispersed polymer spheres (1–45 μm)	Polycarbonate or cloth	Pulsed air or nitrogen jet (oblique incidence)	Optical images with particle counting	Increasing removal with larger flow rate and higher removal rate for large particles
Bedrikovetsky et al., 2012 [110]	2 μm particles	Sand stone bead	Liquid flow in porous media	Breakthrough curves and pressure drop	Release of particles due to abrupt increase of the flow rate
Young et al. [111]	Latex (31 μm)	Glass	Impinging air jet	Image analysis	Decreases of removal efficiency with distance from the nozzle (except at large distances due to dense versus sparse particle distributions)

coherent structures are more likely to occur) since particle sizes are then larger than the typical size of the viscous sublayer. This mechanism for particle resuspension was first proposed by Sutherland in 1967 [117] and, since then, has received several confirmations [116,118,119,120]. More recently, with the coupled use of both particle image velocimetry (PIV) and three-dimensional particle tracking velocimetry (3D-PTV), experimental data have been able to reveal the correlation between particle resuspension and high energy near-wall coherent structures, especially sweep and ejection events that tend to drive particle towards or away from the surface [116,120]. For instance, superposing both PIV and PTV measurements (see Fig. 10), van Hout has confirmed that resuspension is linked with ejection events that are characterised by a local high speed ('burst') perpendicularly to the surface oriented towards the flow (maps showing the link between particle resuspension and instantaneous fluctuating velocity correlations or streamwise velocity are also available in the original article [120]).

It should be noted that the previous discussion of resuspension mechanisms is not strictly speaking related to the division between colloidal particles and inertial particles but rather to the particle size expressed in terms of near-wall units (to evaluate whether particles are within the viscous sublayer or not). However, as underlined by several studies [98,116,119,120], the distinction between the two cases is not always clear-cut since there is a whole range of particle sizes (d_p close to the size of the viscous sublayer) where a rolling/sliding motion can occur together with a 'burst-type' resuspension. Yet, even though these two mechanisms have been reviewed extensively [1,32,88,89], the present choice to analyse experimental data with respect to the particle size sheds light on the range of application of each mechanism.

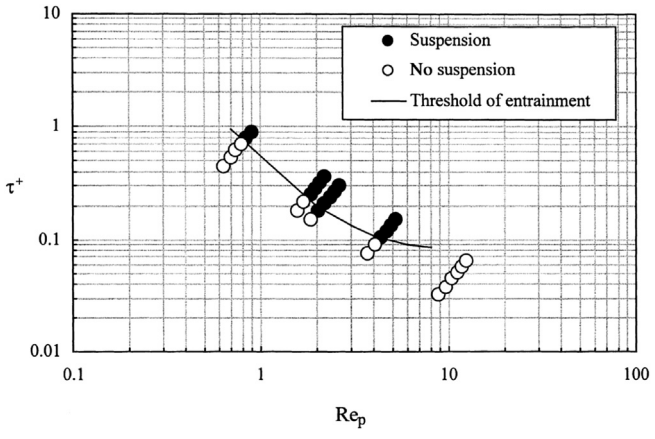

Fig. 8. Particle resuspension as a function of the dimensionless shear stress τ^+ and the particle Reynolds number Re_p for TiO_2 particles on glass substrates: evolution of the threshold velocity (line traced by eye). Adapted from [98]. Copyright 2003 with permission from John Wiley and Sons.

3.1.3. Transport after resuspension

Once particles are resuspended, their trajectory inside the fluid is governed by particle–fluid interactions that are also at play in particle deposition. In that case, particle motion becomes susceptible to near-wall turbulent fluctuations [99] and their trajectory depends on the particle relaxation time. Some particles can be redeposited nearly immediately after detachment [116] while other particles stay in suspension for longer times. This difference in particle behaviour has led to the distinction between saltating and non-saltating particles [7,120]: while small particles (for instance $d_p \lesssim 20$ μm in the atmosphere) usually display long-term suspension, large inertial particles undergo short-term suspension (with parabolic trajectories) and thus impact the surface later on (eventually leading to enhanced resuspension in the case where saltating particles impact large deposited cluster as described in Section 6.2).

3.2. The impact of particle–surface interactions on resuspension

Apart from particle–fluid interactions, particle–surface interactions have been shown to impact significantly particle detachment (see previous reviews [1,88,89]). Indeed, from a mechanical point of view, particles can be detached from a surface only if the adhesion force between the particle and the surface is broken. Atomic force microscopy (AFM) has been widely used to study specifically particle–surface adhesion forces in the wall-normal direction (also called pull-off force) [54,57,124]: the colloidal probe technique [125,126] consists in sticking a colloid on the AFM head and bringing/removing the particle to/from a surface in order to measure particle–surface interactions as well as adhesion properties. There is now a wealth of experimental studies on the adhesion between a particle and a surface (see for instance [125,127–132]) that have shown its dependence on particle properties (size, composition, potential) and surface properties

Table 3
List of experiments that have studied the mechanisms for monolayer resuspension of particles inside the viscous sublayer $d_p \leq \delta_{VS}$

Experiment	Particles	Surface	Flow	Measurement technique	Main observations
Hubbe, 1985 [91]	TiO_2 colloids (144–700 nm) $d_p^+ \leq 10$	Glass	Shear flow and centrifugal techniques (normal and transversal)	Light scattering images	Higher resuspension rate for transversal centrifuge than normal centrifuge, comparison to flow detachment in favour of a process governed by transversal forces
Sharma et al., 1992 [113]	Polystyrene and glass (10–40 μm) $d_p^+ \leq 3$	Glass	Liquid flow in a channel, centrifuge	Image analysis	Difference between resuspension in centrifuges (wall-normal) and in channel flows
Braaten, 1994 [101]	Lycopodium, glass, nickel, pollen (18–34 μm) $d_p^+ \leq 0.6$	Glass	Centrifuge and airflow in wind tunnel	Microscope particle counting	Lower resuspension in centrifuges (wall-normal) than in channel flows
Reeks and Hall, 2001 [114]	Alumina (10–20 μm), Graphite (13 μm) $d_p^+ \lesssim 10$	Stainless steel	Turbulent channel flow (air) and centrifuge	Light reflection (particle concentration)	Smaller tangential force than normal force ($\backsim$1/100) required to remove particles in favour of a contribution of rolling motion
Ibrahim et al., 2003 [94]	Stainless steel, glass and lycopodium (25–77 μm) $d_p^+ \leq 4$	Glass	Turbulent airflow (0–23 m/s) in wind tunnel	Microvideo recording	Removal occurs as rolling/sliding rather than lift-off
Ibrahim et al., 2008 [97]	Soda lime glass (30–111 μm) $d_p^+ \lesssim 2$	Glass	Turbulent airflow in wind tunnel + AFM	Microvideo recording	Effect of rolling motion and turbulent 'burst-sweep' events
Jiang et al., 2008 [115]	Monodispersed Glass (22–41 μm) and PMMA (11–16 μm) $d_p^+ \leq 27$	Stainless steel	Airflow in a rectangular channel	Video analysis	Highlight of rolling motion of particles just before resuspension (see Fig. 9)
Traugott et al., 2011 [116]	700 μm silica $2 \leq d_p^+ \leq 500$	Glass	Turbulent liquid flow in an oscillating grid chamber	PIV and 3D-PTV	Individual particle resuspension at low turbulence intensity versus pattern resuspension at higher turbulence intensity (possibly due to coherent motion), highlight of rolling or sliding motion

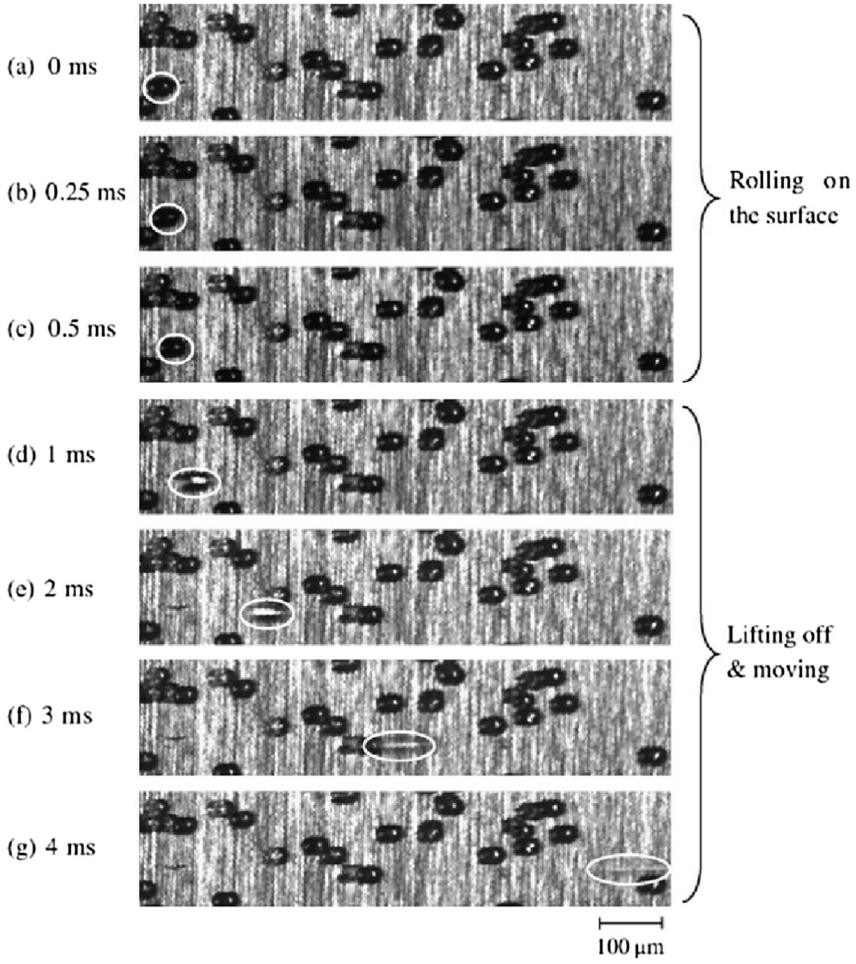

Fig. 9. Snapshots of an entrained glass particle ($d_p = 30$ μm, $d_p^+ = 7$) from a rough substrate as recorded by Jiang et al. Reprinted from [115]. Copyright 2008 with permission from Elsevier.

Table 4
List of experiments that have studied the mechanisms for monolayer resuspension of particles extending within the logarithmic sublayer $d_p \gtrsim \delta_{VS}$.

Experiment	Particles	Surface	Flow	Measurement technique	Main observations
Braaten et al., 1988 and 1990 [121,122]	Monodispersed Lycopodium spores (28 μm) $d_p^+ \simeq 4-6$	Glass	Airflow in wind tunnel	Optical particle detection and hot wire anemometer	Role of turbulent coherent structures in particle removal
Kaftori et al., 1995 [49]	Polystyrene particles (100–900 μm) $d_p^+ \simeq 1.06-17$	Glass	Water flume	Flow visualisation and laser doppler techniques	Role of turbulent coherent structures in particle resuspension
Nino et al., 2003 [98]	Glass (38–94 μm) and silica sand (112–530 μm) $0.6 \leq d_p^+ \leq 21$	Glass	Liquid flow in a rectangular channel	High-speed video	Increasing number of particles affected by near-wall turbulence (coherent structures) for higher flow rates, lower effect on smaller particles, saltation observed for large particles
Ibrahim et al., 2004 [96]	Stainless steel (70 μm) $d_p^+ \leq 4$	Glass	Turbulent airflow in wind tunnel	Microvideo recording	High acceleration of particles probably due to burst-sweep events
Ibrahim et al., 2008 [97]	Soda lime glass (30–111 μm)	Glass	Turbulent airflow in wind tunnel + AFM	Microvideo recording	Effect of rolling motion and turbulent 'burst-sweep' events
Munro et al., 2009 [119]	Sediment (glass, stainless steel, diakon, mustard seed 90–1600 μm) $d_p^+ \gtrsim 50$	Acrylic	Water tank with vortex rings	PIV, high-speed video and light attenuation	Visualisation of the role of coherent structure in sediment resuspension, predominance of viscous effects for smaller particles
Dwivedi et al., 2011 [123]	Spheres 38.3 μm $d_p^+ \gtrsim 10^3$	Glass	Water recirculating flume	PIV and force measurement	High magnitude forces associated with sweep-ejection events, predominance of lift and drag force in resuspension
Traugott et al., 2011 [116]	700 μm silica $2 \leq d_p^+ \leq 500$	Glass	Turbulent liquid flow in an oscillating grid chamber	PIV and 3D-PTV	Individual particle resuspension at low turbulence intensity versus pattern resuspension at higher turbulence intensity (possibly due to coherent motion), highlight of rolling or sliding motion
van Hout, 2013 [120]	Polystyrene (538 μm) $d_p^+ \simeq 10$	Glass	Water channel	PIV and 3D-PTV	Confirmation of the ejection-sweep cycle ('burst') mechanism for resuspension
Kubota and Higuchi [11]	Ceramic spheres (8 μm) $d_p^+ \simeq 2$	Floor	Human foot tapping	Image analysis	Link between particle resuspension and the fluid flow (vortex dynamics)

(composition, potential) as well as on the solution conditions (ion valency, ionic strength, pH).

In the following, attention is focussed on summarising experimental data which reveal the effect of particle–surface interactions on the overall resuspension phenomenon. Since these forces have been studied separately, specific theories have been developed to describe particle–surface interactions (see Section 2 for a presentation of the DLVO theory and Section 4.1.2 for a discussion on adhesion theories). In the present review, we have thus chosen to organise and analyse the experimental data that reveal the impact of particle–surface interactions on resuspension with respect to their relation with the DLVO theory or with extended-DLVO theories (which account for additional forces between interfaces). Therefore, Table 5 lists experiments on particle resuspension that have brought out the dependence of particle reentrainment on properties related to the DLVO theory (particle or surface zeta potential, particle size, particle or surface composition, ionic strength, pH) while Table 6 compiles experiments showing that complex interactions (such as the presence of surfactants or polymers and the hydrophilic or hydrophobic nature of surfaces) can also play a role in particle resuspension.

As emphasised in previous reviews, it appears that similar results are obtained on the effect of particle–surface interactions on resuspension regardless of the flow/chemical conditions. These results are further confirmed by more recent experimental studies on the effect of particle–surface interactions on particle resuspension which have studied different types of particles and surfaces. In addition, it can be noted that most of the experimental data available are concerned with colloidal particles whose sizes are small enough to have a significant contribution of surface forces that can be measured with relative ease.

Drawing on the experiments listed in Table 5, which have quantified the effect of particle–surface interactions (in favour of a DLVO formulation) on resuspension in various flow conditions, it is worth noting that the resuspension rate depends on several properties:

- *pH conditions*: changing the pH of the solution impacts the zeta potential of particles and surfaces, thus modifying the electrostatic interactions between particles and surfaces [90,92,105,113,134,138,139]. For instance, as depicted in Fig. 11, the resuspension rate of $Cr(OH)_3$ colloids (230 nm) from glass substrates exposed to turbulent flows has been shown to decrease between pH 2 and 3 while higher values of pH give rise to higher resuspension rates [90]. This trend appears to be in agreement with measurements of the zeta potentials of particles [92], confirming the role of electrostatic interactions (either repulsive or attractive) in the resuspension phenomenon.
- *Ionic strength*: further confirmations of the impact of electrostatics on resuspension have also been provided by experimental studies of the effect of the ionic strength on resuspension [18,92,100,105,113,134,137–140]. It has been shown that changes in the ionic strength lead to higher resuspension rates due to lower adhesion forces between surfaces [135,138].
- *Particle or surface composition*: experiments have shown that various types of particle or surface display different resuspension rates due to the specific physico-chemical interactions between surfaces (especially van der Waals forces) [90,92,94,99,101,115,136]. For example, glass microspheres of 10 μm are more easily resuspended than polystyrene microspheres of the same diameter from similar glass substrates [113].
- *Particle size and shape*: experiments have also emphasised that the resuspension rate depends on particle sizes, both due to particle–surface interactions and particle–fluid interactions [90,94,113,114,115,134]. Furthermore, the resuspension rate of

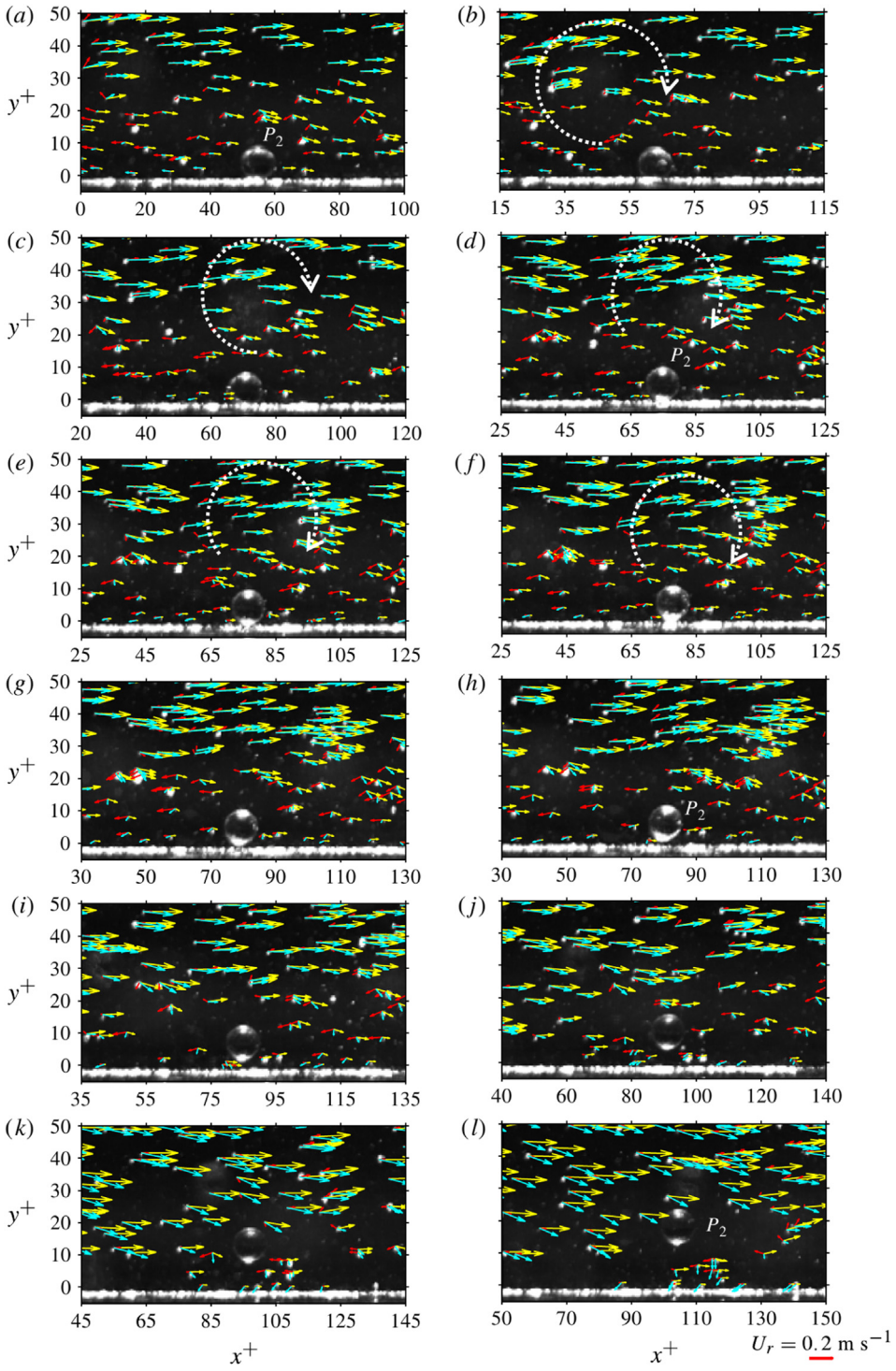

Fig. 10. Sequence of PIV images superposed with PTV vectors showing the resuspension of particle P_2: → instantaneous PTV, → velocity in the particle frame of reference, → velocity fluctuations (Reynolds-decomposed). Reprinted from [120]. Copyright 2013 with permission from Cambridge University Press.

millimetre-sized spherical particles was found to be higher than for millimetre-sized non-spherical particles [136].

However, depending on the solution conditions and on the nature of the particles/surfaces which are considered, more complex physico-chemical interactions can occur between particles and surfaces. From the experiments compiled in Table 6, it appears that four significant contributions can affect particle resuspension:

- *Polymer concentration*: the presence of polymers in the solution can lead to the formation of polymeric bridging between a surface and a particle, thus enhancing the adhesion force and lowering the resuspension rate [93]. Indeed, when two polymer-coated surfaces are brought into contact, the overlap between the two polymer chains lead to complex forces that can significantly enhance adhesion bonds. Yet, the strength of this bond depends strongly on the complex structure of the polymer

Table 5
List of experiments that have studied the effect of particle–surface interactions (in favour of DLVO formulation) on monolayer resuspension.

Experiment	Particles	Surface	Flow	Measurement technique	Main observations
Hubbe, 1985 [90]	TiO_2 colloids (from 144 nm to 700 nm)	Cellulose and glass	Turbulent fluid flow ($0.6 < \tau_f <$ 312 Pa) in coaxial cylinders	Light scattering images	Effect of pH and particle size on detachment
Hubbe, 1987 [92]	TiO_2 (500 nm), $Cr(OH)_3$ (230 nm) and Al_2O_3 (770 nm)	Cellulose and glass	Turbulent fluid flow in coaxial cylinders	Light scattering techniques	Effect of particle composition and solution conditions (pH, ionic strength), link with zeta potential
Taheri and Bragg., 1992 [133]	Glass (20–30 μm)	Glass	Transversal air jet	Image analysis	Log-normal law for particle–surface adhesion
Sharma et al., 1992 [113]	Polystyrene and glass (10–40 μm)	Glass	Liquid flow in a channel, centrifuge	Image analysis	Effect of particle size, particle material and solution conditions (pH, ionic strength) on resuspension
Ryan and Gschwend, 1994 [105]	Hematite (150 nm)	Quartz grains	Liquid flow in packed bed column	Particle concentration derived from turbidity	Higher resuspension rate for increasing ionic strength and effect of pH on reentrainment
Reeks and Hall, 2001 [114]	Alumina (10–20 μm), Graphite (13 μm)	Stainless steel	Turbulent channel flow (air) and centrifuge	Light reflection (particle concentration)	Effect of particle size and nature on resuspension
Negri et al., 2002 [134]	Alumina (0.3 and 3 μm)	Glass	Shear stress flow chamber	Video processing	Decrease of the resuspension with longer resting time, with smaller particles. Effect of pH and ionic strength
Ibrahim et al., 2003 [94]	Stainless steel, glass and lycopodium (25–77 μm) $d_p^+ \leq 4$	Glass	Turbulent airflow (0–23 m/s) in wind tunnel	Microvideo recording	Increasing removal with increasing particle size, dependence on the type of particles
Jiang et al., 2008 [115]	Monodispersed Glass (22–41 μm) and PMMA (11–16 μm) $d_p^+ \leq 27$	Stainless steel	Airflow in a rectangular channel	Video analysis + SEM	Different resuspension rates with various particle types
Canseco et al., 2009 [135]	Polystyrene latex (780 nm)	Silicate	Liquid flow in porous media	Particle concentration	Variations of the removal rate with ionic strength
Rabinovich and Kalman, 2009 [136]	Aluminium, Glass, Plastic, Sand, Salt (0.06–5 mm)	Plexiglass	Turbulent airflow in wind tunnel	Image analysis	Effect of particle nature and shape on resuspension
Keedy et al., 2012 [25]	Polydisperse ceramic (35–60 μm)	Glass	Impinging air jet	Optical methods	Strong dependence of resuspension rate on particle nature (size, ceramic or explosive particles)
Shen et al., 2012 [137]	Carboxylate-modified polystyrene latex (30 and 1156 nm)	Glass bead	Liquid flow in porous media	Spectrophotometry (particle concentration)	Various removal rate for different values of ionic strength
Dagaonkar and Majumdar, 2012 [18]	Polystyrene latex (3 μm)	Whatman filter paper	Filtration experiment (liquid in porous media)	Image analysis	Higher resuspension rate with increasing ionic strength, effect of ion valency

bridge (length, radius of gyration of adsorbed polymers). The reader is referred to Israelachvili's book [56] for further information on polymeric interactions.

- *Surfactant concentration*: the presence of surfactants in the solution can affect surface properties (particularly the zeta potential) and, as a result, change the removal rate [21,138,141,142]. As for polymer concentration, the effect of surfactants on the overall removal rate is complex since various phenomena can occur: the adsorption of surfactants on a surface can increase the contact distance between particles, lowering the interaction, while specific interactions between surfactants and surfaces can lead to enhanced/reduced adhesion forces. Therefore, the overall effect of surfactants on resuspension is highly case-dependent. Besides, above the critical micelle concentration (CMC), surfactants form micelles that have been shown to influence particle resuspension [142] (in a similar way as polymers do).
- *Hydrophilic–hydrophobic interactions*: specific interactions can occur between hydrophilic/hydrophobic surfaces, thus impacting particle resuspension [139,141,143]. However, the effect on the overall resuspension is not straightforward: for instance, Freitas and Sharma [141] found that hydrophobic particles are more easily removed than hydrophilic particles in deionised water but that the opposite is true in an aqueous solution of 0.1 M KCl.
- *Residence time*: some experiments have shown that particles deposited for long times are harder to remove than freshly deposited ones [96,100]. These observations have been attributed to interfacial re-arrangements during particle–surface contact (either visco-elastic deformation of particles or ions reorganisation in the solution).

Besides, in the case of specific experimental conditions, other interactions can play a role in particle resuspension:

- *Magnetic forces*: when magnetic materials are used, magnetic interactions between particles and surfaces arise due to the presence of an electromagnetic field [140]. The effect on particle resuspension depends on the magnetic properties of the materials used which can either lead to attractive or repulsive magnetic forces (thus enhancing or reducing particle resuspension).
- *Capillary forces*: in humid air flows (especially with a relative humidity RH higher than 60–70%), a liquid meniscus can form around the contact area due to the condensation of water [95,144–147]. The resulting capillary force leads to an enhanced

Table 6
List of experiments that have studied the effect of particle–surface interactions (in favour of X-DLVO formulation) on monolayer resuspension.

Experiment	Particles	Surface	Flow	Measurement technique	Main observations
Hubbe, 1987 [93]	TiO_2 (704 nm)	Cellulose and glass	Turbulent fluid flow in coaxial cylinders	Light scattering techniques	Addition of polymers in solution leading to polymeric bridging and thus lower removal
Wu et al., 1992 [99]	Uranine, pollen, polymer, lycopodium (5 μm up to 42 μm)	Glass, plexiglass, leaves	Airflow in wind tunnel	Video analysis	Dependence of resuspension on particle and substrate nature
Meinders and Busscher, 1993 [100]	Polystyrene (736 μm)	Glass	Parallel-plate liquid flow chamber	Image analysis	Influence of ionic strength and residence time on resuspension
Braaten, 1994 [101]	Lycopodium, glass, nickel, pollen (18–34 μm)	Glass	Centrifuge and airflow in wind tunnel	Microscope particle counting	Dependence of particle resuspension on the particle composition
Elzo et al., 1996 [138]	Glass (20 μm)	Cellulose diacetate	Rectangular channel flow (liquid)	Image analysis	Increasing particle removal with increasing pH or surfactant concentration and with decreasing ionic strength or polymer concentration
Freitas and Sharma, 1999 [141]	Glass, polystyrene (10 μm)	Glass, SiO_2, mica	Liquid flow in simple shear flow	Optical microscope (particle counting)	Variations of particle resuspension with ionic strength, surfactant concentration, liquid type, particle or surface type, hydrophobicity
Bergendahl and Grasso, 1999 [139]	Polystyrene latex (1.0 μm)	Glass bead	Liquid flow in porous media	Light scattering	Higher resuspension with increasing pH and with decreasing ionic strength, effect of hydrophobicity
Ryde and Matijević, 2000 [140]	Hematite (66 nm)	Glass bead	Liquid flow in porous media	Light scattering (particle concentration)	Changes of the removal rate with solution conditions (pH and ionic strength), link with particle potential, effect of magnetic forces
Ibrahim et al., 2004 [95]	Stainless steel (70 nm)	Glass	Turbulent airflow in wind tunnel	Microvideo recording	Effect of residence time and relative humidity (decreasing removal for humidity $\gtrsim$30%) on resuspension
Zelenev and Matijević, 2006 [142]	Hematite (29 nm)	Glass bead	Liquid flow in porous media	Light scattering (particle concentration)	Critical surfactant concentration above which resuspension increases
Sharma et al., 2008 [143]	Modified polystyrene spheres ($\simeq$1 μm)	Glass	Liquid channel flow	Image analysis	Changes in the resuspension rate with particle properties (zeta potential, hydrophobic or hydrophilic) with air-water interfaces

adhesion force between the surfaces (see also Israelachvili's book [56] for further information on capillary forces).

3.3. The influence of substrate morphology on resuspension

3.3.1. Effect of morphology on adhesion

Together with particle–fluid and particle–surface interactions, the morphology of substrates (or eventually particles) has been shown to impact the strength of adhesive forces and, as a result, particle resuspension from such substrates. In particular, two main characteristics of surface morphology play a role in particle–surface interactions, namely geometrical heterogeneities (roughness) and surface charge heterogeneities. The presence of such heterogeneities has long been confirmed experimentally using AFM or SEM (Scanning Electron Microscope) techniques to probe the surface (see for instance recent SEM images of glass or PMMA particles and of stainless steel surfaces in Fig. 12). In addition, more recent experiments on adhesion properties between surfaces (using colloidal probe techniques or centrifuge methods to measure particle–surface interactions) have indicated that the presence of a nanoscale roughness on surfaces (characterised using AFM or SEM techniques) can significantly reduce adhesion forces [148–155]. Besides, using modelled rough surfaces, other experiments have investigated the effect of asperity shapes on adhesion forces between rough surfaces [156]. Similarly, the presence of surface charge heterogeneities can induce high dispersion in the distribution of adhesion forces [157,158].

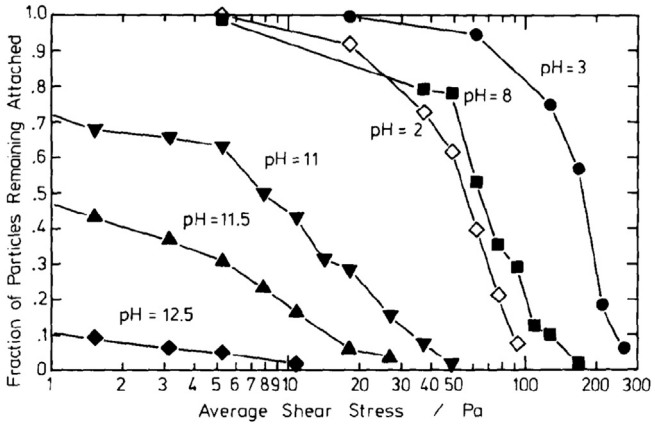

Fig. 11. Evolution of the fraction of $Cr(OH)_3$ particles remaining on a glass substrate with shear stress at various pH conditions. Reprinted from [90]. Copyright 1985 with permission from Elsevier.

3.3.2. Effect of morphology on resuspension

Since the present review addresses more specifically the phenomenon of particle resuspension, the following paragraph proposes a compilation of experimental data showing the effect of substrate morphology on the overall resuspension (see also previous reviews [1,88,89]). In the present work, we have chosen to analyse the existing experimental data with respect to the nature of heterogeneities on the substrate morphology: either geometrical

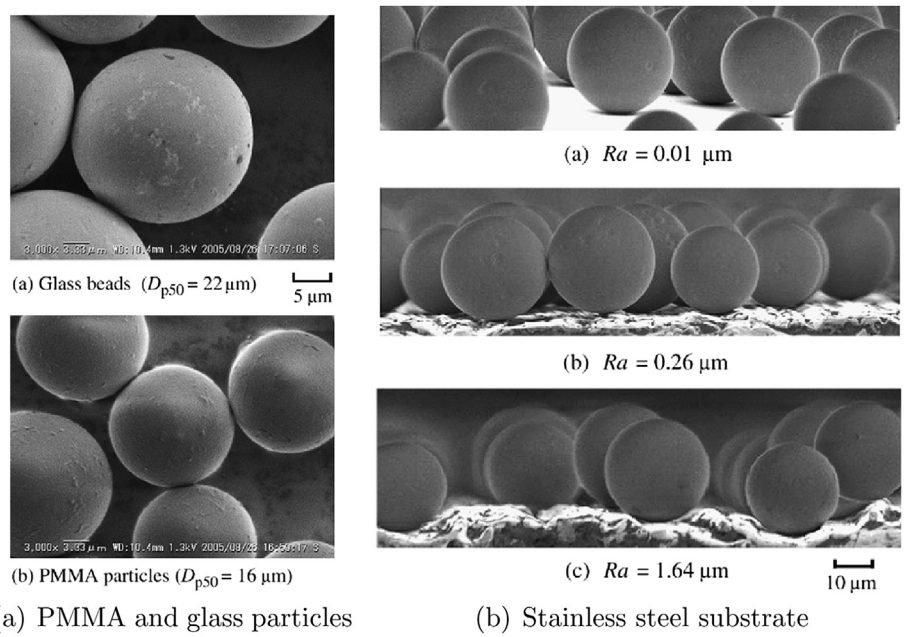

Fig. 12. SEM images of particles (PMMA and glass) and various substrates (stainless steel) showing the presence of surface roughness. Reprinted from [115]. Copyright 2008 with permission from Elsevier.

(roughness) or chemical (surface charge or potential) heterogeneities. Table 7 provides a list of such experiments (both in simple shear flows and in porous media) together with the main conclusions regarding the impacts of surface roughness or surface charge heterogeneities.

- *Roughness*: for instance, the resuspension of PMMA and glass particles (11–41 μm) from stainless steel surfaces with various roughness characteristics (SEM images provided in Fig. 12) has been measured using video recording of particle motion in an airflow channel [115]. Typical results are displayed in Fig. 13: it can be seen that the fraction of resuspended particles increases when surface roughness increases within the submicron range while it is seemingly lower for surface roughness in the micron-scale. Other experimental data have revealed the complex role played by surface roughness in particle resuspension: Mukai et al. [103] have underlined that, whereas microscale roughness significantly affects the adhesion between surfaces thus impacting resuspension, macroscale roughness is likely to modify fluid motion (especially turbulence) in the near-wall

Table 7
List of experiments that have studied the effect of surface heterogeneities on monolayer resuspension.

Experiment	Particles	Surface	Flow	Measurement technique	Main observations
Das et al., 1994 [159]	Glass, Polystyrene (10 μm)	Mica	Flow cell (fluid)	Particle counting (microscope) +SEM	Removal due to the presence of surface roughness (measured at least on particles)
Nino et al., 2003 [98]	Glass (38–94 μm) and silica sand (112–530 μm) $0.6 \leq d_p^+ \leq 21$	Glass	Liquid flow in a rectangular channel	High-speed video	Difference between resuspension on smooth and rough substrates
Ibrahim et al., 2008 [97]	Soda lime glass (30–111 μm)	Glass	Turbulent airflow in wind tunnel + AFM	Microvideo recording	Removal of various particles from a rough substrate
Jiang et al., 2006 [160]	PMMA (9.4 μm) coated with nanoparticles	Stainless steel	Airflow in a rectangular channel	Video analysis	Higher resuspension rate with increasing concentration of nanoparticles on PMMA spheres
Jiang et al., 2008 [115]	Monodispersed Glass (22–41 μm) and PMMA (11–16 μm) $d_p^+ \leq 27$	Stainless steel	Airflow in a rectangular channel	Video analysis + SEM	Increase in the resuspension rate for increasing submicron roughness but further decrease for microscale roughness, dependence on particle diameter
Mukai et al., 2009 [103]	Salt (1–20 μm)	Sheet metal, linoleum, carpet	Airflow in wind tunnel	Light scattering (particle concentration)	Resuspension possibly affected by microscale roughness (lower adhesion) and macroscale roughness (modified turbulence)
Shen et al., 2012 [137]	Carboxylate-modified polystyrene latex (30 and 1156 nm)	Glass bead	Liquid flow in porous media	Spectrophotometry (particle concentration)	Role of surface roughness, heterogeneity and cation exchange on particle resuspension
Dagaonkar and Majumdar, 2012 [18]	Polystyrene latex (3 μm)	Whatman filter paper	Filtration experiment (liquid in porous media) + SEM	Image analysis	Observed (high) resuspension rate explained by the presence of roughness

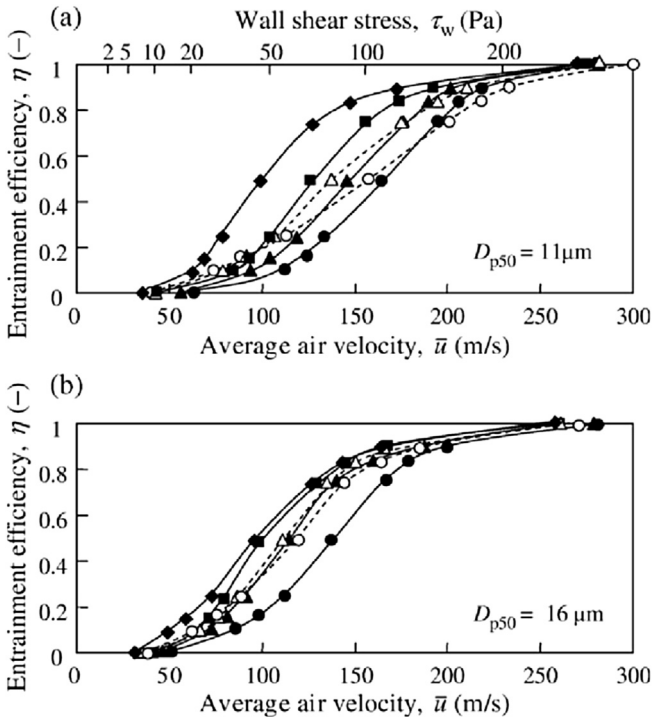

Fig. 13. Entrainment efficiency as a function of air velocity for PMMA particles on rough surfaces (average roughness of ● 0.01, ▲ 0.03, ■: 0.12, ◆ 0.26, △ 0.77, ○ 1.64 μm). Reprinted from [115]. Copyright 2008 with permission from Elsevier.

region. Therefore, the role of surface roughness in particle resuspension can be two-fold.

- *Charge/potential heterogeneities*: surface charge or potential heterogeneities are also brought forward to explain some observations of particle resuspension [137], but these effects have only been studied recently and the articles regarding this contribution are still scarce. The overall effect of charge/potential heterogeneities depends on the situation encountered since such heterogeneities can either increase or decrease the adhesion force and thus the resuspension rate (this issue has been addressed from a theoretical point of view and will be described later in Section 4.1.2).

3.4. Summary and perspectives for future studies

This section has proposed a compilation of experimental data on particle resuspension from monolayers. The discussions have been organised following the fundamental interactions involved, which means that the effects of particle–fluid and particle–surface interactions as well as substrate morphology on particle resuspension have been addressed separately. Furthermore, each effect has been analysed with respect to the corresponding relevant parameters: particle–fluid interactions have been assessed using the dimensionless particle size d_p^+ compared to the extent of the viscous sublayer δ_{VS}^+; particle–surface interactions have been addressed with respect to the DLVO theory; and a distinction between geometrical and chemical heterogeneities has been made.

To summarise, it has been shown that similar observations have been made regardless of the flow/chemical conditions and that particle resuspension depends on a number of parameters (see also previous reviews [1,88,89]): fluid properties (higher resuspension with increasing flow velocity), particle properties (zeta potential, composition, size), solution conditions (pH, ionic strength), surface properties (zeta potential, composition) and surface morphology (roughness, charge or potential heterogeneities). More complex resuspension behaviour arises when surfactants or polymers are present in the solution, or when specific interfacial interactions occur (such as hydrophilic-hydrophobic forces). In addition, the new analysis in terms of the dimensionless particle size has shown that the two well-known mechanisms of particle resuspension (i.e. rolling motion for small particles such that $d_p^+ \lesssim \delta_{VS}^+$ and 'burst-type' resuspension for large particles such that $d_p^+ \gtrsim \delta_{VS}^+$) affect different size of particles and are not necessarily in competition.

Drawing on the present analysis as well as on previous reviews [1,88,89], it appears that a satisfactory level of understanding of monolayer particle resuspension has been reached, especially in the case of simple flows. Indeed, the analysis of recent experiments shows that they have brought further confirmation to the current understanding, with more precise measurements and observations. It appears also that recent experiments have focussed on exploring in detail the effect of turbulence on resuspension [11,120]. This is due to the complexity of turbulence features in the near-wall region, a topic which is still explored in the fluid dynamics field especially in the context of particle-laden flows (since particles can affect near-wall turbulence). Besides, the study of particle interactions with near-wall turbulent features is further motivated by the ongoing need to limit the reentrainment of hazardous particles in the environment [32]. This also explains why most of the recent studies have been performed in the context of walking-induced resuspension [11,161], where the complex fluid motions in the near-wall region are playing a predominant role in resuspension, as well as in the context of indoor resuspension [162] where much progress has still to be done in understanding the impact of complex flow field over intricate geometries (such as carpets or fibers).

4. Mechanisms at play in resuspension from monolayer deposits

Whereas the previous section was devoted to reviewing experiments dealing with particle resuspension from monolayer deposits using a phenomenological point of view, the mechanisms and forces at play in the resuspension phenomenon are analysed in the present section. The question of the forces acting on particles, either embedded in the core of a fluid flow or deposited on a wall surface, is not new and has already been addressed as well as particle motion along walls [1,88,89]. They are nevertheless recalled here for the sake of self-sustainability and to provide a broad picture of all existing theories that are currently available. Yet, the present discussion introduces also new elements, especially with respect to the important issue of surface roughness. Given the role played by surface roughness in experiments as well as in recent models of particle resuspension, this is a central point that justifies to have a specific discussion (following the introduction in Section 2.4) in which the key aspects of the forces acting on particles and of particle motion are addressed separately. In that sense, the descriptions of the fundamental mechanisms and of the main points of particle motion along a wall surface are useful to understand the central points of some modelling approaches that have been developed for particle resuspension and that will be detailed in Section 5.

Layout of this section. Key aspects of particle–fluid interactions are first reviewed in Section 4.1.1, followed by particle–surface interactions in Section 4.1.2 with a specific emphasis on adhesion forces and the effects of surface roughness. Indeed, since readers having a background on fluid mechanics are perhaps inclined to be more familiar with drag and lift forces than with contact theories and adhesion forces, it was chosen to develop more specifically the latter aspect. Then, the basic mechanisms of particle resuspension (i.e. rolling, sliding and lifting motion) are described in Section 4.2.

4.1. A coupling between physical interactions

Particle resuspension results from the intricate competition between disruptive forces (that tend to drive particles away from the surface) and cohesive forces (that tend to keep particles adhered on the surface) [1,13,32,88,89]. Whereas disruptive forces mainly stem from hydrodynamical forces exerted on particles, cohesive forces arise mostly from the physico-chemical interactions between interfaces in contact. This interplay between particle–fluid and particle–surface interactions in the resuspension phenomenon has been investigated extensively, starting with studies which date back to the second half of the 20th century [163–166] as well as in recent works (see for instance Refs. [9,88]).

4.1.1. Particle–fluid interactions

Just as for particles in the bulk of the flow, particles deposited on a surface and exposed to a flow (either turbulent or laminar) are subjected to two main hydrodynamic forces (see also Fig. 14): drag and lift forces (see the introduction on the forces acting on particles in Section 2.1.1). Away from wall surfaces, the expressions usually retained for these forces can have an isotropic form. However, due to the presence of the wall, the properties of the flow in the near-wall region are highly non-homogeneous and, as a result, a distinction between wall-normal and transversal forces is generally made [1].

(a) Drag forces are traditionally expressed by a functional form written as [167,168]

$$\mathbf{F}_{\text{drag}} = \frac{1}{2}\rho_f C_D A_p |\mathbf{U}_r| \mathbf{U}_r \tag{12}$$

where $\mathbf{U}_r$ is the slip velocity, A_p the particle cross-sectional area exposed to the flow and C_D the drag coefficient (introduced in Section 2.1.1). Away from wall boundaries (i.e. in the bulk of the fluid), the drag coefficient is assumed to be isotropic and several correlations have been proposed in the literature (a list is available the book of Clift et al. [167]). For instance, the Oseen relation is a classical correlation for flow with low Reynolds ($\text{Re}_p < 0.01$) [167,168]

$$C_D = \frac{24}{\text{Re}_p} \times \left(1 + \frac{3}{16}\right) \tag{13}$$

where Re_p is the particle Reynolds number. Retaining the analytical factor $24/\text{Re}_p$ appearing in the equation above (which is predominant at small Reynolds Re_p), the classical Stokes drag force is retrieved for creeping (relative) flows, i.e. for $\text{Re} \ll 1$

$$\mathbf{F}_{\text{drag}} = 3\pi d_p \rho_f \nu_f \, \mathbf{U}_r \tag{14}$$

Additional studies on the Oseen approximation have provided higher order asymptotic expansions of the flow past a sphere at low Reynolds number [168–170]:

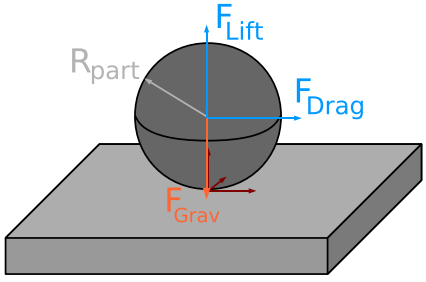

Fig. 14. Sketch of the various hydrodynamical forces exerted on an adhering particle.

$$C_D = \frac{24}{Re_p}\left[1 + \frac{3}{16}\text{Re}_p + \frac{9}{160}\text{Re}_p^2 \ln(Re_p/2)\right] \tag{15}$$

Similarly, semi-empirical correlations have been proposed for higher Reynolds number Re_p and a typical correlation is written as [167]

$$C_D = \frac{24}{Re_p}\left[1 + 0.15 Re_p^{0.687}\right] \quad \text{for } Re_p < 800 \tag{16}$$

Comparing Eq. (16) with Eq. (13), it can be seen that correlations for higher particle Reynolds number can be written as the classical Stokes drag coefficient with the addition of extra correction terms.

However, in near-wall regions, the drag coefficients are now anisotropic and the general formulation of drag forces near or at a wall are expressed as

$$F_{\text{Drag},\parallel} = \frac{1}{2}\rho_f U_r^2 C_{D,\parallel} A_p, \tag{17a}$$

$$F_{\text{Drag},\perp} = \frac{1}{2}\rho_f U_r^2 C_{D,\perp} A_p \tag{17b}$$

For the tangential drag coefficient of a spherical particle attached on a flat surface, an analytical solution has been derived by O'Neill [171] in Stokes flow conditions (i.e. for particles small enough that they are fully immersed in the viscous sublayer and with $\text{Re} \ll 1$):

$$C_{D,\parallel} = 1.7009 \frac{24}{Re_p} \tag{18}$$

This value for the drag coefficient is similar to its value for spherical particles in the bulk of the fluid, but for a correction factor $f_{\text{drag}} = 1.7009$ accounting for the presence of the surface.

Various empirical and analytical formulas have been proposed in the literature for the drag coefficient of particles adhering on a surface for higher values of the particle Reynolds number. For instance, Sweeney and Finlay [172] suggested an empirical drag coefficient valid for a sphere ($0.1 < \text{Re}_p < 250$) in a Blasius boundary layer at a given value of the plate Reynolds number ($\text{Re} = 32{,}400$). Ibrahim et al. [97] used a formula for the drag coefficient with the corrections for inertial particles from Ockendon and Evans [173] (similar to Eq. (15)) and O'Neill corrections for the near-wall effects [171]. The resulting formula is valid provided that $\text{Re}_p < 8$:

$$C_{D,\parallel} = 1.7009 \frac{24}{Re_p}\left[1 + \frac{3Re_p}{16} + \frac{9Re_p^2 \ln(Re_p/2)}{160} + \frac{0.1879 Re_p^2}{4}\right] \tag{19}$$

Similarly, Liu et al [174] proposed a formula for the drag coefficient that remains valid in non-stokesian flows (more precisely in the range $0.1 \le \text{Re}_p \le 250$). For that purpose, an empirical formula for the drag coefficient of spherical particles in a flow was extended with O'Neill corrections for near-wall effects [171]:

$$C_{D,\parallel} = \begin{cases} 1.7009 \dfrac{24}{Re_p}(1 + 0.0916 Re_p) & \text{for } 0.1 \le Re_p < 5 \\ 1.7009 \dfrac{24}{Re_p}\left(1 + 0.158 Re_p^{2/3}\right) & \text{for } 5 \le Re_p < 250 \end{cases} \tag{20}$$

In spite of being a very old and long-addressed question, the issue of coming up with an expression for drag forces even on small spherical particles remains a difficult (and open) one, where available formulas resort to a combination of complex analytical

expansions and empirical correction terms. Thus, it is not too surprising that several correlations can be found. Furthermore, for deposited particles, this difficulty is compounded by the presence of the wall and by the so-called lubrification effects. This explains the various formulas available, such as the ones proposed in Eq. (19) and in Eq. (20) which differ also by their range of validity.

In addition, due to the flow non-uniformity, there is a non-zero moment of the hydrodynamic drag forces which is exerted on deposited particles. This moment due to tangential drag forces has been analytically evaluated by O'Neill [171] for particles in Stokes flow and is given by:

$$M_O\left(F_{\text{drag}}\right) = 1.4 R_{\text{part}} F_{\text{drag}} \tag{21}$$

where the factor 1.4 accounts for the presence of the surface.

For the normal drag coefficient, the influence of the wall is even more pronounced, since the wall blocking effects are felt directly (the pressure-gradient is noticeably affected by the wall in the normal direction). When the wall-normal distance between the particle centre of mass and the wall becomes inferior to one or two particle diameters, the drag coefficient in the wall-normal can rise sharply. Using bipolar coordinates, Brenner [175] came up with an exact expression of the correction, which is expressed as an infinite series sum. The resulting formula is therefore somewhat cumbersome to implement but its main characteristics is that it predicts an infinite value for the correction term at the contact point. A more tractable approximation was proposed just after by Maude [176] for very small particle Reynolds number Re_p:

$$C_{D,\perp} = C_D \times \left(1 + \frac{9}{8}\left(\frac{d_p}{2y_p}\right) + \left(\frac{9}{8}\frac{d_p}{2y_p}\right)^2\right) \tag{22}$$

This expression remains close to the one proposed by Brenner and only separates very near the contact point where it predicts a finite correction term (instead of the infinite value yielded by Brenner's expression) [176]. For example, at the wall itself (distance $y_p = R_{\text{part}}$), the correction term for the drag coefficient in the direction normal to the wall is nearly $g_{\text{drag}} \simeq 3.39$ [176,177] and this value appears therefore as the counterpart of the correction term $f_{\text{drag}} = 1.7009$ which was used for the drag coefficient in the tangential direction. For practical purposes, particularly for deposited particles, this expression is often retained and, in that case, the Stokes drag law in the normal direction is simply written as

$$C_{D,\perp} = 3.39\frac{24}{Re_p} \tag{23}$$

for very small particle Reynolds number Re_p. The same coefficient $C_{D,\perp}$ can be predicted with expressions such as the ones written above in Eqs. (20) by substituting f_{drag} by g_{drag} to obtain general formulas for higher particle Reynolds numbers.

(b) Lift forces: as for drag forces, analytical formulas for lift forces exerted on deposited particles are complex due to the strong non-uniformity of the flow in the near-wall region (in the following, we consider only the component of lift forces in the wall-normal direction). For instance, Leighton and Acrivos [178] calculated the lift force on a small spherical particle in a simple shear flow for small particle Reynolds number:

$$F_{\text{lift}} = 9.22\left(\tau_f \mu_f R_{\text{part}}^2\right)\left(\frac{\tau_f R_{\text{part}}^2}{\nu_f}\right) \tag{24}$$

where τ_f is the shear rate.

For larger particles that are not necessarily fully immersed in the viscous sublayer, near-wall turbulence (with coherent structures) affects particle motion. In these cases, empirical formulas have been proposed by Hall [179] for very large particles ($1.8 < \text{Re}_p/2 < 70$) as well as by Mollinger et al. [180,181] for relatively small particles ($0.3 < \text{Re}_p/2 < 2$) in a fully developed turbulent boundary layer:

$$F_{\text{lift}} = (20 \pm 1.57)\nu_f^2 \rho_f \left(\frac{Re_p}{2}\right)^{2.31\pm0.02} \quad \text{for } 1.8 < Re_p/2 < 70 \tag{25}$$

$$F_{\text{lift}} = (56.9 \pm 1.1)\nu_f^2 \rho_f \left(\frac{Re_p}{2}\right)^{1.87\pm0.04} \quad \text{for } 0.3 < Re_p/2 < 2 \tag{26}$$

Yet, to the authors' knowledge, there is no general similar formula available over a larger range of particle Reynolds numbers. Yet, with the emergence of recent experimental studies on the lift force exerted on bubbles [182,183] as well as numerical works on the lift force on spherical rigid particles [184–186] at various particle Reynolds number and different particle wall-distance, it is believed that new correlations can be reached.

Contrary to drag forces whose functional form is assumed to be well known, following relations such as in Eq. (12), lift forces are much more difficult to fit in a unique framework and to define precisely with a well-accepted general expression. As can be guessed from the expressions given above, different formulations can be found, depending on the situation considered by different authors. It is then essential to be aware of the specific case addressed in each work and, especially, of the defining limitations of each formulation. As a classical example, the well-known Saffman lift force [187] was derived for particles with small relative Reynolds numbers (based on the fluid shear) and in an infinite domain. Clearly, this expression cannot be used for particles in the vicinity of a wall, least of all for particles actually deposited on the surface. However, a very important work was achieved, in particular by McLaughlin and co-workers, in order to come up with a synthesis of the various expressions of lift forces which had been proposed in the literature. This has culminated in the useful formulation of an 'optimal lift force' which was proposed and shown to be applicable in various situations (for various particle Reynolds numbers, distances to the wall and shear intensities), thus overcoming the strict range of validity of previous expressions [188]. Indeed, it is believed that this 'optimal lift force' lives up to its name and represents the best available formulation of lift effects. As indicated by the title of this work [188], this lift force was derived in the context of a study of particle deposition which is, thus, relevant in our present case but also with an emphasis on particles being in the fluid. For particles at the wall, the optimal lift force was shown to follow closely the expressions proposed by Hall and given above in Eq. (25) [188]. In that sense, it can be considered that, for deposited particles, the lift force put forward by Hall represents a reference formulation.

Further investigations of the relative importance of drag and lift forces was performed by Cleaver and Yates [118]: for particles fully immersed in the viscous sublayer ($d_p^+ < 1$), lift forces are negligible compared to drag forces. This conclusion corroborated several experimental data showing that, for small colloidal particles, particles were resuspended due to tangential forces and not wall-normal forces [90,94,104,113,114,189].

4.1.2. Particle–surface interactions

As mentioned in Section 2, physico-chemical interactions occurring between particles approaching a substrate are generally described using the DLVO theory [52,53] (see also [54–57,190,191]). Yet, in the case of particle–surface adhesion, the relevant

interaction is related to contact forces. This explains that two different approaches have been proposed in the literature: contact mechanics (based on surface energies) and adhesion mechanics (based on a DLVO formulation) [56,192]. The main difference between these two theories is whether elastic deformations are accounted for or not and is illustrated in Fig. 15.

Contact mechanics theories have indeed been developed to describe the equilibrium state of two surfaces in contact (that is to determine the size of the contact area in the presence of an external force) while adhesion mechanics theories aim at capturing the dynamics of particle–surface adhesion (i.e. non-equilibrium states such as the contact rupture). In contact mechanics theories, the adhesion force (also called pull-off or separation force) is equal to the external force required to separate the two surfaces (i.e. to obtain a contact radius equal to 0). Besides, the range of validity of these adhesion/contact theories depends strongly on the ability of surfaces to deform [1,56,88,89]. Tabor [193] proposed a dimensionless coefficient to measure the ratio between surface adhesiveness and surface stiffness:

$$\mu_T^3 = R_{part}\Delta\gamma^2 \Big/ \left(K^2 z_0^3\right) \tag{27}$$

with R_{part} the particle radius, $\Delta\gamma$ the surface energy, z_0 the equilibrium separation of surfaces, $K = 4/3((1-\nu_1^2)/E_1 + (1-\nu_2^2)/E_2)$ the elastic moduli and ν the Poisson ratio. In the following, the various adhesion/contact theories are presented with respect to their validity in terms of Tabor's parameter:

(a) JKR theory (named after the work of Johnson–Kendall–Roberts [194]). The JKR theory is one of the first contact theory (i.e. based on surface energies $\Delta\gamma$) and is thus often used in contact mechanics. The key assumption in the JKR theory lies in the fact that particles and surfaces are considered to deform elastically upon contact according to the Hertz theory and that an adhesion between the surfaces occurs within the contact area (due to the surface energy $\Delta\gamma$). Therefore, the JKR theory predicts a contact area larger than the Hertz theory since it also includes the contribution of adhesive forces. The JKR theory is valid only when the criteria? $\mu_T \gg 1$ is respected, i.e. for large or 'soft' (highly deformable) particles.
Under an external force F_{ext}, the JKR theory predicts that the equilibrium contact radius r_c between a sphere and a plate is given by [56,155,192]:

$$r_c^3 = \frac{R_{part}}{K}\left(\sqrt{3\pi R_{part}\Delta\gamma} + \sqrt{F_{ext} + 3\pi R_{part}\Delta\gamma}\right)^2 \tag{28}$$

Pull-off forces (i.e. forces required to separate surfaces) are thus obtained as the forces occurring between surfaces in contact (non-contact forces are neglected) and are given by:

$$F_{JKR} = 3\pi\Delta\gamma R_{part} \tag{29}$$

(b) DMT theory (named after the work of Derjaguin–Muller–Toporov [195]). The DMT theory is another contact theory that considers the elastic deformation of surfaces (according to the Hertzian theory only) but that includes also non-contact forces (van der Waals contribution) which act across the gap between the two surfaces. The DMT theory is valid for $\mu_T \ll 1$, i.e. for small or 'hard' (slightly deformable) particles.
Contact forces are thus obtained as van der Waals forces occurring between surfaces in the close vicinity of the contact point and the corresponding formula for the pull-off force is given by:

$$F_{DMT} = 4\pi\Delta\gamma R_{part} \tag{30}$$

(c) The transition from JKR to DMT theories has been extensively studied in the literature [56,190,196,197]. A simple theory has been proposed by Maugis [198] to connect the JKR and DMT theories and is often referred to as the Maugis–Dugdale model. For that purpose, Maugis simplified the typical Lennard-Jones potential of force-distance curve into a 'Dugdale' (square-well) potential: a constant adhesive force of intensity σ_{Maugis} is assumed within an annular region (within a distance δ_{Maugis}) around the contact area [191,196,198]. As a result, the adhesion force is given by the sum of two component: the contact force given by the Hertz theory and the adhesion force obtained from the 'Dugdale' potential. The theory then naturally retrieves both JKR and DMT theories when a parameter (equivalent to the Tabor parameter μ_T) is changed.

(d) Hamaker approaches [56,199] are adhesion mechanics theories where the adhesion energy (or force) is obtained from the particle–surface interaction energy evaluated, using the DLVO theory, at a given cut-off distance z_0 (whose value is in the molecular range, often taken equal to $z_0 = 0.165$ nm [56]).

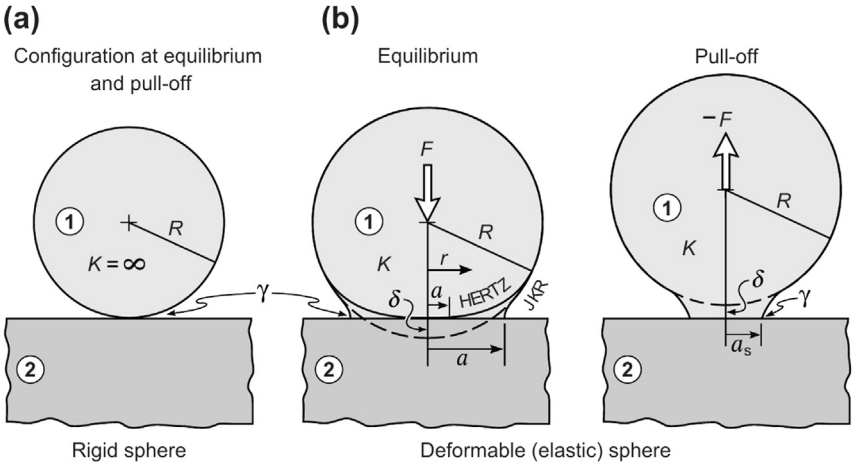

Fig. 15. Sketch of the geometry of surfaces in contact: (a) rigid surfaces, (b-left) deformable elastic sphere on a rigid surface under external compressive force, (b-right) deformable elastic sphere about to detach from a rigid surface. Reprinted from [56]. Copyright 2011 with permission from Elsevier.

Adhesion forces are thus obtained from non-contact interactions between the two surfaces:

$$F_{\mathrm{DLVO}}^{\mathrm{adh}} = F_{\mathrm{VDW}}(z_0) + F_{\mathrm{EDL}}(z_0) \tag{31}$$

where F_{VDW} and F_{EDL} are the van der Waals and electrostatic double-layer forces described in Section 2.2.

However, as pointed out by Eichenlaub et al. [130], the influence of electrostatic conditions on adhesion forces is not always significant. Indeed, depending on the solution conditions (pH, ionic strength), EDL contributions to the adhesion force can be comparable to or greater than VDW attraction (yet, this does not occur frequently in experiments). Thus, the vast majority of Hamaker approaches only include the VDW contribution to adhesion forces [150,152,154,200–204]. Yet, some experimental studies have underlined that the adhesion forces vary with pH conditions [130,205–208], as well as with the ionic strength [128,130]. Therefore, a few studies [128–130,209–212] do include the two aspects of the whole DLVO theory (i.e. both VDW and EDL forces) in the calculation of the adhesion energy.

It should be noted that, even though contact and adhesion mechanics theories have been obtained using different assumptions, they are still closely related (see also the Maugis–Dugdale model): for instance the formula for contact forces obtained with the DMT formula is identical to the formula obtained considering a Hamaker approach but with van der Waals forces only (without any electrostatic forces). This can be understood since, in the DMT theory, the pull-off force is obtained when the radius of the contact area reaches zero (rupture of contact) [197]. More precisely, the link between surface energies and Hamaker constants is given by [213]: $A_{Ham} = \Delta\gamma\ 24\pi z_0^2$.

However, even though these contact and adhesion mechanics theories have been shown to provide satisfying predictions of adhesion forces (as long as their range of validity is respected) [56], they have been developed using simplified assumptions. In particular, both contact and adhesion mechanics theories consider perfectly homogeneous and smooth surfaces whereas many experimental data have shown that surfaces can exhibit non-negligible surface roughness or even surface charge/potential heterogeneities [18,192,211,214]. Furthermore, contact mechanics theories do not consider plastic deformations. For that reason, the M–P theory (named after the work of Maugis–Pollock [215]) has been developed to include the contribution of plastic deformation in the JKR theory. Besides, Hamaker approaches do not include non-DLVO forces in the evaluation of adhesion forces. In the following, existing theoretical works that have studied and extended the range of applicability of these theories are reviewed and analysed.

4.1.2.1. Surface roughness. One of the main difficulties that arise in contact or adhesion theories is linked with the presence of surface roughness. As seen in Section 3.3, AFM and SEM images have shown that surfaces are often rough and that nanoscale surface roughness can significantly reduce adhesion forces. Besides, the random nature of surface roughness (with both inhomogeneous spatial location and size distributions) leads to intricate interactions between rough surfaces [199].

Various models have been proposed to study the impact of surface roughness on particle–surface interactions (see a first account in Section 2.4) and were reviewed recently by Prokopovich and Starov [192]. Since surface deformation can play a significant role in contact forces, the models have been organised with respect to the description of deformation: the resulting classification of the different models is summarised in Fig. 16. With respect to this classification and to the issue of surface roughness (SR in the list below), the following comments can be made:

(SR-i). The use of a Hamaker approach to account for surface roughness is widely used in the literature since this approach has been extensively studied for the description of non-contact particle–surface interactions. The difficulty in that case is to choose a relevant description of surface roughness. As pointed out by Eichenlaub et al. [209], some models consider fractal surfaces while other models are based on Fourier transforms [216] as well as hemispherical asperities [150,152,154,200–204,217,218]. Besides, similar approaches as SEI methods (that have been presented for non-contact forces in Section 2.4) have been proposed to evaluate the adhesion between rough surfaces [219].

Several models based on a Hamaker summation approach with hemispherical asperities have investigated the effect of a single asperity on van der Waals forces between a sphere and a plate [220]. For instance, Rumpf [220] studied the adhesion between a particle (radius R_{part}) and a plate with a single protruding nano-spherical asperity (radius R_{asp}). They obtained the following formula for the adhesion force:

$$F_{\mathrm{adh}} = \frac{A_{\mathrm{Ham}}}{6z_0^2}\left(\frac{R_{\mathrm{part}}R_{\mathrm{asp}}}{R_{\mathrm{part}}+R_{\mathrm{asp}}} + \frac{R_{\mathrm{part}}}{\left(1+R_{\mathrm{asp}}/z_0\right)^2}\right) \tag{32}$$

where z_0 is the contact distance. It can be seen that the overall interaction is the sum of an asperity-particle contact force (first term on the right-hand side) and a non-contact force between the particle and the surface (second term). This simple model has provided insights into the effect of nanoscale roughness on the adhesion force: the presence of an asperity increases the minimum distance between the plate and the particle leading to much lower particle-plate forces, while particle-asperity adhesion forces are significantly smaller than particle-plate adhesion due to the Derjaguin prefactor $R_{\mathrm{part}}R_{\mathrm{asp}}/(R_{\mathrm{part}}+R_{\mathrm{asp}})$. This single-asperity model was refined by Rabinovich et al. [200], who included a more detailed representation of roughness using the root-mean-square (r.m.s.) roughness $R_{\mathrm{asp}}^{\mathrm{rms}}$ and the peak-to-peak distance between asperities λ_{asp}:

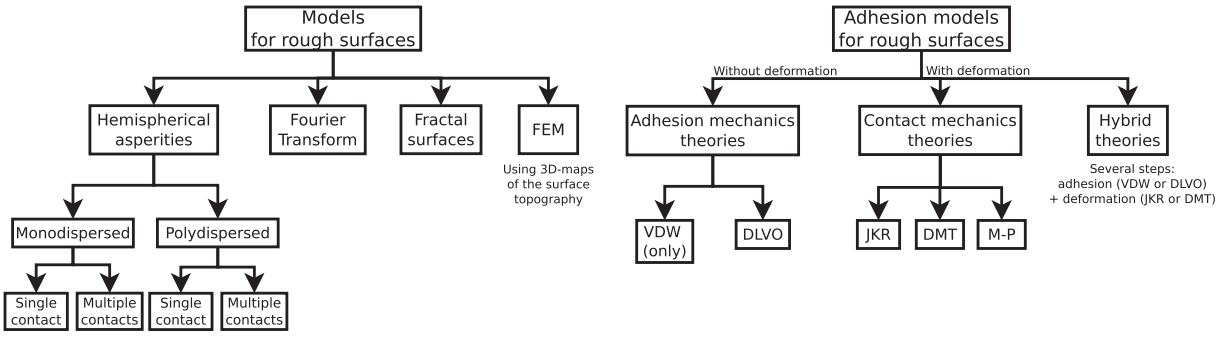

Fig. 16. Sketch summarising the various categories of models to generate a rough surface (left) and to calculate the corresponding particle–surface adhesion forces (right).

$$F_{adh} = \frac{A_{Ham} R_{part}}{6 z_0^2} \left(\frac{1}{1 + \frac{58.144 R_{part} R_{asp}^{rms}}{\lambda_{asp}^2}} + \frac{1}{\left(1 + \frac{1.817 R_{asp}^{rms}}{z_0}\right)^2} \right) \quad (33)$$

This refined model indicates that asperity shapes significantly impact adhesion forces between surfaces but that the complexity of rough surfaces can be captured by detailed models using few statistical characteristics such as R_{asp}^{rms} and λ_{asp}. These models have been compared to various experimental data, showing generally good agreement [150,154,221,222]. Yet, such models do not account for multi-asperity contacts that can occur when two complex rough surfaces are in contact. For that purpose, other refined models have been proposed by considering that multiple contacts can occur with asperities in a given area. For instance, Katainen et al. [223] replaced the first term on the left hand side of Eq. (33) by N times the particle-asperity interaction (N being determined according to the area of contact and the density of asperities). Similar modified Derjaguin approaches have been used but considering the whole DLVO interaction in the adhesion between rough surfaces. In one example, 3D-maps of particle–surface interactions in the presence of one or two hemispherical asperities have been used to study the adhesion and removal behaviour of colloids [211]. Another recent model has explicitly included the distribution in the size of asperities that are in contact with the particle and the adhesion force has been obtained by summing all DLVO components (particle–surface and particle-asperities in contact) [210].

The choice of an appropriate description often boils down to a balance between computational costs and model precision: it can be easily understood that a model using a fractal description of surface roughness is more complex than a simple model using hemispherical asperities. It is also less restrictive (since intricate geometries can be reproduced numerically) but is much more computationally demanding. Yet, models based on hemispherical asperities allow fast evaluations of the adhesion force and can thus provide valuable statistical information on adhesion forces between rough surfaces without requiring too many parameters.

(SR-ii). Other models are based on contact mechanics theories and thus take into account surface deformations in the calculation of adhesive forces between rough surfaces. As for models based on adhesion mechanics theories, the difficulty is to account for the complex nature of surfaces in contact. Greenwood and Williamson [224] have mainly contributed to the development of models for the contact between complex surfaces: they considered a surface covered by an ensemble of identical spherical asperities (constant radius) but with randomly distributed height (following a Gaussian distribution). This model has been widely used in the literature [192,225] and further developed to include a (Gaussian) distribution in the asperity radius [226,227]. More recently, another multi-asperity adhesion model was developed by Prokopovich and Perni [151] that includes the distribution in asperity height and curvature radius but without assuming a specific distribution. A rough surface is also modelled by placing a certain number of asperities (respecting the asperity density) whose size is randomly generated respecting the distribution. The force is then calculated as resulting from the summation of the effect of each asperity taken separately (using JKR or DMT theories) and the adhesion force is extracted from the force-distance curve (the contact force is zero when no contact exists).

(SR-iii). Hybrid approaches have also been proposed [155,201,202,203]: the idea is to couple a contact mechanics theory for surface deformation and a Hamaker summation to determine particle–surface adhesion forces between two rough surfaces.

Some approaches calculate the adhesion between rough surfaces using a Hamaker summation and considering multi-asperities in the contact area, whose size is given by deformation theories. As for Hamaker approaches, such hybrid approaches differ in the level of description of surfaces: some studies assumed hemispherical asperities on a surface [201,202] whereas other models were based on a finite element method (FEM) for surface deformations [155].

More complex hybrid approaches require step-by-step calculations of the adhesion force: the two surfaces are first brought together until contact; the resulting adhesion is then calculated by summing all interactions over the exact topographies; this adhesion force is then used to predict asperities deformation and thus the new separation distance between surfaces; the adhesion-deformation steps are repeated several times (until a certain precision is reached). For instance, Cooper et al. [203] calculated the adhesion force between two surfaces whose topography was characterised experimentally using AFM and SEM measurements and such a hybrid approach.

In that sense, the previous simple hybrid approaches [155,201,202] are specific cases of the complex hybrid approaches, with only a single coupling step. These complex hybrid approaches are much more precise since roughness is considered using the exact surface topography and deformation is explicitly accounted for respecting the adhesion force in a specific geometrical configuration. However, the computational costs associated with such hybrid models can be much higher and thus not adapted to obtain statistics on a large number of particles contacting a rough surface.

4.1.2.2. Charge heterogeneities. Similarly to models for surface roughness, two approaches have been proposed to include surface charge/potential heterogeneities (CH in the list below) in the DLVO interaction.

(CH-i): a first approach is to consider the interaction between two surfaces having constant potentials/charges. The value of the potential/charge is given by the average potential/charge over the area of influence, i.e. the area where surfaces are in very close proximity and where interactions are thus impacting significantly the adhesion properties [219,228]. This approach allows fast evaluations of the statistical information (minimum, maximum, mean value) that quantify the effect of surface charge/potential heterogeneities on particle adhesion [219] and on particle reentrainment [229].

(CH-ii): another approach consists of explicitly summing the interaction between all heterogeneous patches present on the surfaces, using an Hamaker approach [218,228] (similarly to the SEI techniques presented in Section 2.4). This approach has provided insights into the effects of the patch size (very small patches do not influence adhesion), as well as of the patch shape and potential on particle adhesion. The main advantage of this approach lies in the fact that it remains valid even for very complex topographies but it can lead to very high computational costs (depending on the size of the patches).

4.1.2.3. Elasto-plastic transition. Existing contact mechanics theories mainly account for elastic deformation of surfaces upon contact (JKR, DMT theories). The M–P theory includes the contributions from plastic deformation to the contact forces. However, only a few specific models have been proposed to include plastic deformations in more general contact theories of elasto-plastic deformations [230]. Elasto-plastic deformation can play a role in the dynamics of resuspended or bouncing particles: particles impacting the surface with a high wall-normal velocity can indeed give rise to plastic deformations of the surfaces which change the adhesion characteristics. However, due to the complexity of the transition from elastic to plastic deformation, comprehensive models for elasto-plastic deformation have been seldom studied in the literature [225].

4.1.2.4. Shape of interacting surfaces. Another consequence of the short-range of adhesion forces is that particle shapes can significantly impact the strength of adhesion forces. Indeed, adhesion forces between two surfaces are mainly governed by the interaction between areas/volumes that are very close to each other [151,156,210,216,231]. Therefore, as depicted in Fig. 17 for ellipsoidal asperities on a surface, when determining the interaction between two surfaces, the curvature radius of the surfaces facing each other is the relevant parameter [33].

4.1.2.5. X-DLVO theories. In Hamaker approaches, particle–surface interactions are generally described using the DLVO theory and several studies consider only the van der Waals contribution to adhesion forces [192,201]. However, as seen the review of experimental data on resuspension in Section 3.3, more complex forces can play a role in particle–surface adhesion. For instance, acid-base interactions are often added to the classical DLVO theory (leading to so-called X-DLVO theories or Extended-DLVO theories) to describe the adhesion between hydrophilic/hydrophobic surfaces [88,132,139,141,232]. Acid–Base (AB) forces arise from the interaction between electron-donor and electron-acceptor areas on both surfaces. Acid–base interactions can be characterised by two surface tension parameters: the electron-donor surface tension parameter γ^- and the electron-acceptor surface tension parameter γ^+. The acid-base surface tension between two materials across water γ_{1w2}^{AB} is given by [233]:

$$\gamma_{1w2}^{AB} = 2\sqrt{\gamma_w^+}\left(\sqrt{\gamma_1^-}+\sqrt{\gamma_2^-}-\sqrt{\gamma_w^-}\right)+2\sqrt{\gamma_w^-}\left(\sqrt{\gamma_1^+}+\sqrt{\gamma_2^+}-\sqrt{\gamma_w^+}\right)-2\left(\sqrt{\gamma_1^-\gamma_2^+}+\sqrt{\gamma_1^+\gamma_2^-}\right) \quad (34)$$

Acid–base interaction energy between two particles (radius R_1 and R_2) is given by:

$$U_{AB} = -2\pi\frac{R_1R_2}{R_1+R_2}\lambda_{AB}\gamma_{1w2}e^{(h_0-h)/\lambda_{AB}} \quad (35)$$

where γ_{1w2}^{AB} is the surface tension [233], λ_{AB} is the decay length of the liquid molecules (λ_{AB} between 0.2 nm and 1 nm [234,235]) and h_0 is the minimum equilibrium distance ($h_0 = 0.158$ nm) [234,235]). It is worth noting that such forces are naturally included in contact mechanics theories since this contribution is already included in surface energies.

In addition, other studies include the effect of short-ranged Born repulsion in the DLVO theory to evaluate the adhesion between 0.78 μm latex spheres and silicate in porous media [135], or of structural forces [236] as well as specific surface reactions [205].

4.2. Particle motion initiating resuspension

We now turn our attention towards the result of the interplay between the hydrodynamical and adhesion forces and its role in the resuspension phenomenon. This coupling between particle–fluid and particle–surface interactions results in complex mechanisms for particle resuspension: rolling, sliding and lifting motion for particles in contact with a surface have been proposed in the late 20th century [112,118,163,166,237] and there has been a continuous debate regarding the relevance of each mechanism in the resuspension phenomenon [1,89,114]. Following some experimental studies and more fundamental investigations of these mechanisms [113], a common agreement has emerged that lift forces do not play a significant role in the resuspension of colloidal particles which are more sensitive to rolling motion [1,238] but these lift forces can be significant for large particles. This is in line with the analysis made in Section 3.1, where it was shown that the relative importance between rolling motion and coherent structures in resuspension depends on particle sizes (small particles ($d_p \lesssim \delta_{VS}$)) tend to roll on the surface before being reentrained while larger particles ($d_p \gtrsim \delta_{VS}$) are more sensitive to coherent structures). In the following, the mechanisms of particle rolling, sliding or lifting are summarised and illustrated with examples from a few available experimental studies.

4.2.1. Rolling motion

Particles start rolling on a surface when the balance between the moment of hydrodynamic forces and the moment of adhesion forces is broken. For example, the rolling resistance of deformable 21.4 μm polystyrene latex (PSL) particles was studied in detail by Ding et al. [239]. For that purpose, PSL particles were first deposited on the surface and, then, an AFM cantilever was brought in contact with a PSL sphere and a tangential force was exerted on the particle using the AFM (see Fig. 18). The displacement (due to rolling motion) of each particle was recorded using SEM images and the force-displacement relationship was extracted and analysed to underline the rolling resistance exhibited by some particles.

Since rolling motion depends on the balance between hydrodynamic and adhesion forces, theories for rolling particles are based on a moment balance approach describing the evolution of the particle rotational motion, through the evolution equation [1,88,94,97,145,237,240,241]:

$$I\frac{d\omega_p}{dt} = M(F_{rot}) - M(F_{c-rot}) \quad (36)$$

where I is the moment of inertia of the particle, ω_p is the particle angular velocity, $M(F_{rot})$ is the moment of forces that tend to put particles in motion whereas $M(F_{c\text{-}rot})$ is the moment of forces that

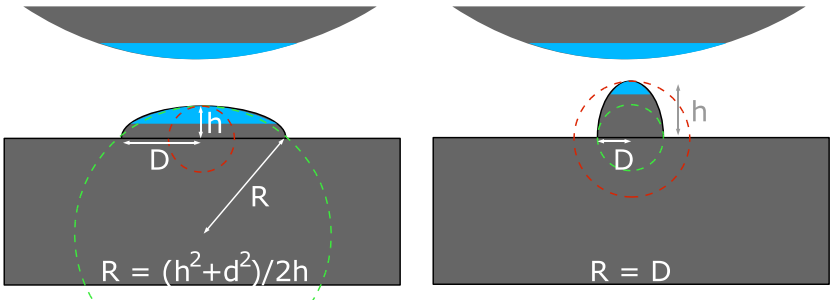

(a) Broad ellipsoidal asperities (b) Slender ellipsoidal asperities

Fig. 17. Illustration of the dependence of adhesion forces on the curvature radius. Reprinted from [33]. Copyright 2012 with permission from Elsevier.

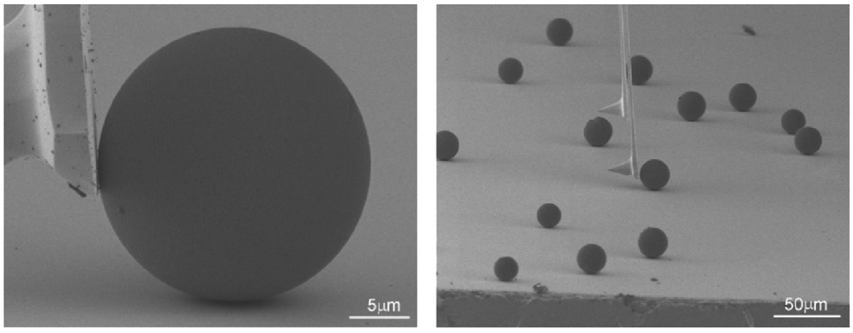

Fig. 18. SEM images of PSL particles showing AFM cantilever used to push particles. Reprinted from [239]. Copyright 2007 with permission from Taylor and Francis.

counter rolling motion. Following the various experimental observations of particle reentrainment due to rolling motions described in Section 3, hydrodynamic drag forces are often considered to be responsible for particle rolling motion while adhesion forces tend to prevent particle from rolling on surfaces.

4.2.2. Sliding motion

Similarly to rolling, sliding motion happens when hydrodynamic and adhesion forces are unbalanced. Yet, contrary to rolling which induces a particle rotation, sliding motion occurs when particles are translated on the surface without rotation. For instance, tangential sliding motions of various cylindrical particles were measured experimentally by Onoe et al. [242]. For that purpose, AFM cantilevers were used to push particles tangentially to the surface and to record the resulting motion of particles (see Fig. 19): this procedure allows to relate the resistance to sliding motion and the binding forces between particles and the substrate. The authors have shown that particles can slide on the surface depending on their shape and size (more complex jump phenomena were reported by the authors but these phenomena are not discussed in the present case since they are out of the scope of the review article).

From a theoretical point of view, particle sliding motion on a surface is described by a force-balance approach in the wall-tangential direction [1,94,97,145,241]:

$$m_p \frac{dU_{p,//}}{dt} = F_{slid} - F_{c-slid} \quad (37)$$

where m_p is the particle mass, $U_{p,//}$ is the particle tangential velocity, F_{slid} corresponds to the sum of all tangential forces acting to move particles while $F_{c\text{-}slid}$ regroups the various forces that prevent sliding motion. Following the various experimental observations of particle reentrainment linked with sliding motions described in Section 3, the forces due to hydrodynamic drag forces are often considered to be responsible for particle sliding motion while friction due to adhesion forces prevent sliding motion. Friction due to adhesion forces is proportional both to the adhesion force and to the coefficients of friction μ_s (static or dynamic): $F_{frict} = \mu_s F_{adh}$.

4.2.3. Lifting motion

Particle lift-off from surfaces has been extensively studied using centrifuge experiments to apply a wall-normal force on deposited particles [91,101,113,114]. Similarly, experiments based on an oscillating surface have also been developed to study the sediment lift-off (see for instance [243]). Following the various experimental data on particle lifting motion described in Section 3, theories for particle lift-off are based on a force-balance approach in the wall-normal direction [1,94,97,241]:

$$m_p \frac{dU_{p,\perp}}{dt} = F_{lift} - F_{c-lift} \quad (38)$$

where m_p is the particle mass, $U_{p,\perp}$ is the wall-normal particle velocity, F_{lift} corresponds to the sum of all wall-normal forces acting to lift particles from the surface while $F_{c\text{-}lift}$ regroups the various forces that prevent it. It is commonly accepted that hydrodynamic lift forces play a role in particle lift-off from surfaces while adhesion forces tend to keep the binding between particles and surfaces (depending on the situation, gravity force can also be significant in lifting motion).

4.3. Summary and perspectives for future studies

With respect to the material introduced in this section, three comments can be made.

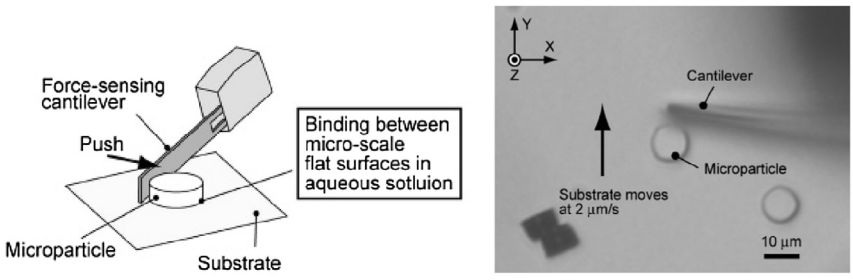

Fig. 19. Illustration and optical image of the measurement method for sliding motions using AFM cantilevers to push particles tangentially to the surface. Reprinted from [242]. Copyright 2005 with permission from American Chemical Society.

First, there is a consensus that the hydrodynamical effects on deposited particles can still be expressed in terms of the classical drag and lift forces, as for particles in the core of the fluid flow. However, the presence of the wall induces strong non-homogeneities that are difficult to capture theoretically. As a result, different formulas are available in the literature and the choice of a specific formulation should be made with care and keeping in mind its range of validity. Among all these formulations, it appeared that the current level of description of lift forces is limited to relatively large particles ($0.3 < \mathrm{Re_p} < 70$). Yet, since it has been shown that lift forces do not play a significant role in the resuspension of colloidal particles, these restrictions are not unsustainable. On the other hand, with the emergence of recent experimental studies on the lift force exerted on bubbles [182,183] as well as numerical works on the lift force on spherical rigid particles [184–186] at various particle Reynolds number and different particle wall-distance, it is believed that new correlations will be developed.

Second, the existing works on particle–surface interactions at contact provide expressions for the adhesion force which is an important element of the resuspension mechanism. It has been shown that the various theories differ depending on whether elastic or plastic deformations, DLVO forces, surface roughness, surface charge heterogeneities or X-DLVO forces are taken into account. These theories are not just mere variations of a common approach that would underly each of the formulations analysed here but appear as widely different. Compared with the situation about the hydrodynamical drag and lift forces, it is seen that the issue of adhesion forces is actually more intricate. On the one hand, well-founded theories are put forward but, on the other hand, they have been developed in different situations which are not easily reconcilable. In that sense, the main difficulty in particle–surface (or particle–particle) forces is that, at the moment, no unified theory that proposes a single view on the question of the adhesion forces acting on deposited particles has been established and that no consensus exists. Clearly, coming up with a clear-cut and well-established picture of adhesion forces is still a goal that requires further work. Yet, drawing on available formulations, it appears that the question of how adhesion forces (and their distributions) are included and accounted for in a particle resuspension model is an important issue. It will be seen that this is a central argument in the discussion of the various modelling proposals in Section 5.

Third, it appears that the different mechanisms of particle motion (i.e. rolling, sliding and lifting) can be gathered in a single formulation if a complete mechanical description, including both particle translational and angular momentum, is applied (as used for instance by Lee et al. [186,244]):

$$\begin{cases} m_{\mathrm{p}} \dfrac{\mathrm{d}\mathbf{U}_p}{\mathrm{d}t} = \sum \mathbf{F}_{\mathrm{transl}} - \sum \mathbf{F}_{\mathrm{c-transl}} \\ I \dfrac{\mathrm{d}\boldsymbol{\omega}_p}{\mathrm{d}t} = \sum \mathbf{M}(F_{\mathrm{rot}}) - \sum \mathbf{M}(F_{\mathrm{c-rot}}) \end{cases} \tag{39}$$

where $\sum \mathbf{F}$ and $\sum \mathbf{M}$, the sum of all forces and torques exerted on the particle, have been decomposed into one part representing the effects acting to move the particle (typically, hydrodynamical forces and moments) and a second part representing the effects acting to prevent the particle from moving (typically, adhesion forces and moments). This description includes naturally all the contributions for rolling, sliding and lifting motion since the effects of hydrodynamic and adhesion forces are properly accounted for. Furthermore, this approach can be easily extended to more complex flows by adding the relevant forces on the rhs of Eq. (39) (such as gravity, added-mass or Basset forces). It is worth noting that the forces at play in particle resuspension are the same, regardless of the particle size. Only their relative importance explains the differences between the behaviour of small and large particles that is observed experimentally (see Section 3: large particles are mainly influenced by gravity and particle–fluid forces, leading to burst-type resuspension events in turbulent flows; small particles are much more sensitive to adhesion forces, leading to rolling motion). Thus, with respect to the description of particle motion made in Eq. (39), it is seen that particle-based approaches represent a natural level of description. In that sense, it is not surprising that they are often found in modelling attempts.

5. Existing resuspension models from monolayer deposits

A wide range of resuspension models has been proposed in the literature and this variety makes reviewing them a rather challenging task. Indeed, not only the resulting forms but also the underlying physical descriptions as well as the assumptions on which these models are built can be very diverse. Therefore, coming up with a clear classification in which all models properly fit in is not straightforward. In previous reviews [1,89,114,189], an often-used classification consists of separating models between two categories: force-balance and energy-accumulation approaches. The former category refers to models where resuspension is addressed by comparing the forces acting on deposited particles while the latter refers to models where resuspension is addressed by assessing particle vibrational energy (through small deformations) and comparing it to adhesive energy barriers. With respect to this classification, two remarks can be made:

(i) there has been a long debate regarding the range of applicability and the accuracy of the force-balance and energy-accumulating models [1]. However, as underlined in Section 3.1, the mechanisms of particle resuspension depend on the particle size with respect to the extent of the boundary layer. As a result, models developed for different purposes cannot be directly compared, rendering the past debate less pertinent. It is thus important to analyse the various modelling attempts with respect to their corresponding context and assumptions, before discussing their interests and limits;

(ii) even though the basis of the force-balance and energy-accumulating approaches are somewhat different, it is worth recalling that these models are actually 'static approaches' in which resuspension is assumed to take place as soon as particle equilibrium on a surface is broken. Thus, these models can be classified as detachment models with respect to (def-2) in Section 1. The terminology of 'static approaches' refers to the fact that particles are not considered as actually moving along the wall and, as such, that there is no proper account of particle dynamics along wall surfaces (even though particles can be vibrating or oscillating, but around the same point, in energy-accumulation models). On the other hand, extended approaches that propose a refined resuspension mechanism (including rupture of equilibrium, particle motion along walls and a specific criterion for the actual detachment) have appeared recently [210,245–247]. In that sense, these new modelling approaches are outside the boundaries of the usual classification.

In the present work, we propose an enlarged classification in which resuspension models are gathered according to the level of description of particle motion on the surface. This new structure is sketched in Fig. 20. A first separation is made between empirical formulas and approaches that rely on a description of deposited

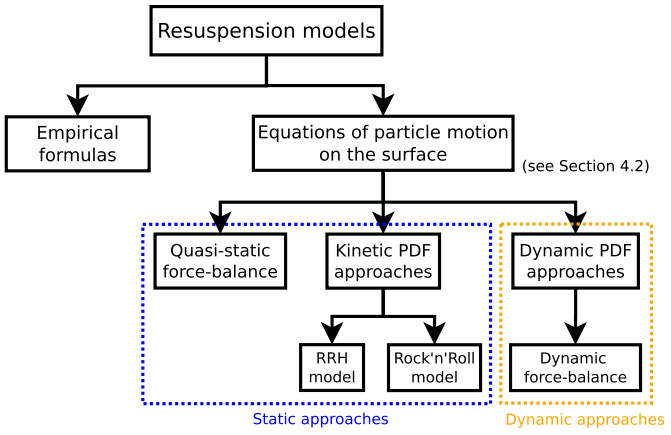

Fig. 20. Sketch summarising the classification of modelling approaches for particle resuspension.

particles through a set of particle equations. This second category is further split between a first ensemble that considers only particle equilibrium (and its rupture) and which encompasses the usual force-balance and energy-accumulating models, and a second ensemble of approaches that retain both particle equilibrium as well as its detailed dynamics on the surface as the relevant description. Following the remark made in point (i), the accuracy and range of validity of each approach is also clarified. In that sense, the presentation of the kinetic-based models is not a mere reformulation of previous accounts but introduces specific comments and corrected expressions (for the Rock'n'Roll model). Moreover, it is useful to be aware of how these models operates to fully grasp the new elements brought in by dynamical approaches. Throughout the discussions of the various modelling attempts, another important objective is to emphasise the nature and the amount of information that needs to be assumed and input in each approach.

Layout of this section. Empirical formulas for particle resuspension are first reviewed in Section 5.1, followed by a description of quasi-static force-balance approaches in Section 5.2. Kinetic-based PDF approaches (such as energetic approaches) are then presented in Section 5.3 while Dynamic-based PDF approaches are detailed in Section 5.4. The various models are briefly summarised in Section 5.5 and analysed with respect to experimental findings (see Section 3) to highlight the potential benefits of recent developments in the framework of dynamic models.

Measuring particle resuspension. Before going into the details of resuspension models, it is worth recalling that particle resuspension is generally expressed in terms of a resuspension rate k_r defined as:

$$k_r = \frac{J_{reent}}{C_{surf}} \tag{40}$$

with C_{surf} the initial surface concentration of particles (in kg.m^{-2}) and J_{reent} the flux of reentrained particles (in kg.m^{-2}.s^{-1}). It is interesting to note that the particle resuspension rate has the dimension of a frequency (in s^{-1}). Indeed, k_r appears as the "intensity" with which the resuspension of particles takes place. For instance, if we consider (for the sake of simplicity) a collection of N monodispersed particles sticking on a surface then, over a small time interval Δt, the number of particles being resuspended is equal to $Nk_r\Delta t$. In other words, if we consider all adhering particles as independent samples, then $k_r\Delta t$ is the probability for one particle of being resuspended during the time interval Δt. This interpretation allows the resuspension rate $k_r(t)$ to be properly expressed for each adhering particle at time t as

$$k_r(t) = \lim_{\Delta t\to 0}\frac{1}{\Delta t}\mathbb{P}\left[y_p(s)>0 \middle| y_p(t)=0; t\le s\le t+\Delta t\right] \tag{41}$$

where $y_p(s)$ denotes the wall-normal particle coordinate (with $y_p(s)=0$ when the particle is sticking on the wall and $y_p(s)>0$ when the particle is reentrained within the flow).

The resuspension rate is most meaningful for a monodispersed set of particles or when it is evaluated for each particle class of diameter. However, in the case where particles are polydispersed, it is best to express the overall resuspension rate by introducing the particle distribution $p(t,\mathbf{x}_s;d_p)$, which measures how particle diameters are distributed for the sticking particles in a unit surface section centered at point $\mathbf{x}_s$ located on the wall surface at time t. Then, the total number of particles (per unit surface) is given by

$$N_{tot}(t,\mathbf{x}_s) = \int p(t,\mathbf{x}_s;d_p)\mathrm{d}d_p \tag{42}$$

while for each class of particle diameter, labelled as [i], and defined as the class of particles whose diameter is in the range $d_p\in[d_{p,min}^{[i]};d_{p,max}^{[i]}]$, the total number of particle $n^{[i]}(t,\mathbf{x}_s)$ within this class is

$$n^{[i]}(t,\mathbf{x}_s) = \int_{d_{p,min}^{[i]}}^{d_{p,max}^{[i]}} p(t,\mathbf{x}_s;d_p)\mathrm{d}d_p. \tag{43}$$

For each particle class, the interpretation expressed in Eq. (41) is valid and provides the value of the resuspension rate for this class, say $k_r^{[i]}(t,\mathbf{x}_s)$. In a continuous sense, the resuspension rate is a function of the particle diameter and can be written as $k_r(t,\mathbf{x}_s;d_p)$. Then, the overall resuspension rate $\widetilde{k_r}(t,\mathbf{x}_s)$ measured over the whole range of particle diameter is given by

$$\widetilde{k_r}(t,\mathbf{x}_s) = \frac{\int k_r(t,\mathbf{x}_s;d_p)m_p(d_p)p(t,\mathbf{x}_s;d_p)\mathrm{d}d_p}{\int m_p(d_p)p(t,\mathbf{x}_s;d_p)\mathrm{d}d_p} \tag{44}$$

and appears as the mass-weighted average of the monodispersed resuspension rates (with $m_p(d_p)=\rho_p\pi d_p^3/6$ the mass of one spherical particle). Note also that the previous equation involves the Mass Density Function (MDF) of the deposited particles on the unit surface at point $\mathbf{x}_s$ and time t, which is indeed the natural distribution to consider in the PDF approach to two-phase flow modelling [35,248], since for the subset made up by the deposited particles we have

$$m_p(d_p)p(t,\mathbf{x}_s;d_p) = \int F_p(t,\mathbf{x}_s;\mathbf{U}_p,d_p)d\mathbf{U}_p \tag{45}$$

where $\mathbf{U}_p$ is the sample-space variable for particle velocities (the same notation d_p have been kept for the particle diameter for sake of simplicity).

It is also worth noting the difference with the reverse process, namely particle deposition from the fluid on a wall surface. Indeed, for particle deposition, the relevant measure is the particle deposition rate which is defined as

$$k_p = \frac{J_{dep}}{C_{vol}} \tag{46}$$

where J_{dep} is the flux of deposited particles (still in kg.m^{-2}.s^{-1}) but where C_{vol} is the particle concentration within the fluid and is thus a volumetric concentration (in kg.m^{-3}). As a result, k_p has the dimension of a velocity (in m.s^{-1}) and stands for the equivalent

velocity with which deposited particles flow from the fluid towards the wall surface. Thus, even if the two corresponding fluxes J_{dep} and J_{reent} are symmetrical quantities having the same dimensions, the deposition process is represented by a characteristic velocity while the resuspension process is represented by a characteristic frequency.

5.1. Empirical models

A first group of models consists of macroscopic empirical models which aim at predicting resuspension by the direct application of given formulas or correlations. As a result, these macroscopic models are highly dependent on the specific context in which these correlations have been devised. Besides, as underlined in a recent review of source term models for particle resuspension from indoor surfaces [9], the complexity of such empirical models depends also on the number of parameters used to describe particle resuspension.

For instance, several empirical formulas have been proposed for dust or radionuclide resuspension in outdoor environment. In that case, particle resuspension is often expressed with the resuspension factor K (in m^{-1}) which corresponds to the air concentration of particles divided by the initial surface deposit (a useful quantity in atmospheric studies). Moreover, these studies of particle resuspension in outdoor environment are focussed on the amount of elements released from the ground after a long time (a few hours up to a few days), where the quantity of resuspended materials is high enough to have an environmental impact (and thus easy to record). Therefore, it is not surprising that most empirical formulas for the resuspension factor K have been expressed with a dependence on time only: either an exponentially decaying function of time [249] or a function inversely proportional to time [250] were shown to fit experimental data. Yet, these models have been derived assuming spatially homogeneous initial deposition (dusts of 2–10 μm) and they remain valid only for outdoor long-term resuspension (i.e. several days of resuspension).

These empirical models for long-term outdoor resuspension fail to capture the features related to resuspension at small times since they have been designed for another purpose. Yet, to extend the validity of such empirical models, other correlations have been obtained for dust resuspension in wind tunnels [251]: the resuspension rate was derived considering both its dependence on time and on the turbulent kinetic energy k. The correlation was shown to remain valid also for short-time resuspension due to the increased complexity of the model, which now includes a parameter related to microscopic features. Other refined empirical models have been proposed by Loosmore [250,252] who extracted correlations from three independent measurements of micrometre particle resuspension ($0.006 < d_p^+ < 0.9$) in wind tunnel experiments with surfaces representative of outdoor environments (grass, concrete, bare soil). These empirical formulas have been developed considering not only the time t but also the friction velocity u_τ, the particle diameter d_p, the surface roughness d_{asp} and on the particle density ρ_p:

$$k_r = 0.01\frac{(u_\tau)^{1.43}}{t^{1.03}} \tag{47a}$$

$$k_r = 0.42\frac{(u_\tau)^{2.13} d_p^{0.17}}{t^{0.92} d_{asp}^{0.32} \rho_p^{0.76}} \tag{47b}$$

It should be noted that Eqs. (47a) and (47b) are formulas for the resuspension rate expressed in s^{-1} but a dimensional analysis shows that, to respect such a condition, the prefactors 0.01 and 0.42 are not dimensionless (this point was not properly mentioned in the original article but certainly deserves attention!). These formulas were shown to fit adequately the experimental results for short-term resuspension (i.e. here ≤24 h). However, the range of validity of such formulas is limited to the conditions involved.

More recently, Kim et al. [9] developed new and more general empirical formulas using a dimensional analysis and choosing the relevant parameters according to the mechanisms that are believed to play a role in particle resuspension. Considering that resuspension occurs due to the balance between van der Waals adhesion forces and hydrodynamic forces, they chose to express the resuspension rate as a function of the particle density ρ_p, the elapsed time t, the friction velocity u_τ, the particle diameter d_p, the asperity diameter d_{asp} and the Hamaker constant A_{Ham}. The resulting correlations were shown to be written as:

$$k_r = c_0\frac{u_\tau}{d_p}\left(\frac{\rho_p}{\rho_f}\right)^{c_1}\left(\frac{u_\tau t}{d_p}\right)^{c_2}\left(\frac{d_{asp}}{d_p}\right)^{c_3}\left(\frac{A_{Ham}}{d_p^3(u_\tau)^2\rho_f}\right)^{c_4} \tag{48}$$

where c_0–c_4 are constant coefficients which are tuned on a selected data set. Compared to the first formulas mentioned above, expressions such as the one entering Eq. (48) are put on a better footing since k_r is now estimated in terms of non-dimensional quantities. These correlations have been compared to various experimental data on resuspension in wind tunnels and indoor environments. However, even though they were shown to capture some of the main features of a set of indoor experiments, they fail to capture the scattering in experimental resuspension rates [9] which have been obtained in different conditions. This can be easily understood since such formulas are based on averaged and/or macroscopic properties (without accounting for the exact distributions of particle diameters, asperity sizes or friction velocity involved).

Therefore, even though empirical models allow fast evaluations of key features of particle resuspension, they can only be relied on and used within their strict domain of validity, which is limited to situations close to the experimental ones on which they have been built. Yet, particle resuspension remains a complex process whose understanding is still in progress and it cannot be assumed that we have definitively extracted the (small) set of relevant and physically-meaningful non-dimensional numbers from which resuspension rates can be safely predicted in every situation. Therefore, we now turn our attention towards approaches that aims to predict particle resuspension rates by considering a model for the evolution of sticking particles.

5.2. Static force-balance approaches

Static force-balance approaches are based on two building blocks: first, it is assumed that an adhering particle is reentrained by the fluid flow as soon as its equilibrium state on the surface is broken and, second, this equilibrium is defined by the balance of the forces, or moments, acting on the particle. Therefore, the equilibrium state of a sticking particle is maintained as long as the balance between external forces and moments remains valid. This balance is expressed as

$$F_{adh} + F_{hydro} + F_{grav} = 0, \tag{49a}$$

$$M_O(F_{adh}) + M_O\left(F_{hydro}\right) + M_O(F_{grav}) = 0 \tag{49b}$$

where $M_O(F)$ refers to the moment of the force F around a point O on the particle surface. It will be seen below that the choice of a

force balance or a moment balance (or a combination of them) depends on the mechanism considered (i.e. rolling, sliding or lifting). Then, particles are considered as reentrained when the hydrodynamical force F_{hydro} overcomes the adhesive force F_{adh} and the particle weight. Thus, resuspension is reduced to the detachment criterion only: resuspension occurs at the first time s when $F_{hydro}(s) > -F = \mathrm{adh}(s) - F_{grav}$. The same is true when the moments are unbalanced and when we have, at a time s, that $M_O(F_{hydro})(s) > -M_O(F_{adh})(s) - M_O(F_{grav})$. In the rest of this section, we will loosely refer to this equilibrium as a 'force-balance' approach and include both force and moment considerations under this terminology.

Since the description of the equilibrium is made for individual particles, force-balance approaches fall naturally in the category of particle methods and are closely related to Lagrangian approaches. Force-balance approaches can indeed provide insights into local (microscopic) phenomena at play in particle resuspension since all forces acting on particles are considered. However, such approaches only address particle detachment, i.e. the rupture of static equilibrium (particle trajectories are not tracked along the wall surface) [94]. In that sense, they do not represent fully-Lagrangian approaches as, for example, the ones discussed in Section 5.4 or DEM methods. Furthermore, it is seen from the forces entering Eq. (49) that randomness can be at play in two different ways: the hydrodynamic force can be random due to fluid turbulence (see also Section 2.1.3 on near-wall turbulence) but the adhesive force can also be random due to surface roughness. It is then useful to distinguish between formulations which have been developed for a given value of the adhesive force and formulations which account for its variations or for the distributions of the hydrodynamic and adhesive forces.

A first type of force-balance approaches describes only the resuspension of single particles, which means here that the hydrodynamical and adhesive forces are assumed to be known. For instance, Ibrahim et al. [94,97] modelled the resuspension of various types of particles (with a size ranging from 29 to 76 μm) used in their wind tunnel experiment. For that purpose, the reentrainment of particles was described considering three resuspension modes (i.e. sliding, rolling and lifting). As illustrated in Fig. 21, the authors considered the action of four forces on particles: drag forces F_{drag} (coupled with a proper model for the near-wall fluid velocity including, or not, burst-sweep events), lift forces F_{lift} (as in Eq. (26)), adhesion forces F_{adh} (calculated using a Lennard-Jones potential with surface deformation issued from JKR theory) and gravity $F_{grav} = m_p g$.

The corresponding formulas for particle resuspension are:

$$F_{lift} > F_{adh} + m_p g \quad \text{for lifting} \tag{50a}$$

$$F_{drag} > \mu_s \left(F_{adh} + m_p g - F_{lift}\right) \quad \text{for sliding} \tag{50b}$$

$$1.4 R_{part} F_{drag} + a F_{lift} > a\left(F_{adh} + m_p g\right) \quad \text{for rolling} \tag{50c}$$

It is seen that this description is based on a combination of force and moment balance. Indeed, the criteria for the lifting (direct pull-off in the vertical direction) and the sliding (the tangential and normal forces are related through the static friction coefficient μ_s) resuspension modes are written using the forces acting on the particle while the rolling criterion is expressed by the rupture of the moment balance around the point O (located at a distance a from the particle axis in the downstream direction and where the factor $1.4R_{part}$ is the same one appearing in Eq. (21), see Fig. 21). As seen in Fig. 22, the results obtained were shown to compare relatively well with the measurements considering the limiting assumptions that were made (i.e. the fact that a single detachment velocity is calculated, that only average and/or macroscopic properties are used and that burst events are neglected) [94]. This force-balance approach was used to evaluate the relative importance of each resuspension mode for small particles ($d_p^+ < 4$), showing that resuspension occurs mainly due to rolling (with possibly some contribution due to sliding) [94]. Yet, similar works [145,253,254] have shown that the effect of sliding can become comparable to rolling motion for much larger particles. Besides, detailed analysis of particle trajectories in the wall-normal direction (using a force-balance approach coupled with a DNS calculation of the fluid phase) have provided further insights in the effects of turbulence on resuspension: large particles ($\tau_p^+ > 780$) are mostly lifted-off by high-speed streaks while small particles ($\tau_p^+ < 0.023$) are removed due to low-speed streaks [255].

Static force-balance approaches have also been used to obtain macroscopic formula for some variables of interest in particle resuspension [18,89,118,237,241]. For instance, Cleaver et al. [118] proposed a condition for particle removal expressed in terms of the wall shear stress considering a balance between lift forces and adhesion forces:

$$\tau_w > B \Big/ d_p^{4/3} \tag{51}$$

with B a constant for the fluid. It should be noted that Eq. (51) provides a criterion for particle resuspension but only when it is assumed that adhesion and hydrodynamic forces are the same for

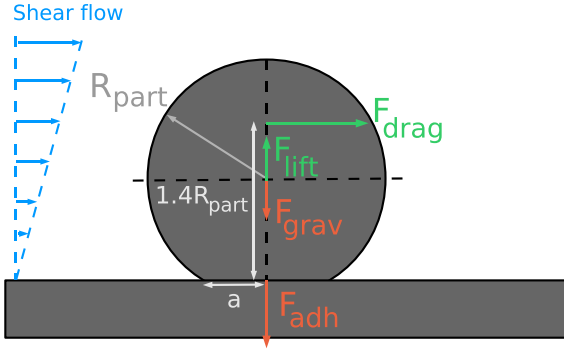

Fig. 21. Forces acting on a micrometre particle on a surface in a shear flow as considered in [94].

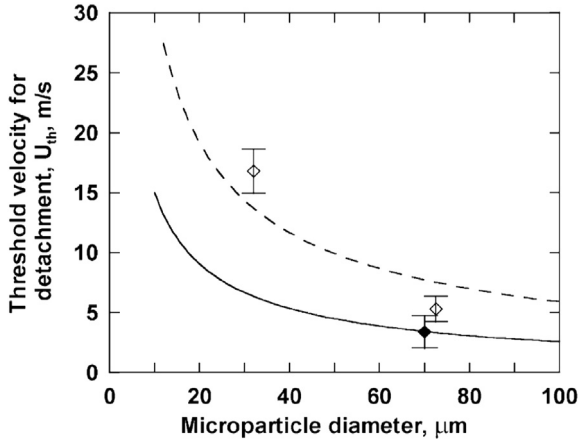

Fig. 22. Evolution of the threshold velocity for resuspension with the particle diameter for glass (dashed curve and open symbols) and stainless steel (solid curve and solid symbols). Symbols represent experimental data while curve were obtained numerically. Reprinted from [94]. Copyright 2003 with permission from Elsevier.

all particles considered. A similar formula was obtained by Ziskind et al. [237] assuming that resuspension occurs when the moment of drag forces exceeds the moment of adhesion forces: in that case, the constant B was defined as $B = \xi\Delta\gamma^{4/3}/K^{1/3}$ (with $\xi = 5.37$ for the DMT theory and $\xi = 7.74$ for the JKR theory).

From these first models, extensions have been proposed in order to start accounting for the effects of surface roughness. In that sense, Ziskind et al. [237] made a first step in that direction by considering the presence of asperities in contact with a sticking particle and by differentiating the case where particles rotate above an asperity or tangentially to it: the condition for removal is similar to the ones expressed in Eq. (51) except that it is proportional to a factor R_{asp}^2/R_{part}^2 (since both the adhesion force and the contact area are lowered due to the presence of an asperity). Similar conclusions on the effect of surface roughness were drawn by Yiantsios and Karabelas [256]. In another study, Nitschke and Schmidt [257] used a force-balance approach (based on lift, drag and adhesion forces) to obtain a formula for the mass transfer coefficient of particles from the surface towards the fluid, which refers to the flux J_{reent} in Eq. (40) rather than the resuspension rate k_r.

More recently, Burdick et al. [258] went further in including the effects of surface roughness in force-balance approaches. They derived a formula for the removal condition in terms of the particle Reynolds number using a force-balance approach for the rolling mode written as $Re_p > Re_{p,c}$, where $Re_{p,c}$ is the critical Reynolds number for resuspension. As depicted in Fig. 23b, the critical Reynolds number for resuspension was obtained using a force-balance approach that included the effect of surface roughness and deformation. Thus, $Re_{p,c}$ is a function of the drag, adhesion and lift forces, as well as of the distance to the pivot point (a_1 in the tangential direction and a_2 in the wall-normal direction). The new aspect is that this critical Reynolds number was evaluated by considering the distribution of the adhesion force due to surface roughness. Using this model, predictions for particle removal were shown to compared relatively well with experimental data but provided that the distribution in $Re_{p,c}$ (which is now a random variable due to the randomness of surface roughness and to the variations in particle size or adhesion forces) is correctly simulated. Another force-balance approach used in the case of bed filtration [18] has shown that, for the particle resuspension rate to be in agreement with experimental data, surface roughness and heterogeneities must be included in the description and properly accounted for in the numerical approach. For that purpose, the authors considered the balance between hydrodynamic lift/drag and adhesion forces obtained with a single protruding asperity between 3 μm particles and the surface.

Still with the purpose of including surface roughness effects, the static force-balance approach developed by Ibrahim et al. [94] (see also Eq. (50)) was used again later but with a refined description that consisted in making the adhesive force a random variable [97]. This was achieved by resorting to Monte Carlo calculation and performing 10,000 single particle simulations to account for the fluctuations related to surface roughness. The resulting threshold removal velocity was shown to decrease with increasing particle diameter and was in agreement with experimental measurements [97]. The strong dependence of the resuspension rate on the substrate roughness was also underlined using this approach (and confirmed recently by other Monte Carlo simulations based on a static force-balance approach [259,260]). A similar model was developed by Bradford et al. [229] for the resuspension of colloidal particles from porous media: a torque-balance approach was used considering both hydrodynamic drag forces and adhesion forces (obtained using the DLVO theory with surface deformation from the JKR theory and including surface roughness). Numerical results highlighted the dependence of particle resuspension on several parameters: the solution ionic strength, the particle radius, the young modulus and the amount of chemical heterogeneity. Another force-balance approach including DLVO adhesion forces and hydrodynamic (drag and lift) forces was used to model particle resuspension from a bulging membrane [19], showing that bulging (which is similar to roughness) increases resuspension by forcing the adhering particles in motion and detachment by collision with an oscillating bulge.

5.3. Kinetic PDF approaches

As it transpires from their name, PDF approaches are probabilistic models that aim to simulate the probability density function (pdf) of some variables of interest attached to particles. This terminology became essentially associated with models that handle directly pdfs and it was believed for some time that this standpoint is different, even opposite, to Monte Carlo simulations as introduced in the previous subsection. This was a misleading statement since, as already recalled, it is equivalent to handle a pdf and a large number of realisations (in a weak sense). Actually, the central element in a PDF approach is the choice of the relevant variables entering the particle state-vector. This has been emphasised for some time in two-phase flow modelling [35,261] and remains valid for particle resuspension models. Only the difference in the chosen variables included in the particle state-vector explains the difference of terminology between the so-called kinetic PDF models considered here and the dynamic PDF models addressed in Section 5.4.

Kinetic-based PDF approaches (especially the Rock'n'roll model) were the first attempts that tried to introduce some effects of particle motion in a resuspension model. As such, they propose an additional element compared to the static force-balance discussed in Section 5.2, which justifies why they are presented in a specific

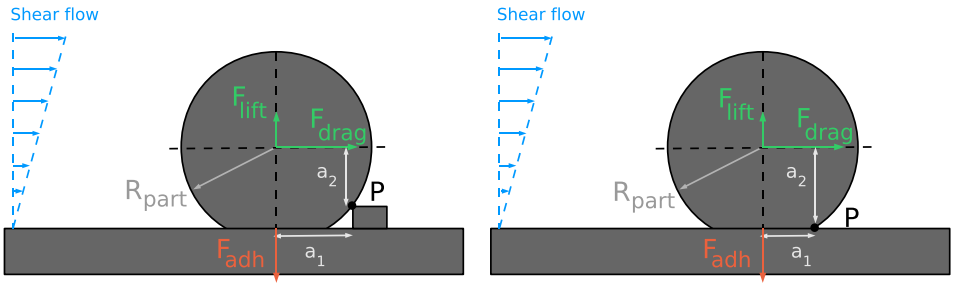

(a) Pivot point (b) Rolling or sliding

Fig. 23. Sketch showing the effect of roughness on the pivot point for particle rolling motion.

section. In the following, three representative kinetic models are analysed while a detailed discussion of their interests as well as their limitations is developed at the end in a specific paragraph.

5.3.1. Kinetic models based on force-balance

A first variety of kinetic PDF models was obtained by considering a (simple) force-balance approach where resuspension is described as the point of rupture between hydrodynamic and adhesion forces written as $F_{\mathrm{adh}} + F_{\mathrm{hydro}} = 0$. For instance, Wen and Kasper [262] obtained a formula for the particle resuspension rate k_r of a particle, knowing the adhesion and hydrodynamic forces:

$$k_{\mathrm{r}}|_{F_{\mathrm{adh}},F_{\mathrm{hydro}}} = n\exp(-q) \tag{52}$$

with n the maximum resuspension rate and q the ratio between adhesion and aerodynamic forces exerted on the particle. At first sight, this expression is surprising and can appear as being non-predictive since it is basically a relation between two values of the resuspension rates and $n = k_{\mathrm{r}}^{\max}$ is not known a priori. Yet, it is possible to work out more explicit expressions from the force-balance equation. Indeed, it is seen that we are only considering a (simple) balance for forces acting in the vertical direction, thus where $F_{\mathrm{hydro}} = F_{\mathrm{lift}}$. Then, n is obtained when there is no adhesion force since, in that case, every positive hydrodynamical vertical force will lift particles off the wall. As such, the maximum resuspension frequency is given by the frequency with which positive fluid motion (able to overcome at least the particle weight) takes place in the vertical direction. In other words, we are already implicitly considering fluid structures and, more specifically, fluid ejections: the maximum resuspension rate in Eq. (52) is thus identical to the frequency of fluid ejections. Then, it is seen that Eq. (52) refers to a Boltzmann-like statistical distribution where the conditional probability to have an ejection with a high-enough intensity to overcome the adhesive force (conditioned on the existence of such an ejection) is given by the scaling factor $\exp(-q) = \exp(-F_{\mathrm{lift}}/F_{\mathrm{adh}})$. In that sense, this formula is similar to the adhesion efficiency used in particle deposition (or agglomeration) studies [33] and has also some similarity with the the Arrhenius formula for the desorption of molecules from a surface or with the Arrhenius factor to express the temperature dependence of chemical reaction kinetic rates.

The model was extended to account for the distributions of the hydrodynamic forces [263] by writing the general condition that the resuspension rate, for a given adhesion force, is given by the probability that the hydrodynamic removal forces exceed the adhesion force [263]:

$$k_{\mathrm{r}}|_{F_{\mathrm{adh}}} = n\int\limits_{F_{\mathrm{hydro}}\geq F_{\mathrm{adh}}} p^{c}\Big|_{\mathrm{ejection}}\left(F_{\mathrm{hydro}}\right)\mathrm{d}F_{\mathrm{hydro}} \tag{53}$$

where $p^{c}\big|_{\mathrm{ejection}}(F_{\mathrm{hydro}})$ is the conditional pdf of the hydrodynamic removal force, conditioned on the existence of an ejection event. More generally (see also Ref. [264]), the resuspension rate for a set of particles exposed to fluctuating hydrodynamic forces and adhesion forces is given by:

$$k_{\mathrm{r}} = n\int\int\limits_{F_{\mathrm{hydro}}\geq F_{\mathrm{adh}}} p^{c}\Big|_{\mathrm{ejection}}\left(F_{\mathrm{hydro}}\right)p(F_{\mathrm{adh}})\mathrm{d}F_{\mathrm{hydro}}\mathrm{d}F_{\mathrm{adh}} \tag{54}$$

where $p(F_{\mathrm{adh}})$ is the pdf of the adhesion force.

A few remarks can be made at this point. First of all, in the initial formula Eq. (52), the assumption of a Boltzmann-like (exponential) factor implies the following assumption: resuspension is described as a statistical equilibrium and corresponds to the response of a particle within a potential well (for the adhesive part) to a random hydrodynamic force. Second, the general formulas written with the maximum resuspension rate and the conditional probability are perhaps slightly cumbersome. Since n is simply the probability of having an 'hydrodynamical event' (meaning here an ejection event) and using the basic definition of conditional probability as well as the probabilistic formulation of the resuspension rate given in Eq. (41) and a new formulation can be expressed by

$$k_{\mathrm{r}} = \lim_{\Delta t\to 0}\left[\iint_{F_{hydro}\geq F_{adh}} p_{\mathrm{hydro}}\left(s;F_{\mathrm{hydro}}\right)\,p_{\mathrm{adh}}(s;F_{\mathrm{adh}})\,\mathrm{d}F_{\mathrm{hydro}}\mathrm{d}F_{\mathrm{adh}}\Big|y_p(t)=0\,;t\leq s\leq t+\Delta t\right] \tag{55}$$

Finally, in the above equations, the relations for the resuspension rates have been written directly using the pdfs of the lift and adhesion forces. Yet, this was already achieved by the force-balance approaches when Monte Carlo estimations are used, with an implicit weak formulation of the pdfs as the sum of Dirac distributions [35,265]. Just as for the force-balance models, the distributions of hydrodynamic and adhesion forces must be assumed but the present force-balance formulation, which is an equilibrium limited to the vertical direction with only direct lift-off effect as the resuspension mechanism, makes this first kinetic-based approach more limited than the models presented in the previous subsection.

5.3.2. Energy accumulation

Another PDF modelling approach for particle resuspension was proposed by Reeks, Reed and Hall [165] and is often referred to as the RRH model or the energy-accumulation model. This model was initially designed to capture burst-type resuspension that has been observed experimentally [117] and which is related to interactions between large particles and near-wall coherent structures [44,120,266].

The RRH model was developed considering that a particle is detached from the surface when it has accumulated enough vibrational energy from the turbulent flow to overcome the adhesion. It is thus clear that the model is meant for deformable particles, though this point was not pointed out in the original work. The second key assumption of the RRH model is that particles are resuspended due to the action of fluctuating lift forces (decomposed as the sum of a mean lift force and a fluctuating lift force, $F_{\mathrm{lift}} = \langle F_{\mathrm{lift}}\rangle + f_{\mathrm{lift}}$) while drag forces are not considered. Thus, a particle moves within a potential well due to the balance between lift, adhesion forces and elastic deformation of surfaces. More precisely, the model describes the time fluctuations of particle/surface deformation $y_p(t)$ (due to fluctuations in the lift force) in the region close to the equilibrium point using a damped harmonic oscillator equation [165] (see also Fig. 24):

$$\frac{\mathrm{d}^2 y_{\mathrm{p}}}{\mathrm{d}t^2} + \beta_{\mathrm{RRH}}\frac{\mathrm{d}y_{\mathrm{p}}}{\mathrm{d}t} + \omega_{\mathrm{RRH}}^2 y_p = m_{\mathrm{p}}^{-1} f_{\mathrm{lift}}(t) \tag{56}$$

with ω_{RRH} the oscillation frequency and β_{RRH} the damping term (related to fluid and mechanical forces). The resuspension rate was then obtained by evaluating the number of particle (per unit time) reaching the maximum potential energy with a positive velocity (i.e. oriented out of the surface), which was described by a Gaussian distribution. Considering the statistics of long-term resuspension of a particle within a potential well of height Q and which accumulates on average a potential energy equal to $\langle \mathrm{PE}\rangle$, Reeks et al. [165] derived a formula for the resuspension rate $k_{\mathrm{r}}|_{Q,\langle PE\rangle}$:

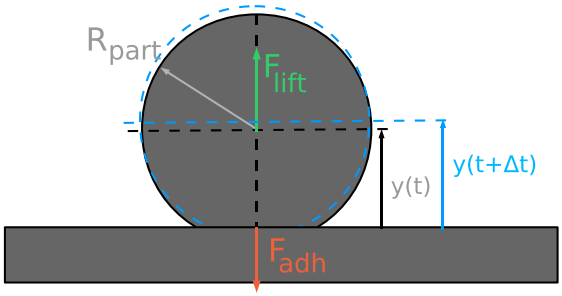

Fig. 24. Sketch of the variations of particle/surface deformation $y(t)$ used in the RRH model.

$$k_r|_{Q,\langle PE\rangle} = \frac{\omega_0}{2\pi}\exp\left(-\frac{Q}{2\langle PE\rangle}\right) \tag{57}$$

with ω_0 the typical vibration frequency (related to the oscillation frequency ω_{RRH}). As emphasised in previous studies [1,89,114,165], this equation is similar to the one obtained by Wen and Kasper [262]. In a more general form, the resuspension rate for a particle with a given adhesion force F_{adh} can be written:

$$k_r|_{F_{adh}} = \frac{\omega_0}{2\pi}\exp\left(-\frac{k\left(F_{adh}-\langle F_{lift}\rangle\right)^2}{\langle f_{lift}^2\rangle(1+\eta_{RRH})}\right) \tag{58}$$

where k is a numerical constant that depends on the shape of the surface potential, η_{RRH} is the enhancement due to resonance (related to the oscillation frequency ω_{RRH} and the damping term β_{RRH}), $\langle F_{lift}\rangle$ and $\langle f_{lift}^2\rangle$ are, respectively, the average and covariance of the lift force. It should be noted that Eq. (58) naturally includes the distribution in lift forces (since the formula has been derived from the oscillations of particle/surface deformation due to fluctuating lift forces) while the adhesion force is considered constant (particles are always facing the same element of surface). The distribution in adhesion forces (due for instance to the presence of roughness) is then included in the calculation of the whole resuspension rate k_r with an integration over all possible values of the adhesion force

$$k_r = \int k_r|_{F_{adh}} p_{adh}(F_{adh})\mathrm{d}F_{adh} \tag{59}$$

In the original RRH model, the average values of adhesion force and surface deformation are determined using the JKR theory (see Eqs. (28) and (29)) while lift forces are evaluated according to Hall formula [179] (see Eq. (25)).

The RRH model was shown to provide accurate predictions of the resuspension rate for large particles [165] but underestimated the resuspension of smaller colloids [267]. In addition, the assumptions of the original RRH model have been widely debated since other models were focussing on rolling motions rather than lift forces and coherent structures. One of the criticism of the RRH theory made by Paw U and Braaten [29] underlined the fact that the RRH approach is limited to specific cases involving large particles that are sensitive to vibration energy. However, in light of the analysis of experimental data made in the present review (see Section 3.1), it is clear that the RRH model was initially designed for large particles only and that the past debate was not that pertinent since other models were focussing on smaller particles where the mechanisms of resuspension are different (except for particle sizes where both rolling motion and coherent structures play a role in resuspension).

A noteworthy point is that the RRH model fails to account for the effect of drag forces on particle resuspension. Another remark is that the RRH model provides a formula for the calculation of the resuspension rate that depends on parameters related to the statistics of the forces exerted on particles: the distribution in the adhesion and lift forces as well as the timescale of these aerodynamic forces. Yet, these distributions are input parameters which are given by presumed probability functions (such as Gaussian distributions for lift forces or log-normal distributions for adhesion forces [165]). Regarding these two remarks, it should be noted that the RRH model has been extended by Vainshtein et al. [1,268], who used the concept of potential well of the RRH model while introducing the effect of surface roughness (with a simplified description including a single asperity) as well as the notion of a tangential drag force necessary to separate the particle from the surface.

5.3.3. Rock'n'roll model

Following the debate and criticism regarding the absence of rolling motion in the RRH model, Reeks and Hall [114] developed a refined model accounting for the drag force as well as the lift force in resuspension. For that purpose, instead of considering the vertical oscillations of particles within a potential well, resuspension was described as resulting from the oscillation of particles around a pivot point: as depicted in Fig. 25, a 2-D model with two-point asperity contact is initially assumed and the particle oscillates around the pivot point P until contact with the other asperity is broken, leaving the particle to roll on the surface until the adhesion at the single-point contact is sufficiently low compared to the lift force for the particle to be resuspended. This model is thus often referred to as the 'Rock'n'Roll' model (later referred to as the RnR model).

Following this mechanical description of resuspension, the RnR model is based on the angle of deflection θ for small oscillations around the pivot point P. Then, as for the RRH model, the RnR model represents the evolution of the deflection angle by a damped oscillator model and is expressed by:

$$\frac{\mathrm{d}^2\theta}{\mathrm{d}t^2} + \beta_{RnR}\frac{\mathrm{d}\theta}{\mathrm{d}t} + \omega_{RnR}\theta = I^{-1}\Gamma'(t) \tag{60}$$

with I the particle moment of inertia about the pivot point P, ω_{RnR} the oscillation frequency, β_{RnR} the damping and Γ' the fluctuating component of the torque Γ exerted on particles. In the original article [114], Γ was expressed in terms of the lift and drag torques only and the adhesion torque was not mentioned. With respect to the notation in Fig. 25, we propose here to correct this expression and express the torque accounting for adhesion and gravity forces as

$$\Gamma = aF_{lift}/2 + rF_{drag} - aF_{adh} - amg_n/2 + rmg_t. \tag{61}$$

In addition, the RnR model considers that the distance r used in the calculation of the moment of drag forces is equal to the particle radius R_{part}. However, in reality, as was done by Burdick et al. [258]

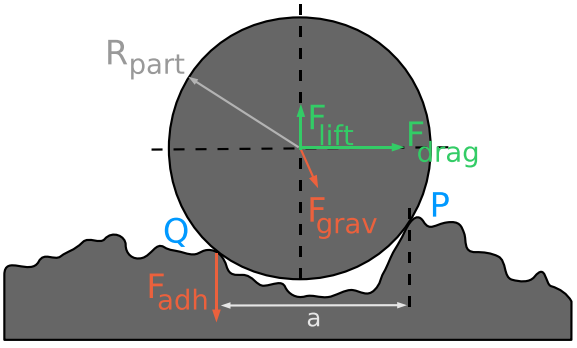

Fig. 25. Particle–surface geometry used in the Rock 'n' Roll model.

(see Fig. 23(a)), the distance r is the vertical distance to the pivot point P. Besides, it should be noted also that an underlying assumption of symmetry in the two-point asperity contact was made in the RnR model (this explains the factor a/2 in the moment of lift forces). The resulting expression for the resuspension rate of a particle exposed to a given constant adhesion force is similar to the one obtained in the RRH model and is given by:

$$k_r|_{F_{adh}} = \frac{\omega_0}{2\pi}\exp\left(-\frac{k(F_{adh} - \langle F\rangle + m_p g_n/2 - (r/a)m_p g_t)^2}{\langle f^2\rangle(1+\eta_{RRH})}\right) \quad (62)$$

where ω_0 is a frequency (proportional to the oscillation frequency ω_{RnR}), η_{RnR} is a contribution to the potential energy from the resonant energy transfer (linked with the oscillation frequency ω_{RnR} and the damping term η_{RnR}), f is the fluctuating component of the force defined as $F(t) = F_{lift}/2 + rF_{drag}/a$ and $\langle f^2\rangle$ its covariance, $m_p g_n$ and $m_p g_t$ are the wall-normal and wall-tangential components of the gravity force. With the corrected expression of the torque given above in Eq. (61), it is then seen that the conditional resuspension rate can be written as

$$k_r|_{F_{adh}} = \frac{\omega_0}{2\pi}\exp\left(-\frac{k\left(\langle\Gamma|_{F_{adh}}\rangle\right)^2}{\langle f^2\rangle(1+\eta_{RRH})}\right) \quad (63)$$

As in the RRH model, the RnR model includes the effects of fluctuating hydrodynamic forces on particle resuspension but assuming a given value of the adhesion force. The (unconditional) resuspension rate is then evaluated by considering the integral of the resuspension probability over all possible adhesion force (weighted by their probability of occurrence), as in Eq. (59). For that purpose, a log-normal distribution of adhesion forces is generally presumed to account for the presence of surface roughness while Gaussian [3,114,269] or non-Gaussian [16,270] distributions of the hydrodynamic force fluctuations are considered.

The RnR model has been widely used in the literature and comparisons to various experimental data have confirmed the accuracy of the model [16,114,270] (see Fig. 26). Compared to the original RRH model, the RnR model can be applied to smaller particles since it includes some effects of the rolling mode and thus some effects of the drag and lift forces. Yet, even though the RnR model has been developed starting from equations of particle motion (i.e. fluctuations of particles around a single pivot point due to fluctuating hydrodynamic forces), it still fails to capture the whole particle dynamics (with fluctuating adhesion forces as particles roll on the surface).

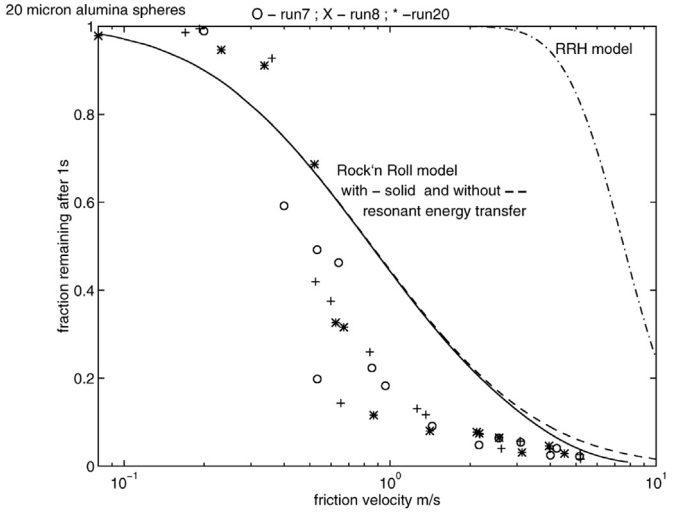

Fig. 26. Fraction of particles remaining on a surface after exposure to a flow with various velocity: comparison between experimental results (symbols) and numerical calculations. Reprinted from [114]. Copyright 2001 with permission from Elsevier.

5.3.4. Discussion

From this overview of kinetic PDF approaches, it appears that the main difference between the various formulations lies in the initial assumptions made in the particle equations of motion: the initial model of Wen and Kasper [262] considered a balance between adhesion and hydrodynamic forces only in the vertical direction for small rigid particles; the RRH model [165] was still developed to account for forces in the vertical direction but introduced the notion of energy accumulation and was thus meant for large deformable particles; the RnR model [114] addressed situations of a particle rolling over asperities in terms of a moment balance that includes the effect of lateral and tangential forces and was also meant for rigid particles. Using the terminology introduced in Section 5.2, it can be said that the Wen and Kasper and RRH models address the lifting mode (with different approaches) while the RnR model addresses the rolling mode. Yet, in spite of differences in their underlying description, the formulas given in Eqs. (52), (58) and (63) for the conditional resuspension rate (conditioned on a given value of the adhesion force) have a similar functional form, namely $k_r \sim n_1 \exp(-n_2\langle F_{df}|_{F_{adh}}\rangle^2)$ where F_{df} stands for the 'driving effect' whose expression changes in each model (with n_1 and n_2 the dimensional parameters that can be found in Eqs. (58) and (63) for example). As a result, satisfactory results can be obtained only if the pdfs of the adhesion forces and hydrodynamic forces are adequately described.

Compared to force-balance approaches, kinetic PDF approaches (such as the RRH and R'n'R models) have proposed new developments for particle resuspension that included the effect of particle motion (oscillations around a stable potential). Nevertheless, these kinetic approaches do not describe explicitly particle dynamics along a wall surface after static equilibrium has been broken. In reality, particles can be rolling on the surface and can thus encounter various adhesion forces and surface geometries, something which is not well-captured in kinetic PDF approaches. In that sense, current kinetic models remain static approaches (this explains the structure sketched in Fig. 20). For instance, if we consider particles deposited on a nearly-smooth surface (such as the one treated later in Fig. 30), particles lying on a rough part of the surface can be set in motion (since adhesion forces are lower) but may be brought back to a standstill afterwards when they reach a smooth part of the surface (where adhesion forces are higher): such situations cannot be captured with present kinetic PDF approaches.

Following recent developments in dynamic PDF models (described in the following section), extensions of such PDF approaches may appear in the near future to try to include particle dynamics along surfaces, resulting in more general PDF approaches (which would not be kinetic anymore). For instance, one possibility will be to include not only the force amplitude but also its duration in the calculation of the resuspension rate as done in a recent study of multilayer resuspension using kinetic PDF approaches [271]. In addition, since the timescale for fluctuations in adhesion forces depends on the particle velocity, further developments of kinetic PDF approaches may have to consider the joint PDF of adhesion and hydrodynamic forces as done recently in multilayer resuspension [264].

5.4. Dynamic PDF approaches

The general framework in which dynamic PDF models for particle resuspension are developed can be defined by three characteristic choices.

(a) Resuspension is not identified with the rupture of static equilibrium but results from an interplay between particle dynamics along the wall and surface roughness.
(b) Particle motion along surfaces is simulated as well as the relations between hydrodynamical/adhesion forces and particle dynamics.
(c) A probabilistic standpoint is adopted since there are random terms (due to aspects of fluid turbulence and surface roughness) that escape a deterministic formulation.

The consequence of these characteristic features is that two elements must be brought into the picture: (i) a new resuspension scenario that distinguishes the process of setting particles in motion from their actual detachment and (ii) a detailed description of surface roughness as met by moving particles along a wall. These two new aspects are intertwined and related to particle dynamics on the surface. From these general statements, it is seen that the aim of dynamic PDF approaches is to explicitly capture particle dynamics in the near-wall region (point(b)) while modelling probabilistic evolutions (point (c)). A trajectory point of view [35] is often adopted where the dynamical variables attached to each particle become stochastic processes, which means that practical calculations belong to the class of dynamical Monte Carlo simulations. For that purpose, once stochastic models are expressed for hydrodynamical/adhesion forces and moments, the particle equations of motion (see Eq. (39) in Section 4.3) are solved for a large number of particles. In that sense, dynamic PDF approaches are similar to classical Lagrangian stochastic approaches where the motion of a large number of particles is explicitly tracked.

It is best to illustrate these characteristics by describing one specific dynamic PDF model which has been recently developed for the resuspension of small particles [210]. This approach was first proposed for particles in air with a simplified account of adhesion forces [245] and was later extended to include a refined description of surface roughness and adhesion forces which makes it applicable to both air and liquid fluid flows [210]. As depicted in Fig. 27, the model is based on a three-stage scenario for particle resuspension (more details can be found in [210,245]):

- Particles are first set in motion when the instantaneous moment of hydrodynamic forces is higher than the moment of adhesion forces (step (a) in Fig. 27).
- Particles can then roll/slide on the surface, depending on the varying hydrodynamical and adhesion forces/moments along their trajectory (step (b) in Fig. 27).
- Upon rocking on a large-scale asperity, particles can detach from the surface if their instantaneous longitudinal kinetic energy is higher than the adhesion potential energy at that point (step (c) in Fig. 27).

This dynamic PDF model builds upon the mechanisms underlying the Rock 'n' Roll model but with a refined description of the whole particle dynamics. Indeed, the model not only accounts for the rupture of the balance between hydrodynamic and adhesion forces that triggers particle motion but also for the dynamics of particles on a complex rough surface where they can gain/lose kinetic energy. Clearly, this new resuspension scenario is more detailed and relies both on particle dynamics and on surface roughness which is seen to play now a central role in the resuspension process. In this approach, rough surfaces are described by two-scale asperities randomly distributed on the surface, according to some statistical information such as their size distribution and their surface coverage. These asperities influence particle dynamics differently: small-scale (meaning typically nanometric) asperities modify the adhesion forces of rolling particles while large-scale (meaning typically micrometric) asperities act as possible detachment locations. The small-scale asperities are small with respect to the particle diameter so that they do not modify the particle line of displacement but are responsible for the magnitude, as well as the timescale, of the adhesion forces seen by particles as they roll/slide along the wall (and on these small-scale asperities). The large-scale asperities have a size roughly comparable to the particle diameter or 'large enough' to be able to change significantly the direction of the particle trajectory upon a rocking event.

Supplementary details on the implementation of each step of this scenario helps to understand how the model is working.

(i) In the first step, the equilibrium (or its rupture) is defined by the balance (or unbalance) between the moment of the adhesion and drag forces (lift forces were neglected in [210,245] since only colloidal particles were considered). The moment of the drag force is given by Eq. (21) with a near-wall fluid velocity given by correlations from Matida et al. [272]. The adhesion force is obtained as the limit of the DLVO force accounting for surface roughness by distributing hemispherical asperities randomly on the particle contact area [210] and using a Derjaguin approximation (see Section 2) to obtain the resulting expression of the force. Then, the adhesion moment is evaluated by multiplying this force with the distance to the pivot point a_0 which is the furthest asperity located in the fluid downstream direction (see Fig. 27(a)).
(ii) In the second step, the translational motion of particles due to rolling on the surface is simulated by solving the dynamical particle moment equation [210,245]:

$$I\frac{\mathrm{d}U_{\mathrm{p},//}}{\mathrm{d}t} \simeq R_{\mathrm{part}} M_0\left(F_{\mathrm{drag},//}\right) - R_{\mathrm{part}} M_0(F_{\mathrm{adh}}) \tag{64}$$

where $I = 7m_{\mathrm{p}}R_{\mathrm{part}}^2/5$ is the moment of inertia of the particle around the pivot point (situated on the particle surface) and $U_{\mathrm{p},//}$ is the streamwise particle velocity (approximated from the angular velocity ω_{p} as $U_{\mathrm{p},//} \simeq R_{\mathrm{part}}\,\omega_{\mathrm{p}}$). For that purpose, the fluid velocity seen by particles U_{s} is included in the particle state-

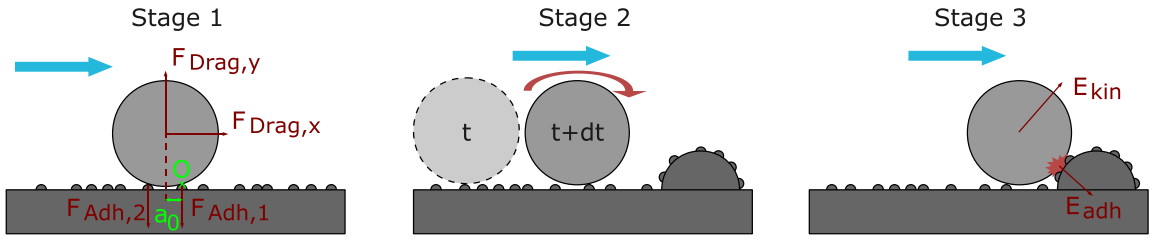

Fig. 27. Resuspension model: a three-stage scenario. Reprinted from [210]. Copyright 2012 with permission from American Chemical Society.

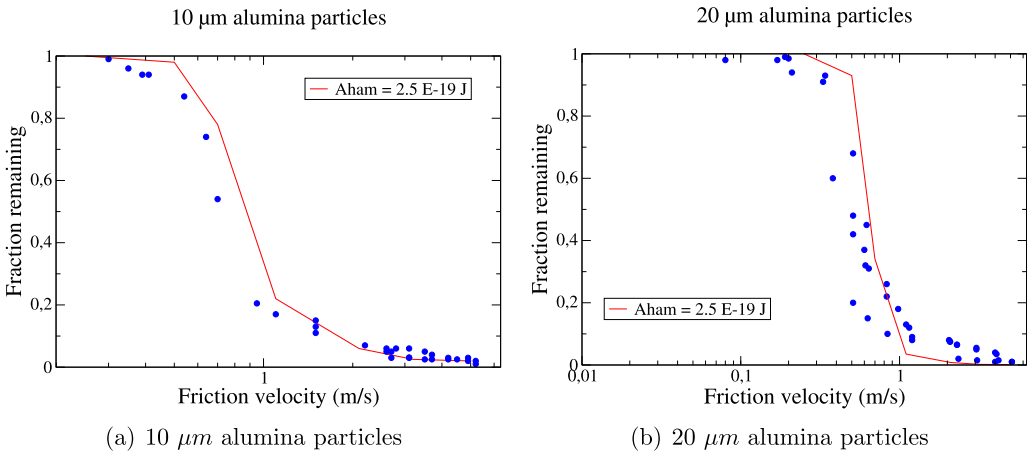

Fig. 28. Adhesion of alumina or graphite particles on stainless steel substrates: ● experimental data [114], — numerical predictions with $\{R_{asp}^{large} = 2\mu m, S_{cov}^{large} = 3.1\%$ and $R_{asp}^{small} = 5$ nm, $S_{cov}^{small} = 0.5\%\}$. Adapted from [210]. Copyright 2012 with permission from American Chemical Society.

vector and is simulated using fluid velocity integral timescales or, in other words, the correlation between the successive value of $U_{s,//}(t + \Delta t)$ and the present fluid velocity seen $U_{s,//}(t)$ is accounted for. Correspondingly, the adhesion moment is also simulated as a stochastic process by tracking in time the number of asperities $n_{asp}(t)$ in contact with each particle and the related distance to the pivot point $a_0(t)$. These variables are attached to each particle and are therefore also included in the particle state-vector. This means that the statistical distributions of adhesion forces are now an outcome of the model.

(iii) In the third stage, the condition for particle detachment is simply given by the condition that $E_{kin} > E_{adh}$ when a rocking event is detected with a large-scale asperity. As large-scale asperities are also randomly distributed along the surface, the probability to hit one such asperity is calculated for each particle displacement and possible events are sampled, while the particle kinetic energy (at the estimated time of the impact) is obtained from the solution of Eq. (64).

The equation of particle motion and the resuspension condition are solved for a large number of particles and statistical information (for instance, the resuspension rate) is directly extracted by Monte Carlo estimations. Satisfactory results have been obtained for the prediction of the particle resuspension rate, for instance in an air flow for a classical resuspension test case (see Fig. 28, which is the same test case addressed in Fig. 26 with a kinetic PDF model) as well as for liquid media which require to have a proper account of electrostatic effects in the adhesion force (through DLVO formulas) and of the influence of the pH of the solution (see Fig. 29). Further details can be found in specific articles [210,245]. Recent numerical results (described in a forthcoming paper [273]) have also underlined the need to properly capture the fluctuations in time of the moments of the hydrodynamic and adhesion forces. The particle velocity (and thus its resulting kinetic energy) is indeed highly dependent on the timescales of the fluctuations of these two moments.

The key advantage of dynamic PDF models, such as the one detailed here, is that the distributions of the adhesion forces and torques are predicted from a detailed calculation of particle–surface interactions which includes the effects of surface roughness. This contrasts with the previous models, where the pdf of adhesion forces must be presumed (often assuming a log-normal or a Gaussian law) from the outset and independently of particle dynamics. In dynamic PDF approaches, these distributions result now from the interplay between particle dynamics and surface roughness. For example, the model described above has been shown to provide accurate predictions for the distribution of adhesion forces due to surface roughness [210]. In particular, this model can account for complex distributions of adhesion forces such as two-peak distributions that are sometimes measured experimentally when surface roughness is small and particles are either in contact with a smooth wall (with high adhesion forces) or with asperities (with lower adhesion forces as seen in Fig. 30(a)). At the same time, the continuous distributions observed when surface roughness is much higher, resulting in a wall surface nearly always covered by asperities is also naturally predicted (see Fig. 30(b)). Consequently, in PDF dynamic approaches, the levels of description for the fluctuations of the hydrodynamic on the one hand and the adhesion forces on the other hand are consistent and both part of the complete description. Yet, these recent developments of dynamic PDF models still need to be improved in the near future to include other mechanisms of particle resuspension since only rolling motion has been considered.

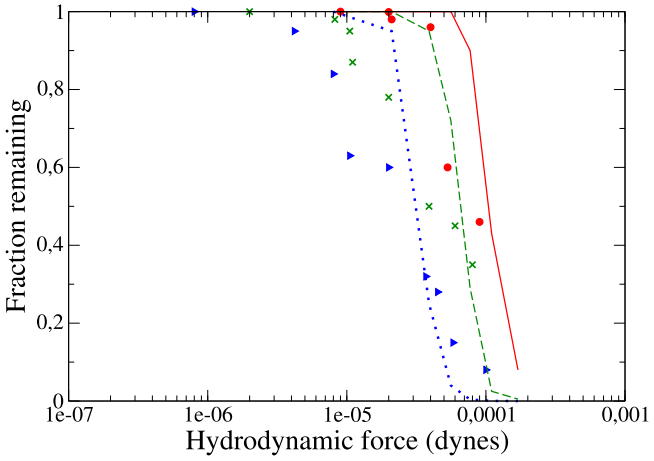

Fig. 29. Effect of solution pH on the release of 10 µm glass particles from a glass surface (symbols correspond to experimental data [113], lines to numerical results): ●— pH 5, x– – pH 7 and ▷ · · · pH 10. Reprinted from [210]. Copyright 2012 with permission from American Chemical Society.

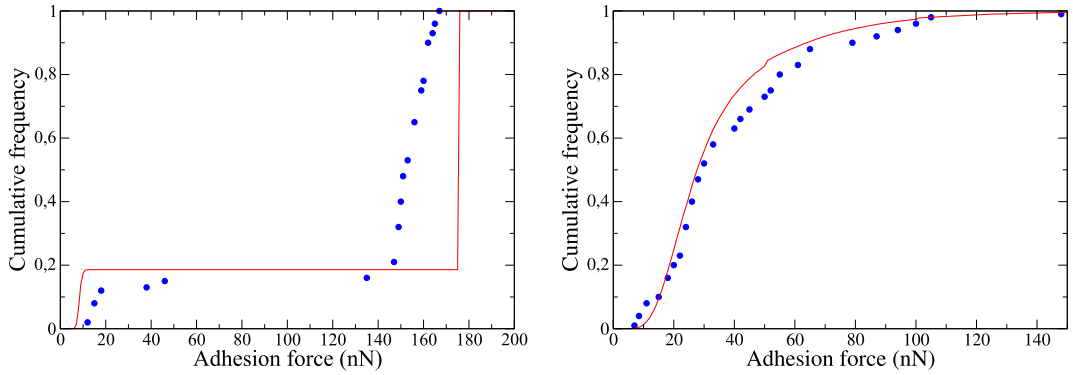

Fig. 30. Adhesion between 10 μm polystyrene particles and aluminum substrate: (a) ● experimental data [154], — predictions with $R_{asp} = 250$ nm ($S_{cov} = 0.5\%$), (b) ● experimental data [154], — predictions with $R_{asp} = 850$ nm ($S_{cov} = 75\%$). Reprinted/adapted with permission from [210]. Copyright 2012 American Chemical Society.

A similar model has been proposed recently by Fu et al. [247] who considered the rolling motion of particles on a smooth plate (adhesion forces described using the JKR theory) under the influence of a turbulent flow (with a stochastic description of fluid fluctuations in the near-wall region). The detachment criterion has been expressed as a critical rotational energy $\omega_p > \omega_c$ (whose value is given either by experimental or theoretical evaluations).

5.5. Open issues concerning unified modelling approaches

Apart from the usual assessment of one formulation compared to the others, there is a more general issue that is worth bringing out: is it possible to come up with a unified modelling framework in which models would be able (by construction) to address the whole range of the phenomenologies involved in the resuspension process? Indeed, the mechanisms playing a role in particle resuspension depend on particle sizes (see Section 3): small particles are influenced by rolling motions while large particles resuspend mostly due to their interaction with near-wall coherent structures. In addition, particles exhibit either rolling, sliding or lifting motion along the surface. Therefore, a unified modelling framework should be able to include all these aspects within a single approach. When considering various modelling choices, this question introduces a new point of view.

With respect to this issue, it is clear that empirical formulas do not provide such a framework: they will need the use of one formula for small particles, another one for large particles, and will involve complex developments for particles of intermediate sizes where the different resuspension mechanisms are coupled. The use of kinetic PDF approaches appears feasible (provided that particle dynamics along surfaces is included) since a formula for the resuspension rate can be developed considering the relevant 'driving force' for each case (i.e. rolling, sliding and lifting). However, separate formulas will be obtained for each mechanism. Then, to include each of them in a general framework, one would have to choose right from the outset which particle will be subject to which mode of resuspension.

In contrast, resuspension models based on a Lagrangian description appear as potential candidates since all the forces acting on deposited particles are naturally included in the description of particle motion. Among such models, current force-balance approaches are limited since they only account for particle detachment (in the sense of the rupture of equilibrium) and not for the complete particle dynamics. For that reason, dynamic PDF models seem to be more adequate, thanks to the fact that a detailed scenario that allows the separate steps to be modelled specifically has been introduced. For instance, if we use the dynamic PDF model presented in Section 5.4 as a reference example, it is seen that the general framework of dynamic PDF approaches can be used to account for all the different mechanisms. To be more specific, it is straightforward to include direct lifting motion simply by considering also the balance of forces in the vertical direction in the first step, the second step of the resuspension scenario can easily be extended to simulate sliding motion, whereas the detachment criterion (third step in the resuspension scenario) can also be easily extended for possible direct lift-off effect upon a rocking event. Furthermore, a noteworthy point is that such dynamic PDF models can include a general description of the interactions between particles and near-wall coherent structures. Indeed, if we use a stochastic model such as the one developed for particle deposition [33,48] which explicitly simulates coherent structures in the buffer and logarithmic regions of a near-wall turbulent layer together with a structure-less viscous sublayer, then adhering particles will naturally be subject to coherent events if they are larger than the size of the viscous sublayer or to smoother and less intermittent fluctuations if they remain embedded in this viscous sublayer. This distinction between the different effects acting on particles does not have to be assumed from the outset but will be made in the course of the calculation for each particle, depending on its dynamics and on its local 'fluid environment' (the local size of the viscous sublayer which can evolve along the surface and the local intensities of turbulent fluctuations). In addition, a further advantage of such a modelling framework for particle resuspension is that models will be consistent with recent developments for particle deposition on rough surfaces [33,48]. This consistency point between models for particle deposition and resuspension is not to be overlooked since these two mechanisms are usually present at the same time.

To put forward a conclusion on the different models which have been discussed in the present section, it is clear that present formulations remain incomplete and that modelling efforts are still needed. However, it is proposed that dynamic PDF models constitute a relevant framework that has all the potential to help researchers develop consistent models that can address the complete process of particle resuspension.

6. Resuspension from multilayer deposits

In the preceding sections, we have addressed particle resuspension for monolayer deposits. This means that sticking particles

were always considered to be in contact with the surface of the material bounding the fluid. In that sense, each adhering particle is said to be in contact with a 'clean surface', whether that surface element is smooth or rough. However, a continuous deposition of particles on a surface can lead to the formation of multilayered deposits [33]. In terms of the fundamental interactions at play, the physical process does not only involve particle–fluid and particle–surface forces (as in previous sections) but now also particle–particle interactions. Note that, even in the case when only one layer is formed, particle–particle interactions can already play a key role: indeed, this situation happens when particle–particle interactions are repulsive enough to overcome any possible particle–fluid forces, thus preventing additional particles from reaching the surface and depositing [33]. In all the other situations, whatever its form and morphology, a multilayer deposit is formed and the reverse process of possible reentrainment means that we are faced with the issue of multilayer particle resuspension.

Layout of this section. In this section, multilayer particle resuspension is addressed with an emphasis put on the mechanisms at play and, more precisely, on the role of particle–particle interactions. Following previous studies on multilayer resuspension [274], and especially the work from Kok et al. [7,31] who proposed three different emission mechanisms for dust/sand aerosols (i.e. aerodynamic entrainment, resuspension after impaction and breakage of saltating particles, see Fig. 31), we have chosen to organise the present review with respect to two important physical mechanisms: first, hydrodynamic resuspension of particles (see Section 6.1) and, second, resuspension due to impaction by moving particles (see Section 6.2).

Each section is presented in a two-fold manner: we first review the experimental works that highlight trends/mechanisms for particle resuspension; second, we focus on the corresponding modelling approaches that have already been developed. Then, we propose a discussion on the open issues that need to be studied in order to come up with a complete description and modelling approach for multilayer particle resuspension.

6.1. Hydrodynamic particle resuspension from multilayers

When several layers of particles are present on the surface (or for high surface particle concentration), resuspension is modified by particle–particle interactions. Compared to monolayer particle resuspension, the number of studies dealing with multilayer resuspension of small colloidal particles is much more limited (whereas large particles have been largely studied in the framework of sediment transport, see for instance [7]). Besides, our understanding of the mechanisms underlying multilayer resuspension remains patchy.

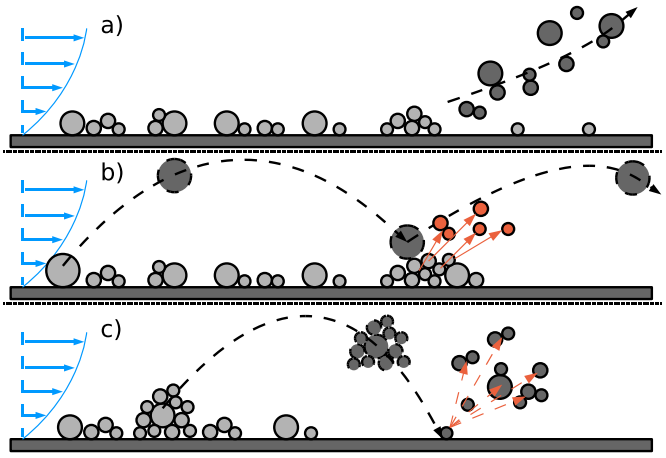

Fig. 31. Illustration of the three dust emission mechanisms proposed by Kok et al. [7]: aerodynamic reentrainment, resuspension following impaction of saltating particles, breakage of saltating particles after impaction.

6.1.1. Experimental evidence of hydrodynamic multilayer resuspension and its mechanisms

One of the first observations of the reentrainment of aggregates from a surface exposed to an airflow was made by Kousaka et al [275]. They measured the resuspension of various dust aggregates deposited on a glass plate using microscope observations and observed that small particles were left on the surface after cluster reentrainment (see Fig. 32).

This trend was further confirmed by measuring the change in the particle size distribution before and after resuspension. These observations suggested that only a part of the cluster is resuspended and that separation occurs inside the cluster and not at the glass substrate (as in the case of single particle resuspension). This trend also indicated that removal due to hydrodynamic forces can lead to a break-up of clusters where the cohesion forces that maintain particle–particle contact are small enough (i.e. close to the small particles, a notion which is illustrated in Fig. 33).

The role played by particle–particle interactions in the resuspension of particles from multilayered systems has been further confirmed by other experimental data involving small particles (where adhesion forces play a dominant role) [276,277]. For instance, Quadt and Schmidt [277] measured the resuspension of micron-sized PMMA particles (either monodispersed or polydispersed) forming a multilayered structure (see also Fig. 34) on ceramic membranes with an optical method (particle counting). Experiments performed using polydispersed suspensions showed that the particle size distribution shifted over time from large to smaller particles, indicating that larger particles are easier to remove than smaller ones. Then, detailed experiments with monodispersed particles under given conditions underlined that, while 20 μm PMMA particles are always resuspended in the conditions considered, 10 μm PMMA particles detach only when they are lying on top of other deposited particles (no reentrainment occurred in the case of a particle–surface contact).

Apart from direct particle–particle interactions, multilayer resuspension has been shown to depend also on the deposit morphology. In particular, a study of the resuspension of particles from hill-shaped deposits [278] revealed that the deposit shape (meaning its height and curvature) has an influence on particle resuspension. In addition, comparing the resuspension of 10 μm particles and 3 mm sediments, the authors underlined the role played by the deposit permeability (or porosity): the presence of a flow inside the porous media formed by the deposits can enhance particle resuspension [278]. Thus, the complex structure formed by deposited particles plays a significant role in the subsequent multilayer resuspension process.

However, as mentioned by Diplas et al. [279], experiments highlighting the mechanisms involved in multilayer resuspension are scarce due to the difficulty to develop non-intrusive techniques for

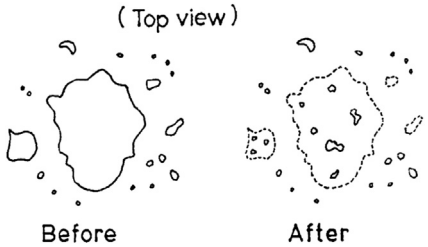

Fig. 32. Typical pattern of dust aggregates observed before and after resuspension due to an airflow. Reprinted from [275]. Copyright 1980 with permission from SCEJ Japan.

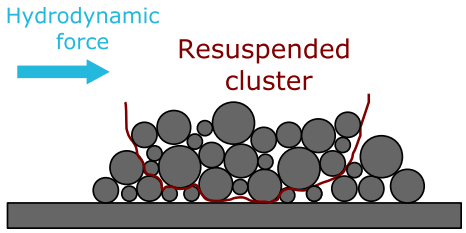

Fig. 33. Drawing showing the weak cohesion forces inside a surface cluster, which can lead to the fragmentation of the cluster upon reentrainment. Reprinted from [33]. Copyright 2012 with permission from Elsevier.

the detection of particle motion in the near-wall region of a deposit bed. Yet, with the development of PIV and PTV techniques, some experiments have provided measurements of particle motion over a bed [279–281]. For that purpose, particle motion is often measured using laser/optical measurements (see for instance Fig. 35). Due to the complexity of the beds formed, these experiments are still often restricted to large sediments (generally of a few millimetres) deposited on top of a deposit with a relatively simple geometry. Nonetheless, they have provided key information on the mechanisms at play in multilayer resuspension. For instance, 8 mm Teflon particles were shown to roll on the glass bed when the hydrodynamic force was strong enough [279]. Besides, the simultaneous measurement of near-wall fluid velocities and sediment motion (size of 5 mm) in a turbulent flow using a 3D-PIV system confirmed the role of near-wall high-velocity coherent structures on multilayer particle resuspension [280,282]. Thus, it appears that the mechanisms underlying multilayer resuspension are similar to those for monolayer resuspension.

As underlined in several experiments [279–281], particle motion on a bed is more intricate than on a typical surface due to the complexity of the bed roughness and of the bed height (or elevation). Multilayer structures are often generated experimentally by gluing particles on a surface (a similar process is used to generate rough surface [98]). In that case, the fact that the fluctuations in the surface height (comparable to roughness) are of the same size as the particle radius leads to complex phenomena such as hiding (or sheltering) effects [98,279–281,283]: particles located partially behind another deposited particles are not fully exposed to the flow and are thus subject to lower hydrodynamic forces.

6.1.2. *Existing modelling approaches for hydrodynamic multilayer resuspension*

From these experimental data on multilayer resuspension, it appears essential to take into account particle–particle interactions as well as the deposit morphology (porosity, roughness, height) in the development of accurate modelling approaches. Theoretical

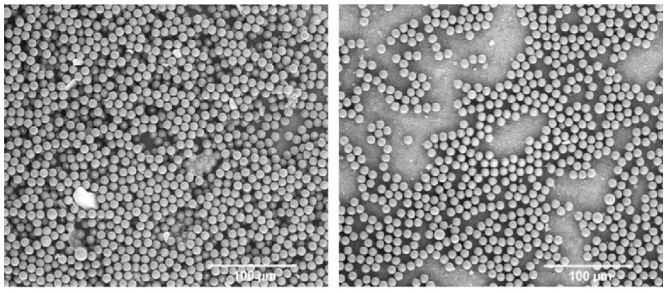

Fig. 34. Light scattering images of TiO_2 particles on glass substrates at pH 3 after 60 s exposure to a constant shear stress τ_f (with increasing increments): (A) initial population, (B) $\tau_f = 14.3$ Pa, (C) $\tau_f = 26.9$ Pa, (D) $\tau_f = 31.9$ Pa, (E) $\tau_f = 42.9$ Pa, (F) $\tau_f = 55.4$ Pa. Reprinted from [277]. Copyright 2012 with permission from John Wiley and Sons.

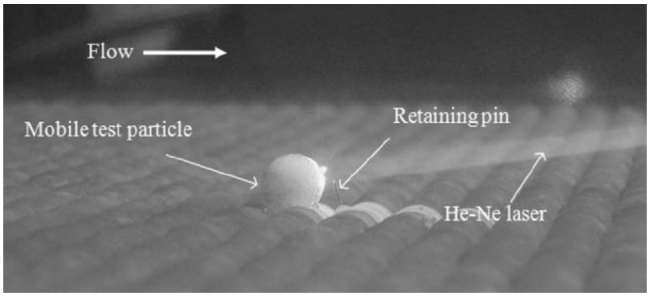

Fig. 35. Optical visualisation of a Teflon test particle (8 mm) over a bed of well-packed glass particles observed using a laser beam. Reprinted from [279]. Copyright 2010 with permission from American Society of Civil Engineering.

considerations and analysis of multilayer resuspension have underlined that the forces at play in multilayer resuspension are identical to those in monolayer resuspension (except that adhesion now depends also on particle–particle interactions): particles are set into motion due to hydrodynamic forces (drag, lift, effect of near-wall coherent structures for large particles in turbulent flows) while physico-chemical adhesion forces prevent it [1,32]. However, two of the main difficulties in modelling multilayer resuspension are related to the issues of how to account for, first, the deposit morphology and, second, the rupture mechanisms associated with the resuspension of large aggregates.

Various approaches for multilayer resuspension have been proposed, particularly in the context of sediments where more detailed experimental data on multilayer resuspension are available. These models can again be organised according to the classification used for monolayer resuspension (see Section 5), with a special emphasis put on the new assumptions or input parameters that have been introduced in these models to remain valid for multilayer resuspension.

- Empirical formulas

In a study of gravel resuspension from sediment beds (with a radius of a few millimetres) [283], a simple modelling approach based on a constant resuspension rate (whose value is chosen to fit the experimental data) showed that the resuspension rate k_r increases with the bed shear stress τ_f (following a power law $k_r = \tau_f^{\alpha}$ with $\alpha > 2$). In addition, the study confirmed the influence of sheltering on sediment resuspension and that detailed information on the surface topography of the bed is required.

- Force-balance approaches

Due to their simplicity, several force-balance or moment balance models have been proposed for multilayer resuspension [4,274,284,285], following the initial works on monolayer resuspension. One of the first force-balance models for multilayer resuspension of aerosols was developed by Friess and Yadigaroglu [284] including the effect of the deposit structure (illustrated in Fig. 36). For that purpose, a deposit is first generated numerically respecting the distribution in particle sizes and a given value of the deposit porosity; second, resuspendable clusters are identified (as unobstructed clusters of particles that have a single contact with the rest of the bed and cannot be extended); third, the resuspension rate of each cluster $k_r\big|_{F_{adh}}$ is evaluated considering a force-balance approach between hydrodynamic forces (due to bursting events) and one value of the adhesion force.

The analysis of numerical results and comparisons with previous experiments (such as the STORM and PARESS experiments

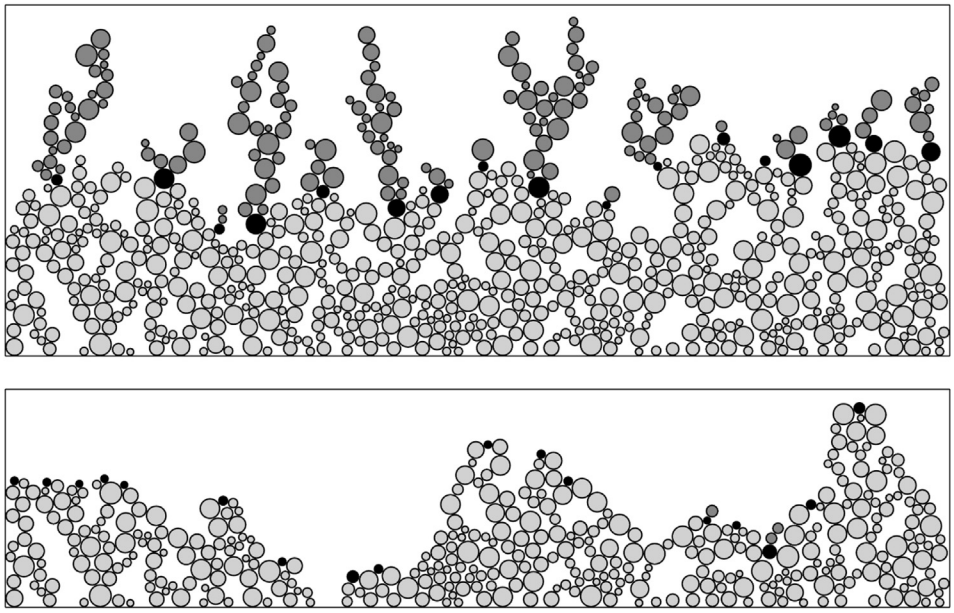

Fig. 36. Visualisation of a numerical aerosol bed (porosity of 0.61, layer number of 10.5, geometric standard deviation of particle size 1.35) before resuspension (top) and after resuspension of 50% of the deposit (bottom). Dark grey circles are resuspendable materials while dark circles represent "cluster feet" where each resuspendable cluster is in contact with the rest of the bed. Reprinted from [284]. Copyright 2002 with permission from Elsevier.

[284]) showed that the resuspension rate depends highly on the bed porosity: structures with a high porosity are very fragile compared to less porous structures where particles are more compactly organised and harder to remove [284]. In addition, the resuspension rate can evolve with the layer number.

Similarly, sediment reentrainment has been simulated using an Eulerian calculation of the fluid phase coupled with a Lagrangian tracking of particles (or clusters) and a force-balance model for particle resuspension [4]. Following the work of Friess and Yadigaroglu [284], the key notion behind this approach is to describe single particle or cluster motion and to develop corresponding models for their resuspension. To that extent, the authors described the reentrainment of a particle (or cluster) moving on a sediment bed with a balance between gravity, hydrodynamic forces and all inter-particle (or inter-cluster) forces.

- Kinetic PDF approaches

An extension of kinetic PDF models based on a force-balance approach towards multilayer resuspension was proposed recently by Tregnaghi et al. [264,280], who studied the reentrainment of sediments in rivers. For that purpose, the authors modified Eq. (54) for the resuspension rate, which is obtained considering that the PDF of adhesion forces and hydrodynamic forces are independent. In the case of multilayer resuspension, both adhesion forces and hydrodynamic forces become dependent on the particle elevation compared to the surrounding deposited particles (see Fig. 37): particles resting in a deep bed hole are harder to remove than particles protruding from the bed.

As a result, the resuspension rate is given by:

$$k_r = n \iint_{F_{hydro} \geq F_{adh}} P\left(F_{\mathrm{hydro}}, F_{\mathrm{adh}}\right) \mathrm{d}F_{\mathrm{hydro}} \mathrm{d}F_{\mathrm{adh}} \tag{65}$$

where $P(F_{\mathrm{hydro}}, F_{\mathrm{adh}})$ is the joint PDF of adhesion and hydrodynamic forces. The authors proposed a refined formula for the resuspension rate that takes into account the dependence of hydrodynamic forces on the particle height compared to the mean bed elevation as well as the distribution in the particle elevation. Statistical information required in the model was derived from experimental results (using PIV) and numerical simulations (based on discrete particle models) provided in another paper [280]. The satisfying results obtained for sediments (of a few millimetres) with this modelling approach have shown that accurate stochastic models can be proposed for multilayer resuspension as long as they properly account for the deposit morphology and particle arrangements.

Another stochastic model for multilayer resuspension has been proposed considering either tangential rolling motion or wall-normal motion [271,286,287]. For that purpose, the model was developed in the framework of static force-balance approaches but considering not only the hydrodynamic force F_{hydro} but also its duration T_{hydro}. The relevant parameter for resuspension is thus the impulse of hydrodynamic forces I_{hydro} defined as:

$$I_{\mathrm{hydro}}(t_i) = \int_{t_i}^{t_i + T_{\mathrm{hydro}}} F_{\mathrm{hydro}}(t) \mathrm{d}t \tag{66}$$

The resuspension rate is then given by Eq. (54) where forces are replaced by impulses (whose distribution is thus accounted for). The main difference with the previous model of Tregnaghi et al. [264] lies in the fact that this model accounts for the contribution of long-lasting 'burst'-events in the near-wall region that lead to resuspension. In the model from Tregnaghi et al. [264], the underlying assumption is that hydrodynamic forces are strong enough to move particles from their resting position but, consequently, it cannot capture resuspension in low flow conditions where hydrodynamic forces are small (whereas this new model can account for resuspension in that case). However, these limitations are inherent to quasi-static force-balance approaches and can be overcome by dynamic approaches.

The RnR model [114] has also been extended to multilayer resuspension [288]. For that purpose, a force-balance approach was retained considering a layer-by-layer model similar to the one initially proposed by Friess and Yadigaroglu [284]: when a particle from the layer labelled i is resuspended, a particle from the underlying layer $i-1$ is exposed to the flow and can later be resuspended.

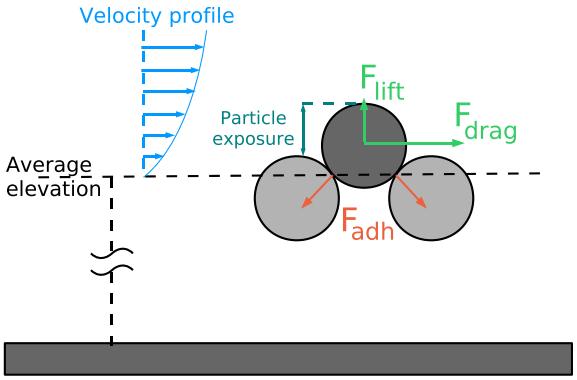

Fig. 37. Geometrical sketch of a particle resting on a sediment bed with a given average elevation above the initial surface.

As a result, the resuspension rate $k_{r,i}$ of each layer labelled i is expressed in terms of both hydrodynamic and adhesion forces (with their distribution) and also in terms of the number of resuspended particles from the above layer $i-1$. Therefore, this model can account for differences in the resuspension rate of each layer. Yet, the difficulty regarding this extended RnR model lies in the resuspension of clusters, which can regroup particles inside various layers.

- Dynamic PDF approaches

To the authors' knowledge, no dynamic PDF approach has yet been proposed for multilayer resuspension. This can be understood as such dynamic PDF approaches are recent proposals [210,245] which, at the moment, have been devised for the case of monolayer resuspension as a first modelling step. Clearly, given the present modelling state-of-the-art discussed in Section 5, this will represent the next challenge for these methods. Furthermore, the lack of dynamic PDF approaches for multilayer resuspension is related to the detailed scenarios which are simulated in a step-by-step manner in these approaches. These scenarios need to be, first, well understood and, second, well characterised from a statistical point of view. At present, the lack of dynamics PDF models is linked with the lack of detailed statistical information on the deposit morphology/structure/porosity and particle arrangement. It is expected that special work will be devoted to this issue in the future.

- Fully Lagrangian approaches

Apart from these models for multilayer resuspension, fully-Lagrangian approaches for particle-laden flows have also been used to simulate resuspension from a bed of particles. For instance, a MD-like algorithm was used to study the resuspension of N aerosol particles (0.6–30 μm) forming a cluster on a surface exposed to a turbulent flow [12]. Particle motion was solved considering the contributions from inter-particle adhesion forces, gravity forces and hydrodynamic forces (both drag and lift forces since lift forces can influence large particle motion [7]). This Lagrangian tracking of particles was coupled with a calculation of the fluid phase (here an eddy-fluid model, which is a method that describes the rotating part of a fluid consisting of many "fluid particles"). Numerical results showed that the dynamics of aerosol clusters depends strongly on the balance between inter-particle, hydrodynamic and gravity forces. DEM methods have also been used to simulate multilayer particle resuspension [289,281]. For example, the modified DEM approach proposed by Iimura et al. [289] describes rotational and translational particle motion (having a 500 nm radius) as resulting from the balance between particle–surface, particle–particle and hydrodynamic forces. Interactions between surfaces were modelled considering van der Waals non-contact forces and a spring repulsive force between contacting surfaces. Hydrodynamic forces were calculated taking into account shielding effects (this was done by discretising each particle surface and integrating hydrodynamic forces on the surface elements exposed to the flow) and using an analytical formula for the fluid velocity around a particle. The numerical simulations showed that, under low flow conditions, the deposit is only deformed and particle resuspension is nearly non-existent. At higher flow velocities, particle resuspension occurs (see Fig. 38).

Moreover, in accordance with the experimental observations of multilayer resuspension (see Section 6.1.1), the amount of resuspended particle as well as the shape of resuspended materials (either single particles or large clusters) was found to depend strongly on the flow velocity, the initial deposit morphology (porosity) and the ratio between particle–surface and particle–particle interactions [289]. It should be noted, though, that such results were possible using very detailed microscopic calculations (and thus time and CPU-consuming) of the hydrodynamic force exerted on each particle (more precisely on the surface exposed to the flow). Other simulations have been performed coupling a LES (Large-Eddy Simulation) calculation of the fluid phase with a DEM approach for the resuspension of sediments (of a few millimetres) [281,290]. The proposed DEM approach described sediment rolling motion on a bed including contributions from drag, lift, gravity and intersurface forces. The modified DEM algorithm was refined to account for five possible states: particles moving in the fluid, particles moving in contact with a single particle, particles moving in contact with two other particles, particles at rest with possible motion, particles at rest without possible motion. In that sense, this DEM algorithm is similar to the dynamic PDF approach for particle resuspension from monolayer deposit (see Section 5.4) since it tries to capture the complex motion of particles on a rough bed composed of similar particles. This modified DEM approach showed that some features of multilayer resuspension can be captured but that quantitative validations require a better characterisation of near-wall velocities close to clusters and deposit morphologies (this limitation being inherent to the choice of an LES simulation).

6.2. *Particle resuspension after impaction*

Multilayer resuspension is more complex than monolayer resuspension since the two processes of hydrodynamic particle

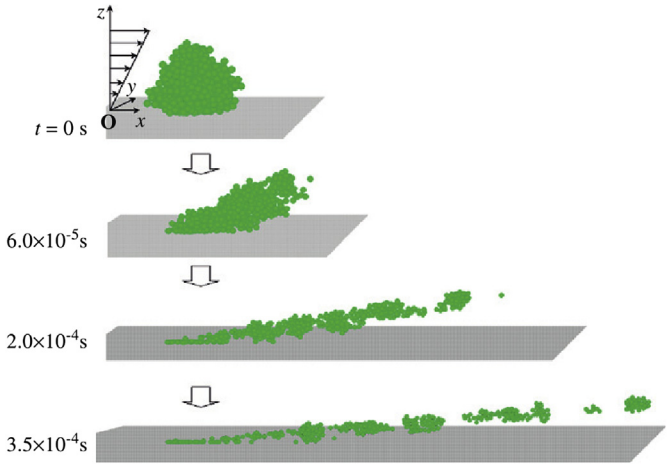

Fig. 38. Snapshots of particle reentrainment from an initially nearly spherical cluster exposed to shear flow (shear stress of 267 Pa) with a Hamaker constant $A_{Ham} = 1.3 \times 10^{-20}$ J for particle–particle and particle–surface interactions. Reprinted from [289]. Copyright 2009 with permission from Elsevier.

resuspension on the one hand and resuspension due to moving particles impacting a deposit on the other hand are coupled [7,31,94,274,291,292]. The resuspension rate due to impacts of particles/agglomerates on the surface can significantly increase the resuspension rate when the flow velocity is high (especially for large particles) [5]. Therefore, this phenomenon cannot be neglected in the multilayer resuspension process and is discussed in the present section. In the following, we review both experiments and models that have studied resuspension from multilayers due to particle impact and we list some of the remaining issues that need to be addressed in this field (another recent review on wind-blown sand and dust emissions mentioned the difficulties related to resuspension after saltation [7]).

Most of the studies on resuspension after impaction are concerned with large cohesionless particles, since such particles are highly subject to gravity which can bring resuspended particles back to the surface. For instance, the effect of 'saltating particles' has been studied extensively in wind-blown sand and dust [7]. Yet, in the present review, we have chosen to use the term 'saltating particles' for any resuspended particle brought back to the surface regardless of the size of the particles involved. In our belief, since the same phenomenon takes place (only the relative importance of forces is changed), making a distinction with respect to particle size is not justified.

6.2.1. Experimental studies on particle resuspension after impaction

As for the case of monolayer resuspension, the difficulty in analysing experimental data for multilayer resuspension after impaction is that the particles involved in this process can have a wide range of sizes (from a few micrometres to a few millimetres or even metres, i.e. large particles where adhesion forces are not significant). Yet, most of the experimental studies on this specific topic considered sand or dust particles due to their strong (and thus measurable) impact on the resuspension rate [7]. For instance, the resuspension rate of large aerosols (with a diameter of 100 or 200 μm) from a surface in a wind tunnel experiment was shown to increase by a factor of nearly 2 when saltating particles are present [292]. Similar observations were made for the removal of submicron-sized and micron-sized spheres from surfaces by dry ice blasting (ice agglomerates with a diameter of a few tens of micrometres) [293,294]: the removal efficiency is mainly due to resuspension by particle impaction, which depends on the jet flow velocity and on the particle size (smaller particles are harder to remove than larger ones).

Following such global observations on the overall resuspension rate, several experiments have been designed with a bed of pre-deposited particles exposed to a particle jet or to a single particle impact [291,293–298]. Such measurements have provided more detailed information on the mechanisms of particle resuspension after impaction and on its consequences on resuspension.

6.2.1.1. Splashing effect. Beladjine et al. [291] used high speed images to measure the effect of a PVC particle impacting a PVC bed (diameter of 6 mm). Typical results are depicted in Fig. 39 which shows that the impact of a single particle on a bed can result in a "splashing" effect (where several particles are ejected from the bed after the impact). This effect has been mostly studied experimentally with large inertial particles which, upon impaction, have a high kinetic energy compared to cohesion forces. Extracting particle velocities before and after impact, the authors also provided a measure of the restitution coefficient $\bar{e}$ (defined as the ratio of the velocity after rebound to the impacting velocity): it was shown to decrease with an increasing impact angle θ_{imp} according to the following law: $\bar{e} = c_1 - c_2 \sin(\theta_{\mathrm{imp}})$ (with c_1 and c_2 two parameters). This result suggests that part of the energy (or momentum) from the impacting particle is transferred to the deposit and that this energy transfer can induce resuspension of other particles within the bed. Other experiments of dust particles (6 mm) impacting a similar bed provided further data on the distribution of particle velocity after impact and on the effect of the incident angle or of the impacting velocity [298].

More recently, PTV systems were used to measure the resuspension of sand particles (diameter ranging from 192 to 303 μm) after impaction [295,296]. The restitution coefficient was shown to be lower for loose (unconsolidated) deposits than for compact (consolidated) ones, meaning that more energy (or momentum) is absorbed by loose deposits. The ejection angles were also smaller for loose deposits than for compact ones, suggesting that the deposit morphology plays a significant role in this resuspension phenomenon. In addition, the distributions in the number of particles ejected from the deposit and in their angle of ejection were found to depend not only on the impacting velocity and angle, but also on the deposit structure as well as on the particle nature (especially its elastic properties). This suggests that the resuspension by impaction is linked with energy propagation through the deposit formed on the surface, with possible energy dissipation through surface deformation.

Other high-speed recordings of resuspension after impact between millimetre-sized particles (1–20 mm) have shown that the phenomenon depends also on the relative size of particles involved as well as on their density ratio [299]. In particular, three different features have been observed: the impacting particle can either rebound on the surface, or move in a direction parallel to the deposit or even penetrate within the deposit depending on its initial velocity and on the impacting angle (see Fig. 40).

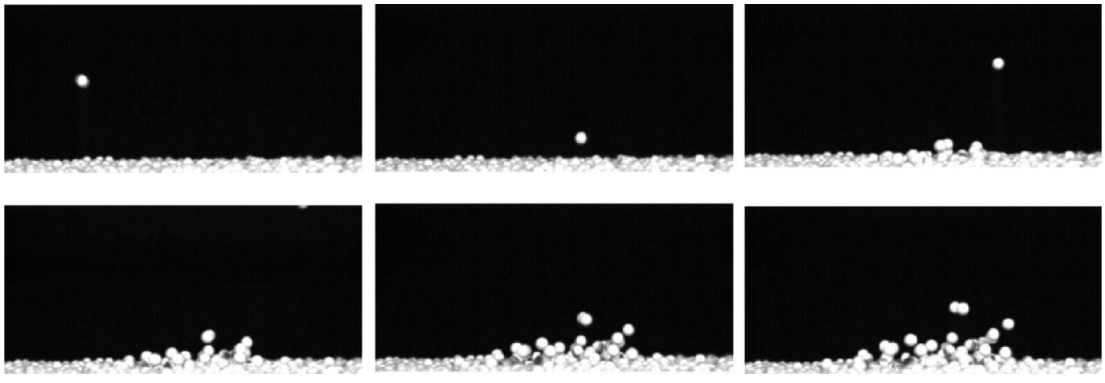

Fig. 39. High-speed images of the splashing of surface particles (of a few millimetres) by an impacting saltation particle (the time between two images is 4 ms). Reprinted from [291]. Copyright 2007 with permission from American Physical Society.

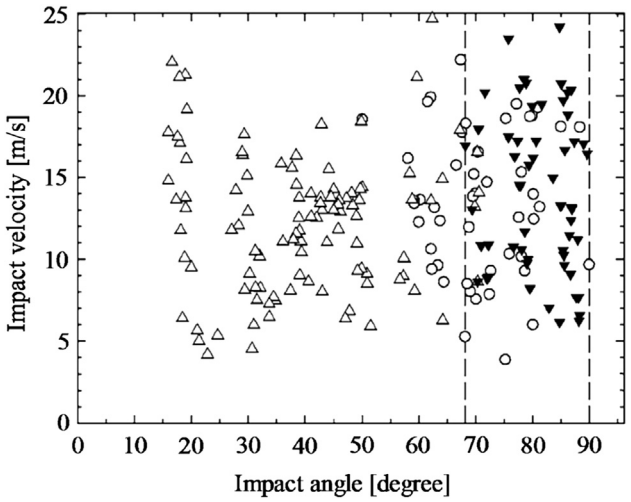

Fig. 40. Particle motion after the impact of 11.1 mm alumina ceramic on 6 mm polystyrene beds (penetration black triangles; rebound white triangles; motion in a direction parallel to the horizontal plane of the granular media: white circles). Reprinted from [299]. Copyright 2010 with permission from Springer.

6.2.1.2. Impact fragmentation. More recent studies have focussed on another aspect linked with resuspension after impaction [300–305]: how do agglomerates fragment after impacting a surface? Indeed, not only single particles can impact the surface after being resuspended but reentrained agglomerates can also reach the surface and, upon impaction, be split with part of them staying on the surface and part of them bouncing off the surface. This effect has been studied recently for small (colloidal) particles, where cohesion forces play an important role. For instance, Froeschke et al. [300] explored the fragmentation of various nanoparticle agglomerates (Ag, Ni and TiO_2 particles of 3–95 nm) on a plate using TEM (Transmission Electron Microscopy) micrographs analysis of agglomerates sticking to the surface. The degree of fragmentation (which is a measure of the amount of fragmented materials) was shown to increase with higher impacting velocities. In addition, the degree of fragmentation depends on the structure of the agglomerate: more compact agglomerates (i.e. with higher coordination numbers) are harder to break. Comparing various nanoparticles, it was also observed that the bond energy between two primary particles significantly affects agglomerate fragmentation. This was further confirmed by Seipenbusch et al. [303–305], who showed that the cohesiveness of nanoparticle powders is significantly impacted by van der Waals forces and possibly by other forces (such as magnetic forces or sintering effects). As a result, impact fragmentation is higher for smaller particles. Besides, detailed analysis of the size distributions after impact fragmentation have highlighted that satisfactory evaluations can be obtained according to Weibull statistics. More recently, Ihalainen et al. [301,302] measured the properties of both deposited particles and bouncing particles after impaction of TiO_2 particles on a surface. The analysis of the fractal dimension (which is a measure of the agglomerate structure) showed no significant difference between bouncing and sticking particles. This experiment further confirmed the dependence of impact fragmentation on the impacting velocity but also brought forward the complex effects of sintering on fragmentation. The authors also underlined that impact fragmentation can vary with the nature of the surface considered.

6.2.2. Numerical models for particle resuspension after impaction

Similar to the models for hydrodynamic multilayer resuspension, particle–particle interactions as well as the deposit structure need to be properly accounted for to obtain satisfactory models for multilayer resuspension after impaction. However, as underlined by John and Sethi [297], the underlying mechanisms for impaction are different than hydrodynamic resuspension. Indeed, numerical results obtained with a simple model based on particle deformation (thus including energy transfer between particles) were shown to capture relatively well experimental data of a micrometre particle bouncing on a bed (composed of micrometre-sized particles) while another simple model based on particle rotational motion underestimated significantly the experimental data. Therefore, models for particle resuspension after impaction include the effect of the transfer of energy upon impaction with eventually dissipation due to deformation coupled with a description of the deposit structure (see the review by John [306]). Yet the difficulty in establishing such models lies in the complex structure of particle deposits and in the wide range of scales involved in the process.

6.2.2.1. Binary-collision models. A first category of models was developed to include the transfer of energy from one particle to another through impact by considering a binary-collision approach [307,308]. In that case, each binary collision is assumed to be independent and is modelled assuming elastic collisions between spherical particles. The post-collisional energy is then modified to account for dissipation (through deformation for instance) using a multiplicative factor $\beta_{\text{diss}} \leq 1$. As a result, the whole transfer of energy through the deposit amounts to a succession (or chain) of independent binary collision (see Fig. 41).

Fig. 41 also reveals that the direction of energy propagation is a complex random function related to the 3D deposit structure (here disordered packing of spheres) and that a part of the impacting momentum/energy can be "backscattered" by the packing eventually leading to the ejection of particles at the surface of the packing. The ejection of particles from the packing then depends on the amount of momentum that has been transferred to them, which again is an intricate function of the deposit structure (since momentum and energy are split upon each binary collision, leading to the fragmentation of energy during propagation) and of the energy dissipation. This 3D model was shown to reproduce correctly the measured statistics showing a dependence of resuspension by impaction (with millimetre particles) on both the impacting velocity and the impacting angle [307].

6.2.2.2. DEM models. Several modelling approaches are based on a DEM formulation of particle motion [298,309–315]. The fact that, in DEM approaches, particle–particle interactions are naturally included in the equation of particle motion makes it a legitimate modelling framework for particle resuspension after impaction. The various DEM models then differ from each other due to the

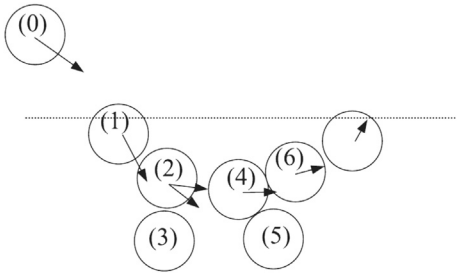

Fig. 41. Sketch of a chain of binary collisions leading to the ejection of a particle in the bed. Reprinted from [307]. Copyright 2007 with permission from the American Physical Society.

level of description of the deposit structure or to the forces that are included in the simulation of particle motion.

For instance, a 2D DEM model with a contact force formulation (including particle elastic deformation) was applied to study the impact of large particles on a 2D granular layer (0.65 m soil particles) [309]. As seen in Fig. 42, numerical results confirmed the role of the deposit structure on the energy propagation and thus on resuspension. In addition, the impacting particle size (as well as the ratio with the size of soil particles) together with its velocity and impacting angle were shown to significantly influence the results.

A specific study of the interaction between the impacting particle and the soil particles provided evidence of a three-phase process in particle rebound [309]: the impacting energy is first exchanged to soil particles, followed by a propagation shockwave that can eventually transfer energy back to the impacting particle and eject it (either through backscattering effects or reflection of the propagation shockwave on the soil surface). The rebound of the impacting particle was shown to depend strongly on the impacting particle size (and thus its initial kinetic properties). This model was further used with soil particles of 0.3 m to evaluate the consequences of the energy propagation on the deposit structure [310]. Numerical results showed that, when the impacting energy is high, the energy propagation can lead to the breakage of contact chains followed by a long recovery-phase where a new equilibrium state is created (with new bonds).

A 2D DEM simulation with an elasto-plastic model for inter-particle interactions was performed for millimetre-sized particles impacting a bed of similar particles and numerical results were compared to experimental data. It was shown that the resuspension depends on the energy propagation, which results from the transmission of energy through contact forces and from the energy reflection on the soil surface. Therefore, the resuspension is a complex function of the number of layers in the deposit, the nature of particles (elastic and plastic properties), the angle of impact and the kinetic energy upon impact.

3D DEM simulations of resuspension after impaction were performed [298,315]. For instance, a 3D DEM model including both adhesion forces between particles and contact deformation (through a spring constant) showed that the rebound or sticking of particles on a bed is affected by the adhesion forces and the spring constant [311]. The structure of the deposit (coordination number, porosity) was also found to be affected by these parameters. Other 3D DEM calculations provided information on statistical properties of interest in the splashing of particles [298,315]. For example, Xing et al. [315] extracted statistical information from their 3D DEM simulation on the average ejection velocity (and its dependence on the initial impact velocity), on the number of ejected particles (which increases with the impact velocity) and on the angle of ejection. Similarly, Oger et al. [298] showed that a 3D DEM simulation including visco-elastic interactions between particles provides satisfactory results for the distribution of the particle ejection velocity, of the ejection angle and of the restitution coefficient compared to 2D experimental data at various initial impacting velocity and impacting angle.

Besides, other DEM simulations of millimetre particle impact on a bed have shown that three cases can occur: the particle can rebound on the surface, it can stick to the surface or even penetrate within it [312,314]. The occurrence of one case instead of another one as well as the depth penetration depends on both impacting properties (particle velocity, impact angle, size) and deposit properties (structural ordering, polydispersity, visco-elastic properties).

6.2.2.3. Other approaches. Simulations have been developed recently for colloidal particles [316,317]. For instance, Grzybowski and Gradoń [316] coupled molecular dynamics and lattice-Boltzmann methods to simulate the reentrainment of particles from powder structures exposed to turbulent flows. Such calculations account for the coupling between particle–fluid, particle–surface and particle–particle interactions while treating each scale involved with detailed evaluations. Similar calculations have explored the effect of adhesion forces and agglomerate structures on the impact fragmentation of nanoparticles on surfaces as well as the possibility of having cluster restructurisation [317].

6.2.3. Summary and open issues concerning multilayer resuspension

Both the experimental data and the modelling approaches to multilayer resuspension have revealed that the forces at play in multilayer resuspension are similar to those in monolayer resuspension (with adhesion forces being now modified by parti cle–particle interactions). Yet, due to the complexity of inter-particle arrangement and interactions, the resulting mechanisms are more intricate: particles can be resuspended either due to hydrodynamic forces or due to the impact of particles/agglomerates on the surface.

Hydrodynamic multilayer resuspension is indeed affected by a number of factors (most of them being related to the deposit morphology) [1,13,32,88,284]: intersurface forces, the deposit structure (including particle arrangement, porosity, the layer location), clustering effects (resuspension of aggregates), ageing effects (including deposit restructuration), hydrodynamic forces

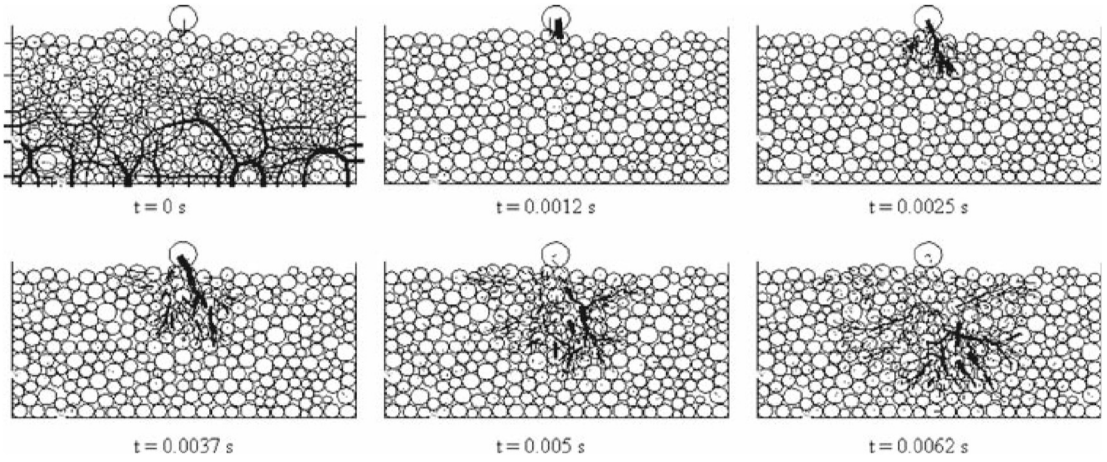

Fig. 42. Snapshots of compression wave propagation obtained with a 2D DEM model. Reprinted from [309]. Copyright 2008 with permission from Springer.

(including hiding/sheltering effects and two-way coupling). As a result, it is not surprising to find that most modelling approaches for monolayer resuspension have been extended and adapted to multilayer resuspension by including the effects of particle–particle interactions and of the deposit morphology (such as the coordination number). However, our present understanding of hydrodynamic multilayer resuspension could be completed with detailed experimental data highlighting the link between resuspension mechanisms (i.e. rolling, sliding and lifting) and the relative importance of forces at play as well as more detailed characterisation of the size distribution of resuspended particles/agglomerates. It is believed that, with recent advances in PTV and PIV techniques [120], such data could be measured. Besides, although modelling approaches appear adapted to small particles (since the forces involved are accounted for), they nevertheless need to be further tested in that case. Further developments of dynamic PDF approaches are also expected in the near future.

Even though experimental data on multilayer resuspension after impaction are still scarce and mostly devoted to large particles, available studies have provided some insights into the basic mechanisms. It has been shown that both the amount of splashing and the amount of impact fragmentation are complex functions of the following parameters: impacting particle velocity, impacting angle, size and nature of impacting particles, size of particles in the deposit, deposit or agglomerate structure (porosity, coordination number, fractal dimension), cohesive forces (eventually related to surface deformation). However, further experiments are needed on the splashing effect with colloidal particles to assess the importance of this phenomenon for small particles compared to impact fragmentation. Besides, the impact of large agglomerates on multilayered structures still has to be explored and characterised experimentally. As far as modelling approaches are concerned, most of them are based on DEM simulations since they can naturally include microscopic details of particle–particle interactions. They have confirmed the fact that resuspension due to impaction is related to the propagation of energy within the deposit, which is a complex function that depends both on particle properties (impact velocity and angle, size, nature) and on agglomerate/cluster properties (structure, visco-elastic properties, nature, size). Also, recent simulations have shown that promising results can be obtained by coupling detailed microscopic methods (MD) with lattice-Boltzmann calculations. It thus appears realistic to assume that new stochastic approaches (for instance in the context of kinetic PDF or dynamic PDF approaches) will be developed in the near future.

6.2.3.1. Open issues. Despite recent advances in the field of multilayer resuspension, there is still a lack of detailed information (both from an experimental and a numerical point of view) on a number of the factors at play in multilayer resuspension [1,4,13,32,88,306].

(i) *Deposit morphology*: whereas the deposit structure (porosity) has been measured for sediments, there is no information on the structure of the deposits for smaller particles (such as colloids). Furthermore, as mentioned in a previous review on deposition [33], the dependence of the deposit/agglomerate structure on the flow and physico-chemical conditions has not been explored experimentally. Some numerical studies have investigated the effect of the deposit shape or of the porosity on resuspension [289] but these situations have not yet been linked with proper real experiments. Characterisations of the deposit morphology as a function of both hydrodynamics and physico-chemical conditions can be obtained experimentally following the recent study of Papanicolaou et al. [318], who described irregular clusters using fractal analysis. This will be relevant in multilayer resuspension since the resulting information is useful in all stochastic approaches as well as in MD or DEM Lagrangian calculations.

(ii) *Restructuration*: for large cohesionless particles, a number of studies have explored how the deposit shapes are modified due to the action of hydrodynamic forces (see for instance wind-driven sand or dust dunes [7]). However, the evolution of the microscopic structure (such as the coordination number) with time and with the amount of particles deposited has not been characterised, especially for small particles. Some experimental data have shown a decrease of the resuspension rate with time [6,104]. This feature has been sometimes attributed to a deposit restructuration of the first deposited layers that are more compact (and thus harder to remove) [284]. Similarly, when a particle impacts a surface, the energy propagation within the deposit structure can eventually lead to a breakage of the contact chains [309,310] followed by a recovery-phase towards a new equilibrium. This deposit restructuration requires further investigations since it can play a crucial role in the formation of more compact deposit which are less likely to be resuspended later.

(iii) *Two-way coupling*: another issue in the context of multilayer resuspension is related to two-way coupling between the fluid and the particles. In the case of large cohesionless particles, several studies have included the effect of multilayer deposits on fluid motions using modified wall-functions that accounted for the evolution of large-scale roughness features due to the deposit [7]. However, in the case of small particles (where adhesion forces are significant), the size of one particle is too small to significantly perturb the flow in the viscous sublayer. As a result, the effect on the flow is harder to model due to the separation of scales involved (DNS-like calculations are also not suitable for large-scale studies due to the large number of colloidal particles). For instance, the use of adaptable-mesh methods requires a proper description of the evolution of the computational grid due to the continuous deposition/resuspension of particles to account for two-way coupling. A new mathematical model for the evolution of the deposit height with time has been proposed recently [319] and has been shown to be applicable with Lagrangian approaches. In addition, the presence of saltating particles can have a significant influence on the near-wall flow velocity [7] which need to be further characterised and modelled.

(iv) *Surface roughness*: the effects of geometrical singularities on the surface of particles on the resuspension after impaction have not been characterised. Similarly to particle deposition or monolayer resuspension, surface roughness can lower the cohesion between surfaces and affect the energy transfer through a deposit.

(v) *Deformation*: plastic deformation can significantly affect the energy propagation and, thus, resuspension.

(vi) *Consolidation phenomenon*: some recent experimental studies on multilayer resuspension have explored the effect of sintering on the bond energy between particle and its consequences on resuspension [301,302]. Sintering occurs at high temperature and leads to the creation of stronger bonds between contacting particles due to the precipitation occurring on surfaces. Such modifications of particle bond energies with time after the formation of a deposit are generally referred to as 'consolidation' processes, which have been studied recently in the context of heat exchanger fouling (see for instance [320–322]).

From the recent experimental and numerical works on multilayer resuspension, it appears that the two main mechanisms at

play (i.e. hydrodynamic multilayer resuspension and resuspension after impaction) have been understood to a certain extent but that significant advances in the fields of hydrodynamics, materials physics and interface chemistry are still required to reach a more mature comprehension of this phenomenon. Yet, since most studies have focussed on large cohesionless particles (with a few being available for small particles), there is still a lack of knowledge on the overall coupling between hydrodynamic resuspension and resuspension after impaction and especially on their relative importance. In fact, whereas it appears clear that saltating particles play a significant role in the case of wind-blown sand and dust [7] (due to the high kinetic energy associated with impacting particles compared to fluid flow stresses), some care should be adopted when conclusions are to be drawn for much-smaller particles such as colloids. Colloids are indeed small low-inertia particles and the energy at impact for colloids can be comparable to hydrodynamic forces exerted on the deposit exposed to the flow (though, large agglomerates can play a significant role in resuspension by impaction due to their higher inertia). For that reason, further experiments and simulations are required to assess the relative importance of these two phenomena with respect to the whole range of particle diameters (and inertia).

7. Conclusion

Particle resuspension is a good example of how a question at the intersection of physics, engineering and even daily concerns can contain intricate issues. Although the present review was devoted to resuspension, it has been mentioned at various moments that resuspension is closely related to deposition and that it can even be regarded as its 'mirror' physical mechanism. These two issues have been the long-term object of investigations, for example in the context of particle fouling in industrial situations where it may be believed that they represent impediments to proper operations of industrial processes. However, this is not necessarily the case. There are more and more applications where deposition and resuspension are fundamental aspects which are used specifically to achieve some predefined objectives. Typical examples are provided by the increasing number of applications in micro-science and biologically oriented developments where new materials and new surface properties are tailored by controlling a desired level of particle deposition and re-entrainment. Clearly, this requires an in-depth understanding of these fundamental phenomena. In turn, this makes the issue of particle resuspension a stimulating and lively subject which raises fundamental questions while still being rooted in practical questions. It also explains why there are continuous interests and active studies devoted to shed light on the mechanisms at play in particle resuspension.

In this paper, we have reviewed recent works on particle resuspension with a view towards bringing out the significant progress which has been achieved over the last years. With respect to the objectives given in the Introduction, a number of conclusions can be set forth:

(i) This review has been presented in terms of the three fundamental physical interactions, namely particle–fluid, particle–surface and particle–particle interactions, whose interplay has been shown to create the variety of phenomena observed. This reflects the structure also adopted in a recent review on particle deposition [33] and indicates that this decomposition is relevant. Furthermore, one of the key interests of this approach is to point clearly to three separate fields of fluid dynamics, interface chemistry and material surface properties (see Section 2). There is not a one-to-one correspondence between the three interactions and the three fields, as particle–surface and particle–particle forces refer both to interface chemistry and material surface properties. Yet, this matrix-like approach remains simple while allowing all aspects of deposition/resuspension issues to be addressed in a straightforward manner.

(ii) The analysis of experimental works (as presented in Section 3) has revealed that an important clarification is gained when we consider also the ratio of the particle diameter with respect to the size of the viscous sublayer. The introduction of this new dimensionless particle size is helpful to distinguish between 'small' and 'large' particles and to show that the separate mechanisms of particle rolling/sliding or interactions with burst-like fluid ejections are mostly valid but for the class of small and large particles respectively. Each of these mechanisms can be the relevant one but for different types of particles, without having to be regarded as competitive explanations of particle resuspension.

(iii) A new classification has been introduced in the discussion of available models for monolayer particle resuspension (see Section 5). This hierarchy allows to separate between the classical static approaches (which gather force-balance and kinetic PDF models) and recent approaches which have been described as dynamic PDF models. Drawing on the physical mechanisms (see Section 4) and on detailed scenarios of re-entrainment, these dynamic PDF models have been shown to represent a marked improvement in the ability of modelling approaches to reproduce particle dynamical aspects of resuspension. It is believed that such developments have brought models to an interesting level of maturity for the simulation of resuspension from monolayer deposits and are thus promising candidates for the development of unified modelling approaches for resuspension. At this point, it is worth noting that such unified modelling approaches (such as dynamic PDF or DEM methods) raise a new specific issue related to the models used for the calculation of the fluid seen by adhering particles (which is needed in the evaluation of hydrodynamic forces). This point has not been extensively developed in Section 5 since it mostly concerns recent dynamic PDF approaches or DEM methods (which rely on a fine level of description of particle motion). In fact, this question is related to the more general issue of the consistency between models for the fluid phase and for the particle phase: it is straightforward to see that very fine levels of description of particle dynamics require similar detailed information on the fluid phase, which can only be obtained with a fine-enough modelling approach for the fluid (for instance, an LES calculation of the fluid phase will not be fully consistent with a detailed DEM method for particle tracking unless proper models are added to reintroduce the filtered information regarding small-scale features of turbulence). This consistency issue between models for particle and fluid motion has been discussed more extensively in the companion paper [33] on particle deposition.

(iv) In contrast with the state-of-the-art achieved by models of monolayer resuspension, the development of modelling approaches for multilayer particle resuspension is still in its infancy. This is explained by our limited understanding of the relevant mechanisms involved. Two such mechanisms, referred to as hydrodynamic resuspension (where clusters are fragmented by fluid actions and entrained away from the surface) and particle impaction (where saltating particles with high kinetic energies can transfer energy to deposited particles), have been brought out and analysed (see Section 6). It may be that these two mechanisms depend on the particle size and its related inertia: particle impaction is significant for

large particles (which can acquire significant kinetic energy when suspended and coming towards wall surfaces) but not necessarily for small colloidal particles whereas hydrodynamical resuspension seems to affect the whole range of particle size (and thus may be more relevant for small colloidal particles compared to particle impaction). Yet, these are just preliminary indications and, clearly, multilayer resuspension is still an open issue where pioneering investigations are needed to come up with a complete picture of resuspension.

In spite of the extent of the present review, a number of issues have been left out of the discussion.

- *Coupling resuspension and deposition*: as recalled above, particle resuspension generally occurs together with particle deposition. The competition between these two phenomena has been shown to be responsible for the formation of complex structures on the surface [323–325]. For instance, measurements of particle deposition and resuspension showed that three different patterns can be obtained depending on the balance between hydrodynamics and interface chemistry: no-layer, striped patterns or filmy deposition [326–329]. The coupling between particle deposition and resuspension is also responsible for the movements of dunes in deserts [7]. Similarly to unified modelling approaches for particle resuspension, coupling particle deposition and reentrainment in modelling approaches requires to have consistent descriptions for the fluid and for the particles (see also [33]). In addition, the models for particle deposition and particle resuspension should also be consistent: for instance, coupling a macroscopic formula for particle resuspension (such as in Eq. (51)) with a very fine Lagrangian method for particle deposition appears inefficient due to the difference in the level of information required.
- *Organic or biological particles*: within the scope of the present review, only the resuspension of solid non-organic particles was considered. However, resuspension can involve organic or biological particles. The phenomenology of resuspension for such particles is similar to solid particles but the forces involved can be different. For instance, microbial resuspension is more complex due to the occurrence of non-DLVO forces in intersurface forces [28]. Experiments with biological and bacterial materials have also shown that detachment from biofilms is governed by a balance between hydrodynamic forces and intersurface forces (such as DLVO forces, with possible inclusions of acid–base forces or interactions with polymers) [14,20,330–333] that can induce particle rolling motions [334]. Similarly, the resuspension of organic materials has also been studied experimentally in the context of the food industry [13,15]: it has been shown that reentrainment is a complex function of the gas velocity, the moisture content and the relative humidity (capillary forces). Lastly, experimental [11,335] and numerical [336] studies of particle resuspension in the environment underlined the role of the flow field, the floor geometry and nature, the intersurface forces (including capillary forces) in the walking-induced resuspension of micron-sized elements.

It is hoped that further works will address these open questions and help to achieve a deeper understanding of the rich and diverse question of particle resuspension.

Acknowledgement

The authors would like to express special thanks to Pr. Jacek Pozorski for useful advice.

Nomenclature

List of symbols

a_0	distance for adhesion moments [m]
A_{Ham}	Hamaker constant [J]
A_p	particle cross-sectional area exposed to flow [m^2]
β	damping term [s^{-1}]
C_A	added-mass coefficient
C_D	Drag coefficient
C_{surf}	surface concentration [$kg\,m^{-2}$]
δ_{VS}	extent of the near-wall viscous sublayer [m]
$\Delta\gamma$	surface energy [$J\,m^{-2}$]
Δt	time interval [s]
d_{asp}	asperity diameter [m]
d_p	particle diameter [m]
$\overline{e}$	restitution coefficient after impact
e	electron charge [C]
ε_0	dielectric permittivity of vacuum [$F\,m^{-1}$]
ε_r	dielectric constant of a medium
E_1 or E_2	elastic modulus [$N\,m^{-1}$]
E_{adh}	adhesion energy for a particle [J]
E_{kin}	kinetic energy of a particle [J]
E_{barr}	energy barrier [J]
F	force [N]
$\langle F\rangle$	average force [N]
f	fluctuations of a force [N]
g	gravitational acceleration [$m\,s^{-2}$]
γ^-	electron-donor surface tension parameter [$J\,m^{-2}$]
γ^+	electron-acceptor surface tension parameter [$J\,m^{-2}$]
h	distance between surfaces [m]
I	particle moment of inertia [$kg\,m^2$]
I_{IS}	solution ionic strength [M]
J	flux [$kg\,m^2\,s^{-1}$]
k_B	Boltzmann constant [$J\,K^{-1}$]
k_p	deposition rate [$m\,s^{-1}$]
k_r	resuspension rate [s^{-1}]
κ^{-1}	Debye length [m]
K	equivalent elastic modulus [$N\,m^{-2}$]
λ_{asp}	peak-to-peak distance between asperities [m]
λ_{AB}	decay length of liquid molecules [m]
m_p	particle mass [kg]
$M_O(F)$	moment of a force around a point O [N m]
μ_f	fluid dynamic velocity [Pa s]
μ_T	Tabor dimensionless coefficient
μ_s	friction coefficient
n_{asp}	number of asperities
ν_1 or ν_2	Poisson ratio
ν_f	fluid kinematic velocity [$m^2\,s^{-1}$]
ϕ	potential of a surface [in V]
$P(F)$	probability density function of a force
r_c	equilibrium contact radius [m]
Re	flow Reynolds number
Re_p	particle Reynolds number
R_{asp}	asperity radius [m]
R_{part}	particle radius [m]
ρ_f	fluid density [$kg\,m^{-3}$]
ρ_p	particle density [$kg\,m^{-3}$]
S_{cov}	surface coverage [%]
t	time [s]
T_f	fluid temperature [K]
τ_p	particle relaxation timescale [s]
τ_f	flow shear stress [Pa]
τ_w	critical shear stress for resuspension [Pa]
θ_{imp}	angle of impact [rad]

u_τ flow shear velocity at the wall [m s^{-1}]
U interaction energy [J]
U_{SA} interaction energy between a sphere and an asperity [J]
U_{SP} interaction energy between a sphere and a smooth plate [J]
U_{SR} interaction energy between a sphere and a rough plate [J]
U_f fluid velocity [m s^{-1}]
U_p particle velocity [m s^{-1}]
U_R fluid velocity relative to the particle [m s^{-1}]
U_s velocity of the fluid seen by particles [m s^{-1}]
x_p particle position [m]
y_p particle wall-normal distance from the wall [m]
z_0 equilibrium separation for surfaces at contact [m]
ω_p particle angular velocity [s^{-1}]
ω frequency [s^{-1}]
Bold symbols represent vectors.

Subscript
// related to the wall-tangential direction
$\perp$ related to the wall-normal direction
AB related to the acid-base interactions
adh related to adhesion
dep related to deposition
drag related to drag
ext related to external contributions
frict related to friction
f→p related to friction
grav related to gravity
hydro related to hydrodynamics
lift related to lift
reent related to reentrainment
rot related to rotational motion
RnR related to the RnR model
RRH related to the RRH model
trans related to translational motion

Superscript
+ normalised by wall units
rms root-mean-square value

List of abbreviations
AB acid-base
AFM atomic force microscopy
BD Brownian dynamics
CFD computational fluid dynamics
CMC critical micelle concentration
CPU central processing unit
DEM distinct element methods
DLVO Derjaguin–Landau Verwey–Overbeek
DMT Derjaguin–Muller–Toporov
DNS direct numerical simulation
DPD dissipative particle dynamics
DPI dry powder inhalers
EDL electrostatic double-layer
FEM finite element method
HTR high temperature reactor
JKR Johnson–Kendall–Roberts
LD Langevin dynamics
LES large-eddy simulation
MD molecular dynamics
MDF mass density function
M–P Maugis–Pollock
PDF probability density function
PSL polystyrene latex
PTV particle tracking velocimetry
PIV particle image velocimetry
PWR pressurised water reactor
PMMA poly(methyl methacrylate)
PVC poly(vinyl chloride)
RH relative humidity
rhs right-hand side
RnR Rock 'n' Roll (model)
RO reverse osmosis
RRH Reeks–Reed–Hall (model)
SEI surface element integration
SEM scanning electron microscope
TEM transmission electron microscopy
VDW van der Waals
X-DLVO extended-DLVO

References

[1] Ziskind G. Particle resuspension from surfaces: revisited and re-evaluated. Rev Chem Eng 2006;22:1–123.
[2] Mani M, Pillai R. Impact of dust on solar photovoltaic (PV) performance: research status, challenges and recommendations. Renew Sustain Energy Rev 2010;14:3124–31.
[3] Stempniewicz MM, Komen EMJ. Comparison of several resuspension models against measured data. Nucl Eng Des 2010;240:1657–70.
[4] Coleman SE, Nikora VI. A unifying framework for particle entrainment. Water Resour Res 2008;44:W04415.
[5] Harris AR, Davidson CI. A Monte Carlo model for soil particle resuspension including saltation and turbulent fluctuations. Aerosol Sci Technol 2009;43:161–73.
[6] Chiou SF, Tsai CJ. Measurement of emision factor of road dust in a wind tunnel. Powder Technol 2011;118:10–5.
[7] Kok JF, Parteli EJR, Michaels TI, Karam DB. The physics of wind-blown sand and dust. Rep Prog Phys 2012;75:106901.
[8] Hu B, Freihaut JD, Bahnfleth WP, Thran B. Measurements and factorial analysis of micron-sized particle adhesion force to indoor flooring materials by electrostatic detachment method. Aerosol Sci Technol 2008;42:513–20.
[9] Kim Y, Gidwani A, Wyslouzil BE, Sohn CW. Source term models for fine particle resuspension from indoor surfaces. Build Environ 2010;45:1854–65.
[10] Zhou B, Zhao B, Tan Z. How particle resuspension from inner surfaces of ventilation ducts affects indoor air quality – a modeling analysis. Aerosol Sci Technol 2011;45:996–1009.
[11] Kubota Y, Higushi H. Aerodynamic particle resuspension due to human foot and model foot motions. Aerosol Sci Technol 2013;47:208–17.
[12] Gac J, Sosnowksi TR, Gradon L. Turbulent flow energy for aerosolization of powder particles. Aerosol Sci 2008;39:113–26.
[13] Hanus MJ, Langrish TAG. Resuspension of wall deposits in spray dryers. J Zhejiang Univ Sci A 2007;8:1762–74.
[14] Mercier-Bonin M, Dehouche A, Morchain J, Schmitz P. Orientation and detachment dynamics of Bacillus spores from stainless steel under controlled shear flow: modelling of the adhesion force. Int J Food Microbiol 2011;146:182–91.
[15] Hanus MJ, Langrish TAG. Re-entrainment of wall deposits from a laboratory-scale spray dryer. Asia-Pacific J Chem Eng 2007;2:90–107.
[16] Kissane MP, Zhang F, Reeks MW. Dust in HTRs: its nature and improving prediction of its resuspension. Nucl Eng Des 2012;251:301–5.
[17] Ouf FX, Delcour S, Azema N, Coppalle A, Ferry L, Gensdarmes F, et al. Contribution to the study of particle resuspension kinetics during thermal degradation of polymers. J Hazard Mater 2013;250–251:298–307.
[18] Dagaonkar M, Majumdar U. Morphology of fibrous material on colloid filtration. J Eng Fibers Fabrics 2012;7:62–74.
[19] Gac J, Gradon L. Computational analysis of displacement of particles with given size on the nonstationary bulging membrane as a theoretical model of membrane fouling. Chem Process Eng 2013;34:109–19.
[20] Johnson WP, Li X, Assemi S. Deposition and re-entrainment dynamics of microbes and non-biological colloids during non-perturbed Transp Porous Media in the presence of an energy barrier to deposition. Adv Water Resour 2007;30:1436–54.
[21] Du Y, Shen C, Zhang H, Huang Y. Effects of flow velocity and nonionic surfactant on colloid straining in saturated porous media under unfavorable conditions. Transp Porous Media 2013;98:193–208.
[22] Garny K, Horn H, Neu TR. Interaction between biofilm development, structure and detachment in rotating annular reactors. Bioprocess Biosyst Eng 2008;31:619–29.
[23] Phares DJ, Holt JK, Smedley GT, Flagan RC. Method for characterization of adhesion properties of trace explosives in fingerprints and fingerprint simulations. J Forensic Sci 2000;45:774–84.
[24] Fletcher R, Briggs N, Ferguson E, Gillen G. Measurement of air jet removal efficiencies of spherical particles from cloth and planar surfaces. Aerosol Sci Technol 2008;42(12):1052–61.

[25] Keedy R, Dengler E, Ariessohn P, Novosselov I, Aliseda A. Removal rates of explosive particles from a surface by impingement of a gas jet. Aerosol Sci Technol 2012;46:148–55.
[26] Yiantsios SG, Sioutopoulos D, Karabelas AJ. Colloidal fouling of RO membranes: an overview of key issues and efforts to develop improved prediction techniques. Desalination 2005;183:257–72.
[27] Epstein N. Thinking about heat transfer fouling: a 5–5 matrix. Heat Transfer Eng 1983;4:43–56.
[28] Busscher HJ, Norde W, Sharma PK, van der Mei HC. Interfacial rearrangement in initial microbial adhesion to surfaces. Curr Opin Colloid Interf Sci 2010;15:510–7.
[29] Paw U KT, Braaten DA. New perspectives on rebound and reentrainment processes. Aerosol Sci Technol 1995;23:72–9.
[30] Murphy DM, Cziczo DJ, Hudson PK, Thomson DS, Wilson JC, Kojima T, et al. Particle generation and resuspension in aircraft inlets when flying in clouds. Aerosol Sci Technol 2004;38:401–9.
[31] Shao Y. Physics and Modelling of Wind Erosion. Springer; 2008.
[32] Boor BE, Siegel JA, Novoselac A. Monolayer and multilayer particle deposits on hard surfaces: literature review and implications for particle resuspension in the indoor environment. Aerosol Sci Technol 2013;355:417–22.
[33] Henry C, Minier JP, Lefèvre G. Towards a description of particulate fouling: from single particle deposition to clogging. Adv Colloid Interf Sci 2012;185-186:34–76.
[34] Pope SB. The PDF approach to turbulent reactive flows. Prog Energy Combust Sci 1985;11:119–92.
[35] Minier JP, Peirano E. The PDF approach to turbulent and polydispersed two-phase flows. Phys Rep 2001;352(1–3):1–214.
[36] Gatignol R. The Faxén formulae for a rigid particle in an unsteady non-uniform Stokes flow. J Méc Théor Appl 1983;1(2):143–60.
[37] Maxey MR, Riley JJ. Equation of motion for a small rigid sphere in a nonuniform flow. Phys Fluids 1983;26(4):883–9.
[38] Pope SB. Turbulent flows. Cambridge University Press; 2000.
[39] Kim J, Moin P, Moser R. Turbulence statistics in fully developed channel flow at low Reynolds number. J Fluid Mech 1987;177:133–66.
[40] Lelouvetel J, Bigillon F, Doppler D, Vinkovic I, Champagne JY. Experimental investigation of ejections and sweeps involved in particle suspension. Water Resour Res 2009;45:W02416.
[41] van Hout R. Time-resolved PIV measurements of the interaction of polystyrene beads with near-wall-coherent structures in a turbulent channel flow. Int J Multiphase Flow 2011;37:346–57.
[42] Bernardini M, Pirozzoli S, Orlandi P. The effect of large-scale turbulent structures on particle dispersion in wall-bounded flows. Int J Multiphase Flow 2013;51:55–64.
[43] Vinkovic I, Doppler D, Lelouvetel J, Buffat M. Direct numerical simulation of particle interaction with ejections in turbulent channel flows. Int J Multiphase Flow 2011;37:187–97.
[44] Marchioli C, Soldati A. Mechanisms for particle transfer and segregation in a turbulent boundary layer. J Fluid Mech 2002;468:283–315.
[45] Marchioli C, Giusti A, Salvetti MV, Soldati A. A direct numerical simulation of particle wall transfer in upward turbulent pipe flow. Int J Multiphase Flow 2003;29:1017–38.
[46] Soldati A, Marchioli C. Physics and modelling of turbulent particle deposition and entrainment: review of a systematic study. Int J Multiphase Flow 2009;35:827–39.
[47] Rouse DWI, Eaton JK. On the preferential concentration of solid particles in a turbulent channel flow. J Fluid Mech 2001;428:149–69.
[48] Guingo M, Minier JP. A stochastic model of coherent structures for particle deposition in turbulent flows. Phys Fluids 2008;20(5):053303.
[49] Kaftori D, Hetsroni G, Banerjee S. Particle behavior in the turbulent boundary layer. I. Motion, deposition, and entrainment. Phys Fluids 1995;7:1095.
[50] Kaftori D, Hetsroni G, Banerjee S. Particle behavior in the turbulent boundary layer. II. Velocity and distribution profiles. Phys Fluids 1995;7:1107.
[51] Soldati A, Marchioli C. Sediment transport in steady turbulent boundary layers: potentials, limitations, and perspectives for Lagrangian tracking in DNS and LES. Adv Water Resour 2012;48:18–30.
[52] Derjaguin B, Landau L. Theory of the stability of strongly charged lyophobic sols and of the adhesion of strongly charged particles in solution of electrolytes. Acta Physicochim USSR 1941;14:633–62.
[53] Verwey E, Overbeek JTG. Theory of stability of lyophobic colloids. Elsevier; 1948.
[54] Hunter RJ. Foundations of colloid science. 2nd ed. Oxford University Press; 2001.
[55] Liang Y, Hilal N, Langston P, Starov V. Interactions forces between colloidal particles in liquid: theory and experiment. Adv Colloid Interf Sci 2007;134-135:151–66.
[56] Israelachvili JN. Intermolecular & surface forces. 3rd ed. Academic Press; 2011.
[57] Elimelech M, Gregory J, Jia X, Williams RA. Particle deposition and aggregation: measurement, modelling and simulation. Butterworth Heinemann; 1995.
[58] Parsegian VA. van der Waals forces: a handbook for biologists, chemists, engineers, and physicists. Cambridge University Press; 2005.
[59] Adamczyk Z, Warszyński P. Role of electrostatic interactions in particle adsorption. Adv Colloid Interf Sci 1996;63:41–149.
[60] Adamczyk Z, Weroński P. Application of the DLVO theory for particle deposition problems. Adv Colloid Interf Sci 1999;83:137–226.
[61] Mohaupt M, Minier JP, Tanière A. A new approach for the detection of particle interactions for large-inertia and colloidal particles in a turbulent flow. Int J Multiphase Flow 2011;37:746–55.
[62] Henry C, Minier JP, Mohaupt M, Profeta C, Pozorski J, Tanière A. A stochastic approach for the simulation of collisions between colloidal particles at large time steps. Int J Multiphase Flow 2014;61:94–107.
[63] Henry C, Minier JP, Pozorski J, Lefèvre G. A new stochastic approach for the simulation of agglomeration between colloidal particles. Langmuir 2013;29:13694–707.
[64] von Smoluchowski M. Experiments on a mathematical theory of kinetic coagulation of colloid solutions. Z Phys Chem 1917;92:129–68.
[65] Friedlander SK. Smoke, dust and haze - fundamentals of aerosol dynamics. 2nd ed. Oxford University Press; 2000.
[66] Suresh L, Walz JY. Effect of surface roughness on the interaction energy between a colloidal sphere and a flat plate. J Colloid Interf Sci 1996;183:199–213.
[67] Suresh L, Walz JY. Direct measurement of the effect of surface roughness on the colloidal forces between a particle and flat plate. J Colloid Interf Sci 1997;196:177–90.
[68] Bhattacharjee S, Ko CH, Elimelech M. DLVO interaction between rough surfaces. Langmuir 1998;14:3365–75.
[69] Hoek EMV, Bhattacharjee S, Elimelech M. Effect of membrane surface roughness on colloid-membrane DLVO interactions. Langmuir 2003;19:4836–47.
[70] Martines E, Csaderova L, Morgan H, Curtis ASG, Riehle MO. DLVO interaction energy between a sphere and a nano-patterned plate. Colloids Surf A: Physicochem Eng Aspects 2008;318:45–52.
[71] Zhao H, Bhattacharjee S, Chow R, Wallace D, Masliyah JH, Xu Z. Probing surface charge potentials of clay basal planes and edges by direct force measurements. Langmuir 2008;24:12899–910.
[72] Huang X, Bhattacharjee S, Hoek EMV. Is surface roughness a “Scapegoat” or a primary factor when defining particle–substrate interactions? Langmuir 2010;26:2528–37.
[73] Vaidyanathan R, Tien C. Hydrosol deposition in granular media under unfavorable surface conditions. Chem Eng Sci 1991;46:967–83.
[74] Velegol D, Thwar PK. Analytical model for the effect of surface charge nonuniformity on colloidal interactions. Langmuir 2001;17:7687–93.
[75] Kemps JAL, Bhattacharjee S. Interactions between a solid spherical particle and a chemically heterogeneous planar substrate. Langmuir 2005;21:11710–21.
[76] Nazemifard N, Masliyah JH, Bhattacharjee S. Particle deposition onto charge heterogeneous surfaces: convection–diffusion–migration model. Langmuir 2006;22:9879–93.
[77] Duffadar RD, Davis JM. Interaction of micrometer-scale particles with nanotextured surfaces in shear flow. J Colloid Interf Sci 2007;308:20–9.
[78] Duffadar RD, Davis J. Dynamic adhesion behavior of micrometer-scale particles flowing over patchy surfaces with nanoscale electrostatic heterogeneity. J Colloid Interf Sci 2008;326:18–27.
[79] Henry C, Minier JP, Lefèvre G, Hurisse O. Numerical study on the deposition rate of hematite particles on polypropylene walls: role of surface roughness. Langmuir 2011;27:4603–12.
[80] Bhattacharjee S, Elimelech M. Surface element integration: a novel technique for evaluation of DLVO interaction between a particle and a flat plate. J Colloid Interf Sci 1997;193:273–85.
[81] Bhattacharjee S, Elimelech M, Borkovec M. DLVO interactions between colloidal particles: beyond Derjaguin’s approximation. Croat Chem Acta 1998;71:883–903.
[82] Bhattacharjee S, Chen JY, Elimelech M. DLVO interaction energy between spheroidal particles and a flat surface. Colloids Surf A: Physicochem Eng Aspects 2000;165:143–56.
[83] Bhattacharjee S, Sharma A. Apolar, polar, and electrostatic interactions of spherical particles in cylindrical pores. J Colloid Interf Sci 1997;187:83–95.
[84] Kline TR, Chen G, Walker SL. Colloidal deposition on remotely controlled charged micropatterned surfaces in a parallel-plate flow chamber. Langmuir 2008;24:9381–5.
[85] Chatterjee R, Mitra SK, Bhattacharjee S. Particle deposition onto janus and patchy spherical collectors. Langmuir 2011;27(14):8787–97.
[86] Rotsch C, Radmacher M. Mapping local electrostatic forces with the atomic force microscope. Langmuir 1997;13:2825–32.
[87] Ma H, Pazmino E, Johnson WP. Surface heterogeneity on hemispheres-in-cell model yields all experimentally-observed non-straining colloid retention mechanisms in porous media in the presence of energy barriers. Langmuir 2011;27:14982–94.
[88] Gradoń L. Resuspension of particles from surfaces: technological, environmental and pharmaceutical aspects. Adv Powder Technol 2009;20:17–28.
[89] Ziskind G, Fichman M, Gutfinger C. Resuspension of particulates from surfaces to turbulent flows - review and analysis. J Aerosol Sci 1995;26:613–44.
[90] Hubbe MA. Detachment of colloidal hydrous oxide spheres from flat solids exposed to flow – 1. Experimental system. Colloids Surf 1985;16:227–48.
[91] Hubbe MA. Detachment of colloidal hydrous oxide spheres from flat solids exposed to flow – 2. Mechanism of release. Colloids Surf 1985;16:249–70.
[92] Hubbe MA. Detachment of colloidal hydrous oxide spheres from flat solids exposed to flow – 3. Forces of adhesion. Colloids Surf 1987;25:311–24.

[93] Hubbe MA. Detachment of colloidal hydrous oxide spheres from flat solids exposed to flow – 4. Effect of polyelectrolytes. Colloids Surf 1987;25:325–39.
[94] Ibrahim AH, Dunn PF, Brach RM. Microparticle detachment from surfaces exposed to turbulent air flow: controlled experiments and modeling. J Aerosol Sci 2003;34:765–82.
[95] Ibrahim AH, Dunn PF, Brach RM. Microparticle detachment from surfaces exposed to turbulent air flow: effect of flow and particle deposition characteristics. J Aerosol Sci 2004;35:805–21.
[96] Ibrahim AH, Brach RM, Dunn PF. Microparticle detachment from surfaces exposed to turbulent air flow: microparticle motion after detachment. J Aerosol Sci 2004;35:1189–204.
[97] Ibrahim AH, Dunn PF, Qazi MF. Experiments and validation of a model for microparticle detachment from a surface by turbulent air flow. J Aerosol Sci 2008;39:645–56.
[98] Nino Y, Lopez F, Garcia M. Threshold for particle entrainment into suspension. Sedimentology 2003;50:247–63.
[99] Wu YL, Davidson CI, Russel AG. Controlled wind tunnel experiments for particle bounceoff and resuspension. Aerosol Sci Technol 1992;17:245–62.
[100] Meinders JM, Busscher HJ. Influence of ionic strength and shear rate on the desorption of polystyrene particles from a glass collector as studied in a parallel-plate flow chamber. Colloids Surf A: Physicochem Eng Aspects 1993;80:279–85.
[101] Braaten DA. Wind tunnel experiments of large particle reentrainment-deposition and development of large particle scaling parameters. Aerosol Sci Technol 1994;21:157–69.
[102] Phares DJ, Smedley GT, Flagan RC. Effect of particle size and material properties on aerodynamic resuspension from surfaces. J Aerosol Sci 2000;31:1335–53.
[103] Mukai C, Siegel JA, Novoselac A. Impact of airflow characteristics on particle resuspension from indoor surfaces. Aerosol Sci Technol 2009;43:1022–32.
[104] Wang S, Zhao B, Zhou B, Tan Z. An experimental study on short-time particle resuspension from inner surfaces of straight ventilation ducts. Build Environ 2012;53:119–27.
[105] Ryan JN, Gschwend PM. Effects of ionic strength and flow rate on colloid release: relating kinetics to intersurface potential energy. J Colloid Interf Sci 1994;164:21–34.
[106] Smedley GT, Phares DJ, Flagan RC. Entrainment of fine particles from surfaces by gas jets impinging at normal incidence. Exp Fluids 2001;26:324–34.
[107] Smedley GT, Phares DJ, Flagan RC. Entrainment of fine particles from surfaces by gas jets impinging at oblique incidence. Exp Fluids 2001;30:135–42.
[108] Bergendahl J, Grasso D. Prediction of colloid detachment in a model porous media: hydrodynamics. Chem Eng Sci 2000;55:1523–32.
[109] Zhang XW, Yao ZH, Hao PF, Hu HQ. Study on particle removal efficiency of an impinging jet by an image-processing method. Exp Fluids 2002;32:376–80.
[110] Bedrikovetsky P, Zeinijahromi A, Siqueira FD, Furtado CA, de Souza ALS. Particle detachment under velocity alternation during suspension Transp Porous Media. Transp Porous Media 2012;91:173–97.
[111] Young RM, Hargather MJ, Settles GS. Shear stress and particle removal measurements of a round turbulent air jet impinging normally upon a planar wall. J Aerosol Sci 2013;62:15–25.
[112] Visser J. Measurement of the force of adhesion between submicron carbon-black particles and a cellulose film in aqueous solution. J Colloid Interf Sci 1970;34:26–31.
[113] Sharma MM, Chamoun H. Sita Rama Sarma, D.S.H., Schechter, R.S.. Factors controlling the hydrodynamic detachment of particles from surfaces. J Colloid Interf Sci 1992;149:121–34.
[114] Reeks MW, Hall D. Kinetic models for particle resuspension in turbulent flows: theory and measurement. J Aerosol Sci 2001;32:1–31.
[115] Jiang Y, Matsusaka S, Masuda H, Qian Y. Characterizing the effect of substrate surface roughness on particle-wall interaction with the airflow method. Powder Technol 2008;186:199–205.
[116] Traugott H, Hayse T, Liberzon A. Resuspension of particles in an oscillating grid turbulent flow using PIV and 3D-PTV. J Phys Conf Series 2011;318:052021.
[117] Sutherland AJ. Proposed mechanism for sediment entrainment by turbulent flows. J Geophys Res 1967;72:6183–94.
[118] Cleaver J, Yates B. Mechanism of detachment of colloidal particles from a flat substrate in a turbulent flow. J Colloid Interf Sci 1973;44(3):464–74.
[119] Munro RJ, Bethke N, Dalziel SB. Sediment resuspension and erosion by vortex rings. Phys Fluids 2009;21:046601.
[120] van Hout R. Spatially and temporally resolved measurements of bead resuspension and saltation in a turbulent water channel flow. J Fluid Mech 2013;715:389–423.
[121] Braaten DA, Paw U KT, Shaw RH. Coherent turbulent structures and particle detachment in boundary layer flows. J Aerosol Sci 1988;19:1183–6.
[122] Braaten DA, Paw U KT, Shaw RH. Particle resuspension in a turbulent boundary layer: observed and modelled. J Aerosol Sci 1990;21:613–28.
[123] Dwivedi A, Melville BW, Shamseldin AY, Guha TK. Flow structures and hydrodynamic force during sediment entrainment. Water Resour Res 2001;47:W01509.
[124] Lyklema J. Fundamentals of interface and colloid science. Particulate colloids, vol. IV. Elsevier Academic Press; 2005.
[125] Kappl M, Butt HJ. The colloidal probe technique and its application to adhesion force measurements. Part Part Syst Char 2002;19:129–43.
[126] Butt HJ, Cappella B, Kappl M. Force measurements with the atomic force microscope: technique, interpretation and applications. Surface Science Reports 2005;59:1–152.
[127] Drelich J, Tormoen GW, Beach ER. Determination of solid surface tension from particle-substrate pull-off forces measured with the atomic force microscope. J Colloid Interf Sci 2004;280:484–97.
[128] Dreschler A, Petong N, Zhang J, Kwok DY, Grundke K. Force measurements between Teflon AF and colloidal silica particles in electrolyte solutions. Colloids Surf A: Physicochem Eng Aspects 2004;250:357–66.
[129] Dreschler A, Grundke K. The influence of electrolyte ions on the interaction forces between polystyrene surfaces. Colloids Surf A: Physicochem Eng Aspects 2005;264:157–65.
[130] Eichenlaub S, Kumar G, Beaudoin S. A modeling approach to describe the adhesion of rough, asymmetric particles to surfaces. J Colloid Interf Sci 2006;299:656–64.
[131] Elmahdy MM, Dreschler A, Gutsche C, Synytska A, Uhlmann P, Kremer F, et al. Forces between blank surfaces as measured by the colloidal probe technique and by optical tweezers - a comparison. Langmuir 2009;25:12894–8.
[132] Freitas AM, Sharma MM. Detachment of particles from surfaces: an AFM study. J Colloid Interf Sci 2001;233:73–82.
[133] Taheri M, Bragg GM. A study of particle resuspension in a turbulent flow using a preston tube. Aerosol Sci Technol 1992;16:15–20.
[134] Negri F, Bedel E, Schmitz P. Experimental study of alumina particle removal from a plane surface. J Adhes 2002;78:79–95.
[135] Canseco V, Djehiche A, Bertin H, Omari A. Deposition and re-entrainment of model colloids in saturated consolidated porous media: experimental study. Colloids Surf A: Physicochem Eng Aspects 2009;352:5–11.
[136] Rabinovich E, Kalman H. Incipient motion of individual particles in horizontal particle-fluid systems: A. Experimental analysis. Powder Technol 2009;192:318–25.
[137] Shen C, Lazouskaya V, Jin Y, Li B, Ma Z, Zheng W, et al. Coupled factors influencing detachment of nano- and micro-sized particles from primary minima. J Contam Hydrol 2012;134–135:1–11.
[138] Elzo D, Schmitz P, Houi D, Joscelyne S. Measurement of particle/membrane interactions by a hydrodynamic method. J Membr Sci 1996;109:43–53.
[139] Bergendahl J, Grasso D. Prediction of colloid detachment in a model porous media: thermodynamics. AIChE J 1999;45:475–84.
[140] Ryde NP, Matijević E. Deposition and detachment studies of fine particles by the packed column technique. Colloids Surf A: Physicochem Eng Aspects 2000;165:59–78.
[141] Freitas AM, Sharma MM. Effect of surface hydrophobicity on the hydrodynamic detachment of particles from surfaces. Langmuir 1999;15:2466–76.
[142] Zelenev A, Matijević E. Surfactant-induced detachment of monodispersed hematite particles adhered on glass. J Colloid Interf Sci 2006;299:22–7.
[143] Sharma P, Flury M, Zhou J. Detachment of colloids from a solid surface by a moving air-water interface. J Colloid Interf Sci 2008;326:143–50.
[144] Ahmadi G, Guo S, Zhang X. Particle adhesion and detachment in turbulent flows including capillary forces. Part Sci Technol 2007;25:59–76.
[145] Ahmadi G, Guo S. Bumpy particle adhesion and removal in turbulent flows including electrostatic and capillary forces. J Adhes 2007;83:289–311.
[146] Zhang X, Ahmadi G. Effects of capillary force and surface deformation on particle removal in turbulent flows. J Adhes Sci Techn 2007;21:1589–611.
[147] Zhang X, Ahmadi G. Effects of electrostatic and capillary forces and surface deformation on particle detachment in turbulent flows. J Adhes Sci Technol 2011;25:1175–210.
[148] Audry MC, Ramos S, Charlaix E. Adhesion between highly rough alumina surfaces: an atomic force microscopy study. J Colloid Interf Sci 2009;331:371–8.
[149] George M, Goddard DT. The characterisation of rough particle contacts by atomic force microscopy. J Colloid Interf Sci 2006;299:665–72.
[150] Götzinger M, Peukert W. Particle adhesion force distributions on rough surfaces. Langmuir 2004;20:5298–303.
[151] Prokopovich P, Perni S. Multiasperty contact adhesion model for universal asperity height and radius of curvature distributions. Langmuir 2010;26:17028–36.
[152] Rabinovich YI, Adler JJ, Ata A, Singh RK, Moudgil BM. Adhesion between nanoscale rough surfaces: II. Measurement and comparison with theory. J Colloid Interf Sci 2000;232:17–24.
[153] Yang S, Zhang H, Hsu SM. Correction of random surface roughness on colloidal probes in measuring adhesion. Langmuir 2007;23:1195–202.
[154] Zhou S, Götzinger M, Peukert W. The influence of particle charge and roughness on particle-substrate adhesion. Powder Technol 2003;135–136:82–91.
[155] Zhou S, Peukert W. Modeling adhesion forces between deformable bodies by FEM and Hamaker summation. Langmuir 2008;24:1459–68.
[156] Greiner C, del Campo A, Arzt E. Adhesion of bioinspired micropatterned surfaces: effects of pillar radius, aspect ratio and preload. Langmuir 2007;23:3495–502.
[157] Taboada-Serrano P, Vithayaveroj V, Yiacoumi S, Tsouris C. Surface charge heterogeneities measured by Atomic Force Microscopy. Environ Sci Technol 2005;39:6352–60.
[158] Drelich J, Wang YU. Charge heterogeneity of surface charges: mapping and effects on surface forces. Adv Colloid Interf Sci 2011;165:91–101.

[159] Das SK, Schechter R, Sharma MM. The role of surface roughness and contact deformation on the hydrodynamic detachment of particles from surfaces. J Colloid Interf Sci 1994;164:63–77.
[160] Jiang Y, Matsusaka S, Masuda H, Yokohama T. Characterizing the effect of surface morphology on particle-wall interaction by the airflow method. Adv Powder Technol 2006;17:413–24.
[161] Zhang X, Ahmadi G, Qian J, Ferro A. Particle detachment, resuspension and transport due to human walking in indoor environments. J Adhes Sci Technol 2008;22:591–621.
[162] Goldasteh I, Ahmadi G, Ferro AR. Wind tunnel study and numerical simulation of dust particle resuspension from indoor surfaces in turbulent flows. J Adhes Sci Technol 2013;27:1563–79.
[163] Francis JRD. Experiments on the motion of solitary grains along the bed of a water stream. Proc R Soc A 1973;332:443–71.
[164] Otani Y, Namiki N, Eni H. Removal of fine particles from smooth flat surfaces by consecutive pulse air jets. Aerosol Sci Technol 1995;23:665–73.
[165] Reeks MW, Reed J, Hall D. On the resuspension of small particles by a turbulent flow. J Phys D: Appl Phys 1988;21:574–89.
[166] Wang HC. Effects of inceptive motion on particle detachment from surfaces. Aerosol Sci Technol 1990;13:386–93.
[167] Clift R, Grace JR, Weber M. Bubbles, drops and particles. Academic Press; 1978.
[168] Brennen CE. Fundamentals of multiphase flows. Cambridge University Press; 2005.
[169] Proudman I, Pearson JRA. Expansions at small Reynolds number for the flow past a sphere and a circular cylinder. J Fluid Mech 1957;2:237–62.
[170] Kaplun S, Lagerstrom PA. Asymptotic expansions of Navier-Stokes solutions for small Reynolds numbers. J Math Mech 1957;6:585–93.
[171] O'Neill M. A sphere in contact with a plane in a slow shear linear flow. Chem Eng Sci 1968;23:1293–8.
[172] Sweeney LG, Finlay WH. Lift and drag forces on a sphere attached to a wall in a Blasius boundary layer. J Aerosol Sci 2007;38:131–5.
[173] Ockendon JR, Evans GA. The drag on a sphere in low Reynolds number flow. J Aerosol Sci 1972;3:237–42.
[174] Liu CN, Chien CL, Lo CC, Lin GY, Chen SC, Tsai CJ. Drag coefficient of a spherical particle attached on the flat surface. Aerosol Air Qual Res 2011;11:482–6.
[175] Brenner H. The slow motion of a sphere through a viscous fluid towards a plane surface. Chem Eng Sci 1961;16:242–51.
[176] Maude A. The movement of a sphere in front of a plane at low Reynolds number. Br J Appl Sci 1963;14:894–8.
[177] Arcen B, Tanière A, Oesterlé B. On the influence of near-wall forces in particle-laden channel flows. Int J Multiphase Flow 2006;32:1326–39.
[178] Leighton D, Acrivos A. The lift on a small sphere touching a plane in the presence of a simple shear flow. J Appl Math Phys 1985;36:174–8.
[179] Hall D. Measurements of the mean force on a particle near a boundary in turbulent flow. J Fluid Mech 1988;187:451–66.
[180] Mollinger AM, Nieuwstadt FTM, Bessem JM. A new device to measure the lift force on a particle in the viscous sublayer. Measure Sci Technol 1995;6:206–13.
[181] Mollinger AM, Nieuwstadt FTM. Measurement of the lift force on a particle fixed to the wall in the viscous sublayer of a fully developed turbulent boundary layer. J Fluid Mech 1996;316:285–306.
[182] Takemura F, Takagi S, Magnaudet J, Matsumoto Y. Drag and lift forces on a bubble rising near a vertical wall in a viscous liquid. J Fluid Mech 2002;461:277–300.
[183] Takemura F, Magnaudet J. Drag and lift forces on a bubble rising near a vertical wall in a viscous liquid. J Fluid Mech 2003;495:235–53.
[184] Zeng L, Balachandar S, Fischer P. Wall-induced forces on a rigid sphere at finite Reynolds number. J Fluid Mech 2005;536:1–25.
[185] Zeng L, Balachandar S, Fischer P, Najjar F. Interactions of a stationary finite-sized particle with wall turbulence. J Fluid Mech 2005;594:271–305.
[186] Lee H, Balachandar S. Drag and lift forces on a spherical particle moving on a wall in a shear flow at finite Re. J Fluid Mech 2010;657:89–125.
[187] Saffman PG. The lift on a small sphere in a slow shear flow. J Fluid Mech 1965;22:385–400.
[188] Wang Q, Squires KD, Chen M, McLaughlin JB. On the role of the lift force in turbulence simulations of particle deposition. Int J Multiphase Flow 1997;23:749–63.
[189] Hubbe MA. Theory of detachment of colloidal particles from flat surfaces exposed to flow. Colloids Surf 1984;12:151–78.
[190] Rimai DS, DeMejo LP. Physical interactions affecting the adhesion of dry particles. Annu Rev Mater Sci 1996;26:21–41.
[191] Cappella B, Dietler G. Force-distance curves by atomic force microscopy. Surf Sci Rep 1999;34:1–104.
[192] Prokopovich P, Starov V. Adhesion models: from single to multiple asperity contacts. Adv Colloid Interf Sci 2011;168:210–22.
[193] Tabor D. Surface forces and surface interactions. J Colloid Interf Sci 1977;58:2–13.
[194] Johnson KL, Kendall K, Roberts A. Surface energy and contact of elastic solids. Proc R Soc A 1971;324:301–13.
[195] Derjaguin BV, Muller VM, Toporov YP. Effect of contact deformations on adhesion of particles. J Colloid Interf Sci 1975;53:314–26.
[196] Johnson KL, Greenwood JA. An adhesion map for the contact of elastic spheres. J Colloid Interf Sci 1997;192:326–33.
[197] Grierson DS, Flater EE, Carpick RW. Accounting for the JKR-DMT transition in adhesion and friction measurements with atomic force microscopy. J Adhes Sci Technol 2005;19:291–311.
[198] Maugis D. Adhesion of spheres: the JKR-DMT transition using a dugdale model. J Colloid Interf Sci 1992;150(1):243–69.
[199] Kumar D, Battacharya S, Ghosh S. Weak adhesion at the mesoscale: particles at an interface. Soft Matter 2013;9:6618–33.
[200] Rabinovich YI, Adler JJ, Ata A, Singh RK, Moudgil BM. Adhesion between nanoscale rough surfaces: I. Role of asperity geometry. J Colloid Interf Sci 2000;232:10–6.
[201] Cooper K, Ohler N, Gupta A, Beaudoin S. Analysis of contact interactions between a rough deformable colloid and a smooth substrate. J Colloid Interf Sci 2000;222:63–74.
[202] Cooper K, Gupta A, Beaudoin S. Substrate morphology and particle adhesion in reacting systems. J Colloid Interf Sci 2000;228:213–9.
[203] Cooper K, Gupta A, Beaudoin S. Simulation of the adhesion of particles to surfaces. J Colloid Interf Sci 2001;234:284–92.
[204] Thoreson EJ, Martin J, Burnham NA. The role of few-asperity contacts in adhesion. J Colloid Interf Sci 2006;298:94–101.
[205] Spalla O, Kékicheff P. Adhesion between oxide nanoparticles: influence of surface complexation. J Colloid Interf Sci 1997;192:43–65.
[206] Tsukruk VV, Bliznyuk VN. Adhesive and friction forces between chemically modified silicon and silicon nitride surfaces. Langmuir 1998;14:446–55.
[207] Kreller DI, Gibson G, vanLoon GW, Horton JH. Chemical force microscopy investigation of phosphate adsorption on the surfaces of iron(III) oxyhydroxyde particles. J Colloid Interf Sci 2002;254:205–13.
[208] Ong QK, Sokolov I. Attachment of nanoparticles to the AFM tips for direct measurements of interactions between a single nanoparticle and surfaces. J Colloid Interf Sci 2007;310:385–90.
[209] Eichenlaub S, Gelb A, Beaudoin S. Roughness models for particle adhesion. J Colloid Interf Sci 2004;280:289–98.
[210] Henry C, Minier JP, Lefèvre G. Numerical study on the adhesion and reentrainment of nondeformable particles on surfaces: the role of surface roughness and electrostatic forces. Langmuir 2012;28:438–52.
[211] Shen C, Lazouskaya V, Zhang H, Wang F, Li B, Jin Y, et al. Theoretical and experimental investigation of detachment of colloids from rough collector surfaces. Colloids Surf A: Physicochem Eng Aspects 2012;410:98–110.
[212] Shen C, Wu L, Zhang S, Ye H, Li B, Huang Y. Heteroaggregation of microparticles with nanoparticles changes the chemical reversibility of the microparticles attachment to planar surfaces. J Colloid Interf Sci 2014;421:103–13.
[213] Israelachvili JN. Intermolecular & surface forces. 2nd ed. Academic Press; 1991.
[214] Zhang H, Ding W, Law KY, Cetinkaya C. Adhesion properties of nanoparticle-coated emulsion aggregation toner. Powder Technol 2011;208:582–9.
[215] Maugis D, Pollock HM. Surface forces, deformation and adherence at metal microcontacts. Acta Metall 1984;32(9):1323–34.
[216] Jaiswal RP, Kumar G, Kilroy CM, Beaudoin SP. Modeling and validation of the van der Waals force during the adhesion of nanoscale objects to rough surfaces: a detailed description. Langmuir 2009;25:10612–23.
[217] Shen C, Huang Y, Li B, Jin Y. Predicting attachment efficiency of colloid deposition under unfavorable attachment conditions. Water Resour Res 2010;46:W11526.
[218] Shen C, Lazouskaya V, Zhang H, Li B, Jin Y, Huang Y. Influence of surface chemical heterogeneity on attachment and detachment of microparticles. Colloids Surf A: Physicochem Eng Aspects 2013;433:14–29.
[219] Bradford SA, Torkzaban S. Colloid interaction energies for physically and chemically heterogeneous porous media. Langmuir 2013;29:3668–76.
[220] Rumpf H. Particle technology. Chapman & Hall; 1990.
[221] Beach ER, Tormoen GW, Drelich J, Han R. Pull-off force measurements between rough surfaces by atomic force microscopy. J Colloid Interf Sci 2002;247:84–99.
[222] Li Q, Rudolf V, Peukert W. London-van der Waals adhesiveness of rough particles. Powder Technol 2006;161:248–55.
[223] Katainen J, Paajanen M, Ahtola E, Pore V, Lahtinen J. Particle adhesion and removal in model systems III. monodispersed ferric oxide on steel. J Colloid Interf Sci 2006;304:524–9.
[224] Greenwood JA, Williamson JPB. Contact of nominally flat surfaces. Proc R Soc A 1966;295:300–19.
[225] Persson BNJ. Contact mechanics for randomly rough surfaces. Surf Sci Rep 2006;61:201–27.
[226] Bush AA, Gibson RD, Thomas TR. The elastic contact of a rough surface. Wear 1975;35:87–111.
[227] Bush AA, Gibson RD, Keogh GP. Strongly anisotropic rough surfaces. J Lubri Technol 1979;101:15–20.
[228] Bradford SA, Torkzaban S. Colloid adhesive parameters for chemically heterogeneous porous media. Langmuir 2012;28:13643–51.
[229] Bradford SA, Torkzaban S, Shapiro A. A theoretical analysis of colloid attachment and straining in chemically heterogeneous porous media. Langmuir 2013;29:6944–52.
[230] Krupp H. Particle adhesion-theory and experiment. Adv Colloid Interf Sci 1967;1:111–239.
[231] Farshchi-Tabrizi M, Kappl M, Cheng Y, Gutmann J, Butt HJ. On the adhesion between fine particles and nanocontacts: an atomic force microscope study. Langmuir 2006;22:2171–84.

[232] Brant JA, Childress AE. Colloidal adhesion to hydrophilic membrane surfaces. J Membr Sci 2004;241:235–48.
[233] Hoek EMV, Agarwal GK. Extended DLVO interactions between spherical particles and rough surfaces. J Colloid Interf Sci 2006;298:50–8.
[234] Brant JA, Childress AE. Assessing short-range membrane-colloid interactions using surface energetics. J Membr Sci 2002;203:257–73.
[235] Wu W, Giese RF, van Oss CJ. Linkage between ζ-potential and electron donicity of charged polar surfaces: 1. Implications for the mechanism of flocculation of particle suspensions with plurivalent counterions. Colloids Surf A: Physicochem Eng Aspects 1994;89:241–52.
[236] Thio BJR, Lee JH, Meredith JC, Keller AA. Measuring the influence of solution chemistry on the adhesion of Au nanoparticles to mica using colloid probe atomic force microscopy. Langmuir 2010;26:13995–4003.
[237] Ziskind G, Fichman M, Gutfinger C. Adhesion moment model for estimating particle detachment from a surface. J Aerosol Sci 1997;28:623–34.
[238] Bergendahl J, Grasso D. Colloid generation during batch leaching tests: mechanics of disaggregation. Colloids Surf A: Physicochem Eng Aspects 1998;135:193–205.
[239] Ding W, Howard AJ, Murthy Peri MD, Cetinkaya C. Rolling resistance moment of microspheres on surfaces: contact measurements. Philos Mag 2007;87:5685–96.
[240] Maniero R, Climent E, Bacchin P. Adhesion and detachment fluxes of microparticles from a permeable wall under turbulent flow conditions. Chem Eng Sci 2012;71:409–21.
[241] Rabinovich E, Kalman H. Incipient motion of individual particles in horizontal particle-fluid systems: B. Theoretical analysis. Powder Technol 2009;192:326–38.
[242] Onoe H, Gel M, Hoshino K, Matsumoto K, Shimoyama I. Direct measurement of the binding force between microfabricated particles and a planar surface in aqueous solution by force-sensing piezoresistive cantilevers. Langmuir 2005;21:11251–61.
[243] Medina P, Sánchez MA, Redondo JM. Grid stirred turbulence: applications to the initiation of sediment motion and lift-off studies. Phys Chem Earth 2001;26:299–304.
[244] Lee H, Ha MY, Balachandar S. Rolling/sliding of a particle on a flat wall in a linear shear flow at finite Re. Int J Multiphase Flow 2011;37:108–24.
[245] Guingo M, Minier JP. A new model for the simulation of particle resuspension by turbulent flows based on a stochastic description of wall roughness and adhesion forces. J Aerosol Sci 2008;39:957–73.
[246] Harris AR, Davidson CI. Particle resuspension in turbulent flow: a stochastic model for individual soil grains. Aerosol Sci Technol 2008;42:613–28.
[247] Fu SC, Chao CYH, So RMC, Leung WT. Particle resuspension in a wall-bounded turbulent flow. J Fluids Eng 2013;135:041301.
[248] Minier JP, Peirano E, Chibbaro S. PDF model based on langevin equation for polydispersed two-phase flows applied to a bluff-body gas-solid flow. Phys Fluids 2004;16:2419–31.
[249] Anspaugh LR, Shinn JH, Phelps PF, Kennedy NC. Resuspension and redistribution of plutonium in soils. Health Phys 1975;29:571–82.
[250] Loosmore GA. Evaluation and development of models for resuspension of aerosols at short times after deposition. Atmos Environ 2003;37:639–47.
[251] Lengweiler P, Nielsen P, Moser A, Heiselberg P, Takai H. Deposition and resuspension of particles: which parameters are important?. In: Proceedings of roomvent 98: 6th international conference on air distribution in rooms, Stockolm, Swedenvol. 1; 1998. pp. 317–23.
[252] Loosmore GA, Hunt JR. Dust resuspension without saltation. J Geophys Res 2000;105:20663–71.
[253] Fan FG, Soltani M, Ahmadi G, Hart SC. Flow-induced resuspension of rigid-link fibers from surfaces. Aerosol Sci Technol 1997;27:97–115.
[254] Soltani M, Ahmadi G. On particle adhesion and removal mechanisms in turbulent flows. J Adhes Sci Technol 1994;8:763–85.
[255] Zhang H, Ahmadi G. Aerosol particle removal and re-entrainment in turbulent channel flows – a direct numerical simulation approach. J Adhes 2000;74:441–93.
[256] Yiantsios SG, Karabelas AJ. Detachment of spherical microparticles adhering on flat surfaces by hydrodynamic forces. J Colloid Interf Sci 1995;176:74–85.
[257] Nitschke D, Schmidt E. A new approach to model the re-entrainment of settled particles based on film theory of fluid mass transfer processes. Part Part Syst Char 2009;26:58–68.
[258] Burdick GM, Berman NS, Beaudoin SP. Hydrodynamic particle removal from surfaces. Thin Solid Films 2005;488:116–23.
[259] Goldasteh I, Ahmadi G, Ferro A. A model for removal of compact, rough, irregularly shaped particles from surfaces in turbulent flows. J Adhes 2012;88:766–86.
[260] Goldasteh I, Ahmadi G, Ferro AR. Monte Carlo simulation of micron size spherical particle removal and resuspension from substrate under fluid flows. J Aerosol Sci 2013;66:62–71.
[261] Pozorski J, Minier JP. Probability density function modelling of dispersed two-phase turbulent flows. Physical Review E 1998;59:855–63.
[262] Wen HY, Kasper G. On the kinetics of particle re-entrainment from surfaces. J Aerosol Sci 1989;20:483–98.
[263] Jurcik B, Wang HC. The modeling of particle resuspension in turbulent flow. J Aerosol Sci 1991;22:S149–52.
[264] Tregnaghi M, Bottacin-Busolin A, Marion A, Tait S. Stochastic determination of entrainment risk in uniformly sized sediment beds at low transport stages: 1. Theory. J Geophys Res 2012;117:F04004.
[265] Chibbaro S, Minier JP. Stochastic methods in fluid mechanics. CISM courses and lectures, vol. 548. Springer; 2013.
[266] Soldati A. Particles turbulence interactions in boundary layers. Z Angew Math Mech 2005;85:683–99.
[267] Lazaridis M, Drossinos Y. Multilayer resuspension of small identical particles by turbulent flow. Aerosol Sci Technol 1998;28:548–60.
[268] Vainshtein P, Ziskind G, Fichman M, Gutfinger C. Kinetic model of particle resuspension by drag force. Phys Rev Lett 1997;78:551–4.
[269] Biasi L. de los Reyes, A., Reeks, M.W., de Santi, G.F.. Use of a simple model for the interpretation of experimental data on particle resuspension in turbulent flows. J Aerosol Sci 2001;32:1175–200.
[270] Zhang F, Reeks M, Kissane M. Particle resuspension in turbulent boundary layers and the influence of non-Gaussian removal forces. J Aerosol Sci 2013;58:103–28.
[271] Valyrakis M, Diplas P, Dancey CL. Entrainment of coarse grains in turbulent flows: an extreme value theory approach. Water Resour Res 2011;47:W09512.
[272] Matida EA, Nishino K, Torii K. Statistical simulation of particle deposition on the wall from turbulent dispersed pipe flow. Int J Heat Fluid Flow 2000;21:389–402.
[273] Henry C, Minier JP. A stochastic approach for the simulation of particle resuspension from rough substrates: model and numerical implementation. Submitted to Aerosol Sci 2014.
[274] Theerachaisupakij W, Matsusaka S, Akashi Y, Masuda H. Reentrainment of deposited particles by drag and aerosol collision. J Aerosol Sci 2003;34:261–74.
[275] Kousaka Y, Okuyama K, Endo Y. Re-entrainment of small aggregate particles from a plane surface by air stream. J Chem Eng Jpn 1980;13:143–7.
[276] Matsusaka S, Masuda H. Particle reentrainment from a fine powder layer in a turbulent air flow. Aerosol Sci Technol 1996;24:69–84.
[277] Quadt T, Schmidt E. Resuspension of abiotic particles from ceramic membranes. Chem Eng Technol 2012;35:1885–91.
[278] Rabinovich E, Kalman H. Pickup velocity from particle deposits. Powder Technol 2009;194:51–7.
[279] Diplas P, Celik AO, Dancey CL, Valyrakis M. Nonintrusive method for detecting particle movement characteristics near threshold flow conditions. J Irrig Drain Eng 2010;136:774–80.
[280] Tregnaghi M, Bottacin-Busolin A, Marion A, Tait S. Stochastic determination of entrainment risk in uniformly sized sediment beds at low transport stages: 2. Experiments. J Geophys Res 2012;117:F04005.
[281] Schmeeckle MW, Nelson JM. Direct numerical simulation of bedload transport using a local, dynamic boundary condition. Sedimentology 2003;50:279–301.
[282] Bottacin-Busolin A, Tait SJ, Marion A, Chegini A, Tregnaghi M. Probabilistic description of grain resistance from simultaneous flow field and grain motion measurements. Water Resour Res 2008;44:W09419.
[283] Measures R, Tait S. Quantifying the role of bed surface topography in controlling sediment stability in water-worked gravel deposits. Water Resour Res 2008;44:W04413.
[284] Friess H, Yadigaroglu G. Modelling of the resuspension of particle clusters from multilayer aerosol deposits with variable porosity. J Aerosol Sci 2002;33:883–906.
[285] Theerachaisupakij W, Matsusaka S, Kataoka M, Masuda H. Effects of wall vibration on particle deposition and reentrainment in aerosol flow. Adv Powder Technol 2002;13:287–300.
[286] Celik AO, Diplas P, Dancey CL, Valyrakis M. Impulse and particle dislodgement under turbulent flow conditions. Phys Fluids 2010;22:046601.
[287] Valyrakis M, Diplas P, Dancey CL, Greer K, Celik AO. Role of instantaneous force magnitude and duration on particle entrainment. J Geophys Res 2010;115:F02006.
[288] Zhang F, Reeks MW, Kissane MP, Perkins RJ. Resuspension of small particles from multilayer deposits in turbulent boundary layers. J Aerosol Sci 2013;66:31–61.
[289] Iimura K, Watanabe S, Suzuki M, Hirota M, Higashitani K. Simulation of entrainment of agglomerates from plate surfaces by shear flows. Chem Eng Sci 2009;64:1455–61.
[290] Furbish DJ, Schmeeckle MW. A probabilistic derivation of the exponential-like distribution of bed load particle velocities. Water Resour Res 2013;49:1537–51.
[291] Beladjine D, Ammi M, Oger L, Valance A. Collision process between an incident bead and a three-dimensional granular packing. Phys Rev E 2007;75:061305.
[292] Fairchild CI, Tillery MI. Wind tunnel measurements of the resuspension of ideal particles. Atmos Environ 1982;16:229–38.
[293] Liu YH, Maruyama H, Matsusaka S. Effect of particle impact on surface cleaning using dry ice jet. Aerosol Sci Technol 2011;45:1519–27.
[294] Liu YH, Hirama D, Matsusaka S. Particle removal process during application of impinging dry ice jet. Powder Technol 2012;217:607–13.
[295] Gordon M, Neuman CM. A comparison of collisions of saltating grains with loose and consolidated silt surfaces. J Geophys Res 2009;114:F04015.
[296] Gordon M, Neuman CM. A study of particle splash on developing ripple forms for two bed materials. Geomorphology 2011;129:79–91.
[297] John W, Sethi V. Threshold for resuspension by particle impaction. Aerosol Sci Technol 1993;19:57–68.

[298] Oger L, Ammi M, Valance A, Beladjine D. Study of the collision of one rapid sphere on 3D packings: experimental and numerical results. Comput Math Appl 2005;55:132–48.
[299] Nishida M, Okumura M, Tanaka Y. Effects of density ratio and diameter ratio on critical incident angles of projectiles impacting granular media. Granular Matter 2010;12:337–44.
[300] Froeschke S, Kohler S, Weber AP, Kasper G. Impact fragmentation of nano-particle agglomerates. J Aerosol Sci 2003;34:275–87.
[301] Ihalainen M, Lind T, Torvela T, Lehtinen KEJ, Jokiniemi J. A method to study agglomerate breakup and bounce during impaction. Aerosol Sci Technol 2012;46:990–1001.
[302] Ihalainen M, Lind T, Arffman A, Torvela T, Jokiniemi J. Break-up and bounce of TiO_2 agglomerates by impaction. Aerosol Sci Technol 2014;48:31–41.
[303] Seipenbusch M, Froeschke S, Weber AP, Kasper G. Investigation on the fracturing of nanoparticle agglomerates: first results. Proc Inst Mech Eng Part E – J Process Mech Eng 2002;216:219–25.
[304] Seipenbusch M, Toneva P, Peukert W, Weber AP. Impact fragmentation of metal nanoparticle agglomerates. Part Part Syst Char 2007;24:193–200.
[305] Seipenbusch M, Rothenbacher S, Kirchhoff M, Schmid H, Kasper G, Weber AP. Interparticle forces in silica nanoparticle agglomerates. J Nanopart Res 2010;12:2037–44.
[306] John W. Particle-surface interactions: charge transfer, energy loss, resuspension, and deagglomeration. Aerosol Sci Technol 1995;23:2–24.
[307] Crassous J, Beladjine D, Valance A. Impact of a projectile on a granular medium described by a collision model. Phys Rev Lett 2007;99:248001.
[308] Valance A, Crassous J. Granular medium impacted by a projectile: experiment and model. Eur Phys J E 2009;30:43–54.
[309] Bourrier F, Nicot F, Darve F. Physical processes within a 2D granular layer during an impact. Granular Matter 2008;10:415–37.
[310] Bourrier F, Nicot F, Darve F. Evolution of the micromechanical properties of impacted granular materials. C R Mec 2010;338:639–47.
[311] Kobayashi T, Tanaka T, Shimada N, Kawaguchi T. DEM-CFD analysis of fluidization behavior of Geldart Group A particles using a dynamic adhesion force model. Powder Technol 2013;248:143–52.
[312] Kondic L, Fang X, Losert W, O'Hern CS, Behringer RP. Microstructure evolution during impact on granular matter. Phys Rev E 2012;85:011305.
[313] Nishida M, Tanaka Y. DEM simulations and experiments for projectile impacting two-dimensional particle packings including dissimilar material layers. Granular Matter 2010;12:357–68.
[314] Seguin A, Bertho Y, Gondret P, Crassous J. Sphere penetration by impact in a granular medium: a collisional process. EPL 2009;88:44002.
[315] Xing M, He C. 3D ejection behavior of different sized particles in the grain-bed collision process. Geomorphology 2013;187:94–100.
[316] Grzybowski K, Gradoń L. Modeling of the re-entrainment of particles from powder structures. Adv Powder Technol 2005;16:105–21.
[317] Grzybowski K, Itoh M, Gradoń L. Restructurization of nanoaggregates in the impact breakage process. Chem Process Eng 2009;30:99–110.
[318] Papanicolaou ANT, Tsakiris AG, Storm KB. The use of fractals to quantify the morphology of cluster microforms. Geomorphology 2012;139–140:91–108.
[319] Bozzi S, Passoni G. Mathematical modelling of bottom evolution by particle deposition and resuspension. Appl Math Modell 2012;36:4186–96.
[320] Abd-Elhady MS, Clevers SH, Adriaans TNG, Rindt CCM, Wijers JG, van Steenhoven AA. Influence of sintering on the growth rate of particulate fouling layers. Int J Heat Mass Transfer 2007;50:196–207.
[321] Coletti F, Ishiyama EM, Paterson WR, Wilson DI, Macchietto S. Impact of deposit aging and surface roughness on thermal fouling: distributed model. AIChE J 2010;56:3257–73.
[322] Ishiyama AM, Paterson WR, Wilson DI. Exploration of alternative models for the aging of fouling deposits. AIChE J 2011;57:3199–209.
[323] Barth T, Reiche M, Banowski M, Oppermann M, Hampel U. Experimental investigation of multilayer particle deposition and resuspension between periodic steps in turbulent flows. J Aerosol Sci 2013;64:111–24.
[324] Barth T, Ludwig M, Kulenkampff J, Gründig M, Franke K, Lippmann-Pipke J, et al. Positron emission tomography in pebble beds. Part 1: liquid particle deposition. Nucl Eng Des 2014;267:218–26.
[325] Barth T, Kulenkampff J, Bras S, Gründig M, Franke K, Lippmann-Pipke J, et al. Positron emission tomography in pebble beds. Part 2: graphite particle deposition and resuspension. Nucl Eng Des 2014;267:227–37.
[326] Adhiwidjaja I, Matsusaka S, Yabe S, Masuda H. Simultaneous phenomenon of particle deposition and reentrainment in charged aerosol flow - effects of particle charge and external electric field on the deposition layer. Adv Powder Technol 2000;11:221–33.
[327] Adhiwidjaja I, Matsusaka S, Tanaka H, Masuda H. Simultaneous phenomenon of particle deposition and reentrainment: effects of surface roughness on deposition layer of striped pattern. Aerosol Sci Technol 2000;33:323–33.
[328] Matsusaka S, Adhiwidjaja I, Nishio T, Masuda H. Formation of striped pattern deposition layers by an aerosol flow - analysis of thickness and interval of layers. Adv Powder Technol 1998;9(3):207–18.
[329] Matsusaka S, Theerachaisupakij W, Yoshida H, Masuda H. Deposition layers formed by a turbulent aerosol flow of micron and sub-micron particles. Powder Technol 2001;118:130–5.
[330] Abe Y, Skali-Lami S, Bock JC, Francius G. Cohesiveness and hydrodynamic properties of young drinking water biofilms. Water Res 2012;46:1155–66.
[331] Adoue M, Bacchin P, Lorthois S, Combes D, Schmitz P, Mercier-Bonin M. Experimental methodology for analysing macromolecular interactions in the context of marine bacterial adhesion to stainless steel. Chem Eng Res Des 2007;85:792–9.
[332] Nejadnik MR, van der Mei HC, Busscher HJ, Norde W. Determination of the shear force at the balance between bacterial attachment and detachment in weak-adherence systems, using a flow displacement chamber. Appl Environ Microbiol 2008;74:916–9.
[333] Sharma PK, Gibcus MJ, van der Mei HC, Busscher HJ. Influence of fluid shear and microbubbles on bacterial detachment from a surface. Appl Environ Microbiol 2005;71:3668–73.
[334] Mercier-Bonin M, Adoue M, Zanna S, Marcus P, Combes D, Schmitz P. Evaluation of adhesion force between functionalized microbeads and protein-coated stainless steel using shear-flow-induced detachment. J Colloid Interf Sci 2009;338:73–81.
[335] Qian J, Ferro AR. Resuspension of dust particles in a chamber and associated environmental factors. Aerosol Sci Technol 2008;42:566–78.
[336] Rosati JA, Thornburg J, Rodes C. Resuspension of particulate matter from carpet due to human activity. Aerosol Sci Technol 2008;42:472–82.